### 3.4.2.3 Percentage yield

This is the total amount of nanoparticles recovered after formulation expressed as a percentage. The formulated powder was weighed immediately after retrieval from the freeze drier. The percentage yield of TDF-PLGA and AZT-PLGA complexes was determined using the following formula:

$$Percentage\ yield(\%) = \frac{Mass\ of\ nanoparticles\ recovered}{Mass\ of\ PLGA, drug\ and\ excipients\ used\ in\ formulation} x100$$

*Equation 3.2*

### 3.4.2.4 Drug entrapment efficiency

Drug entrapment efficiency is defined as the ratio of the drug loaded in the polymer to the theoretical amount of drug expected to have been loaded. To determine this, the theoretical and actual drug loading percentages were first determined, using the following equations:

$$Theoretical\ drug\ loading\ (TDL)(\%) = \frac{weight\ of\ drug\ added}{weight\ of\ polymer\ and\ drug\ added}\ x\ 100$$

*Equation 3.3*

$$Actual\ drug\ loading\ (\%) = \frac{weight\ of\ drug\ in\ nanoparticles}{weight\ of\ nanoparticles} x100$$

*Equation 3.4*

$$Drug\ Entrapment\ efficiency(\%) = \frac{actual\ drug\ loading}{theoretical\ drug\ loading} x100$$

*Equation 3.5*

### 3.4.2.5 Encapsulation efficiency

The encapsulation efficiency determines the actual amount of drug found in the nano-complex after formulation. The amount of drug encapsulated in the polymer was

determined by dissolving 5 mg of the nano-complex in 0.5 ml of ethyl acetate (in a 5 ml Eppendorf tube) with vortexing. The ethyl acetate was evaporated, and 3 ml of phosphate buffer solution (PBS) was added to the Eppendorf tube. The tube was vortexed, and the contents centrifuged at a speed of 10000 rpm for 15 minutes. Thereafter, the supernatant was collected, and the absorbance measured using the UV-spectrometer and HPLC-DAD system. The concentration of the drug in that sample was determined by extrapolating the absorbance value from a calibration plot of the APIs. The amount of API and the encapsulation efficiency was determined using the equation below:

$$Encapsulation\ efficiency(\%) = \frac{total\ amount\ of\ drug\ in\ the\ yield}{amount\ of\ drug\ added\ during\ encapsulation} x100$$

*Equation 3.6*

#### 3.4.2.6 *In-vitro* drug release

*In-vitro* release kinetics of TDF and AZT loaded nanoparticles was carried out as described by Cetin, Atila and Kadioglu (2010) with slight modifications (sample and separate method).[3,4] Weighed amounts (20 mg) of each nano-formulation was suspended in an Eppendorf tube with 1 ml of PBS (at either pH 1.2 or pH 7.4) containing 0.1% v/v of tween 80. The sample was incubated at 37°C in a shaker incubator at 120 rpm. Subsequently, 0.5 ml was withdrawn with replacement at predetermined time intervals. The isolated samples were centrifuged at 15000 rpm for 20 minutes and the supernatant analyzed for drug content by the UV-spectrometry and HPLC-DAD methods described below.

## 3.5 Preparation of phosphate buffer solution (PBS) - pH 7.4 and pH 1.2 for *in-vitro* release

### 3.5.1 Ingredients

Sodium chloride = 8 g

dissolution of the API. Serial dilutions of the stock solution were performed to obtain working solutions of 0.02 µg/ µl, 0.04 µg/ µl, 0.06 µg/ µl, 0.08 µg/ µl, 0.10 µg/ µl and 0.12 µg/ µl.

**Optimization of chromatographic conditions**

The HPLC method was based on the method developed by Bhavsar et *al* (2012) with some slight modification to the flow rate. The final chromatographic conditions consisted of 70 volumes of methanol to 30 volumes of PBS (pH adjusted to 5.0 using 10% orthophosphoric acid) as the mobile phase. A flow rate of 0.8 ml/min was observed to be suitable for elution for both APIs within 10 minutes, with good symmetrical peaks that were acceptable when compared to those obtained at a flow rate of 1.0 ml/min. The final column temperature was set to 40°C.

**Method validation**

The method for simultaneous estimation of TDF and AZT separately in PLGA nanoparticles was developed and validated in accordance with the International Conference on Harmonisation (ICH) guidelines [5,6].

**Linearity**

The linearity of the method was assessed by preparing standard solutions of different concentrations (0.02 µg/ µl to 0.12 µg/ µl) for both TDF and AZT in different PBS solutions (at pH 1.2 or pH 7.4). Each preparation and measurement was done in triplicate as per the chromatographic conditions mentioned above. The obtained peaks were used to plot a graph of absorbance against concentration to obtain a calibration graph for each compound (API).

**Sensitivity**

The sensitivity of the analytical method was evaluated by determining the limits of detection (LOD) and the limits of quantification (LOQ) in accordance with the ICH guidelines.

**Determination of accuracy and precision**

The accuracy and precision for this method was determined by taking sample readings in triplicate. Three concentrations of the API within the calibration range were used, and the precision was determined by inter-day (intermediate precision) and intraday (reproducibility) analyses. Over a period of three consecutive days, the samples were assayed and the average values, standard deviation and % relative standard deviation (RSD) were compared to determine the inter-day and intra-day precision. The accuracy of the method was determined by the percentage difference of the mean measurements.

## 3.7 Assessment of loaded nanoparticle stability

Following preparation, the nano-formulations were stored between 2 and 8˚C. The particle size, zeta potential and PDI were assessed over a period of 10, 20, 30, 60 and 90 days after formulation.

Chapter 4 will follow with the results obtained during formulation and characterization of the formulated nanoparticles using TDF, PLGA 50:50 and PLGA 85:15.

## Bibliography

1. Liu, J., Qiu, Z., Wang, S., Zhou, L., and Zhang, S., (2010). 'A modified double-emulsion method for the preparation of daunorubicin-loaded polymeric nanoparticle with enhancedin vitroanti-tumor activity', *Biomedical Materials*, 5(6), pp. 065002.
2. Blanco, E., Shen, H., and Ferrari, M., (2015). 'Principles of nanoparticle design for overcoming biological barriers to drug delivery', *Nature Biotechnology*, 33(9), pp.941-951.
3. Cetin, M., Atila, A., and Kadioglu, Y., (2010). 'Formulation and In vitro Characterization of Eudragit® L100 and Eudragit® L100-PLGA Nanoparticles Containing Diclofenac Sodium', *AAPS Pharm SciTech*, 11(3), pp.1250-1256.
4. Agnihotri, S., and Vavia, P., (2009). 'Diclofenac-loaded biopolymeric nanosuspensions for ophthalmic application', *Nanomedicine: Nanotechnology, Biology and Medicine*, 5(1), pp.90-95.
5. Bhavsar, D., Patel, B. and Patel, C. (2012). 'RP-HPLC method for simultaneous estimation of tenofovir disoproxil fumarate, lamivudine, and efavirenz in combined tablet dosage form', *Pharmaceutical Methods*, 3(2), pp.73-78.
6. Bapatla J, Sai N, Hari HD, Theja K, Ramalingam P, Reddy Y., (2011). 'Validated HPTLC Method for the Determination of Tenofovir as Bulk Drug and in Pharmaceutical Dosage Form', *Pelagia Res Library*, (2), pp.163–8.

# CHAPTER 4: RESULTS AND DISCUSSION FOR TENOFOVIR DISOPROXIL FUMARATE LOADED NANOPARTICLES

*This chapter presents the results and discussion obtained when Tenofovir disoproxil fumarate (TDF) was investigated. Emphasis is placed on the different ratios of poly-lactic-co-glycolic acid (PLGA 50:50 and 85:15) used in this study.*

## 4.1 Introduction

The objective of this study was two-fold of which the formulation of TDF as a nanoparticle presented the following specific sub-objectives:

- to characterize TDF and PLGA (50:50 and 85:15)
- to formulate non-covalent complexes of TDF with PLGA of different ratios (50:50 and 85:15);
- to characterize and compare physicochemical properties of the formulated complexes using various analytical techniques;
- to compare the pharmaceutical properties (i.e. particle size, stability and *in-vitro* release) of both formulations (TDF-PLGA 50:50 and TDS-PLGA 85:15) as a means of addressing some of the limitations associated with optimal oral delivery of TDF (i.e. low permeability, low bioavailability).

## 4.2 Characterization of TDF and PLGA (50:50 and 85:15)

Prior to formulation of the nanoparticle proper, TDF and two PLGA ratios (PLGA 50:50 and PLGA 85:15) were characterized individually, and in combination as a physical mixture (TDF-PLGA 50:50 and TDF-PLGA 85:15). Data from the characterization studies are as follows:

### 4.2.1 Fourier-transform infra-red (FT-IR) spectroscopy

Infra-red spectroscopy (FTIR) was used to identify the functional groups in TDF, PLGA (50:50 and 85:15), and the TDF-PLGA (50:50 and 85:15) formulations. This was done

to identify the susceptibility of these functional groups to chemical reactions *via* reduction in band intensities or complete disappearance of characteristic bands. The samples were also used as reference samples for assessment of the nano-formulation process. Figure 4.2 presents the spectra of TDF, PLGA 50:50, PLGA 85:15 and a combination of TDF-PLGA 50:50 and TDF-PLGA 85:15 physical mixtures. TDF was ground with each polymer separately to form the physical mixtures. The FTIR spectra of these mixtures were compared to those of the single component compounds (TDF, PLGA 50:50 and PLGA 85:15) to identify characteristic functional groups as a physical mixture, as well as the appearance of or disappearance of such functional groups in the combination (Figure 4.2 and Table C1.3 in appendix C).

TDF (Figure 4.2a) showed a characteristic peak band at 3459.12 $cm^{-1}$, attributed to the N-H stretching vibration bands of the amine group. The intensity bands at 2981.38 $cm^{-1}$ and 2814.22 $cm^{-1}$ were assigned to the hydroxyl (O-H) stretching, the band at 2081.44 $cm^{-1}$ was attributed to the C=C, and the intensity bands at 1752.31 $cm^{-1}$ and 1671.87 $cm^{-1}$ were assigned to C=O. Figure 4.1a presents the structure of TDF.

The pure PLGA 50:50 (Figure 4.2b) showed characteristic peak bands at 2950.52 $cm^{-1}$ which was attributed to the chelated O-H stretching vibrations. The peak band at 1750.32 $cm^{-1}$ was attributed to the C=O stretching of the carbonyl group. The pure PLGA 85:15 (Figure 4.2c) also showed characteristic peak bands at 2996.25 $cm^{-1}$ which was attributed to chelated O-H bridge stretching and 1746.64 $cm^{-1}$ attributed to strong C=O stretching of the carbonyl group. Figure 4.1b below presents the structure of PLGA.

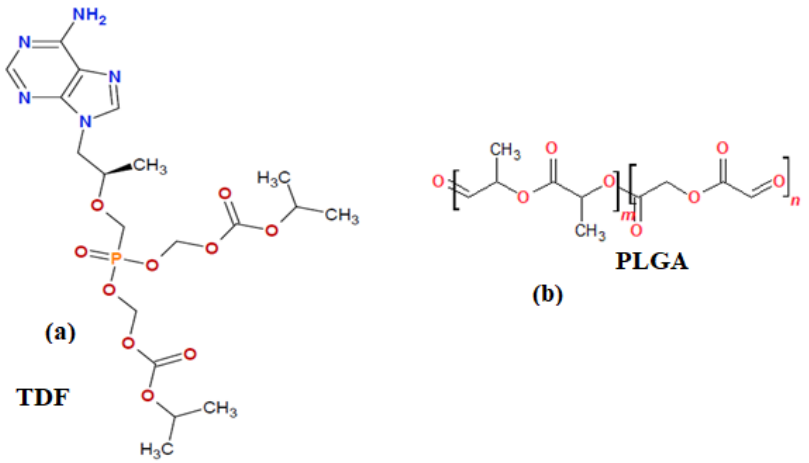


*Figure 4.1: Structure of (a) TDF and (b )PLGA (**n** represents the number of lactic acid units while **m** represents the number of glycolic acid units)*

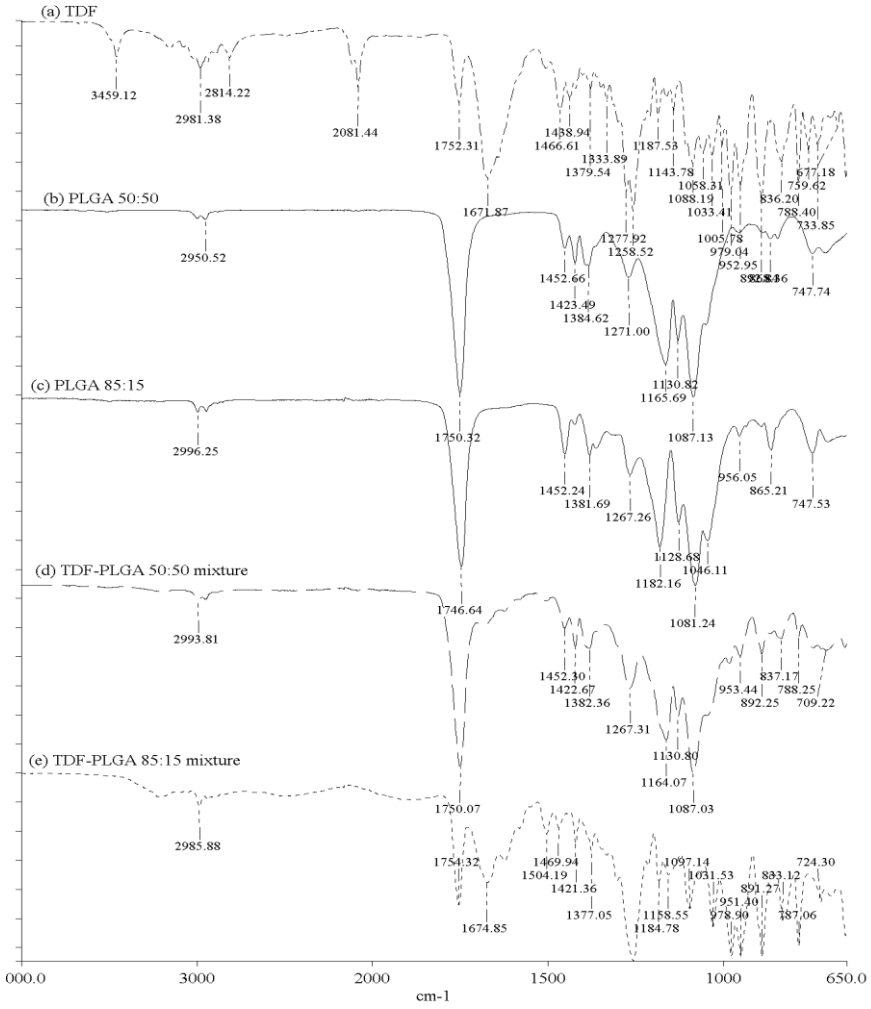


Figure 4.2: *FT-IR spectra of (a) TDF, (b) PLGA 50:50, (c) PLGA 85:15, (d) TDF-PLGA 50:50 physical mixture, (e) TDF-PLGA 85:15 physical mixture*

The FT-IR spectra of TDF-PLGA 50:50 and TDF-PLGA 85:15 physical mixtures (Figure 4.2d and Figure 4.2e, respectively) showed shifts in the characteristic peak bands of the components in the resulting physical mixture. TDF-PLGA 50:50 physical mixture (Figure 4.2d) showed characteristic peak bands at 2993.81 $cm^{-1}$, attributed to chelated O-H bridge stretching and at 1750.07 $cm^{-1}$, attributed to the C=O stretching vibration. The peaks at 3459.12 $cm^{-1}$ 2814.22 $cm^{-1}$ 2081.44 $cm^{-1}$ and 1671.87 $cm^{-1}$ had disappeared while the intensity of the peak at 1752.31 $cm^{-1}$ had increased when compared to the parent AZT. On the other hand, TDF-PLGA 85:15 physical mixture (Figure 4.2e) also showed similar characteristic peak bands at 2985.88 $cm^{-1}$ attributed to chelated O-H bridge stretching, and at 1754.32 $cm^{-1}$ and 1674.85 $cm^{-1}$, both attributed to the C=O stretching vibration. The spectra also presented with peaks that had disappeared just like in AZT-PLGA 50:50 with the exception of the peak at 1671.87 $cm^{-1}$ which was available but with decrease intensity and we also experienced a decrease in intensity for the peak at 1754.32 $cm^{-1}$ when compared to the parent compounds.

Overall both physical mixtures showed slight shifts, disappearance, increase and decrease in intensity of characteristic peaks when compared to the parent compounds, thus indicating an interaction between the TDF and PLGA. A summary of the bands is in Table C1.3 in appendix C.

### 4.2.2 Hot stage microscopy (HSM)

The results presented below were obtained during sample analysis using hot stage microscopy (HSM). The compounds were analyzed individually (TDF, PLGA 50:50, PLGA 85:15) and in combination as a physical mixture of the polymer with TDF (mixed by grinding). The samples where heated up to a maximum temperature of 200°C at a temperature increase rate of 10°C per min.

Figure 4.3(a) shows images of TDF taken during HSM analysis. The melting of TDF commenced in the temperature range, 113°C to 118°C. At 120°C, the sample had completely melted, and at this temperature, bubbles were noticed. The appearance of bubbles could be because of gas (due to sublimation) accumulation between the glass slides (cover slide and sample holder). The results obtained from this analysis were in line with the certificate of analysis which indicated that the melting point of TDF was between 114°C and 118°C. The degradation of TDF started at about 180°C, observed by discoloration of the sample.

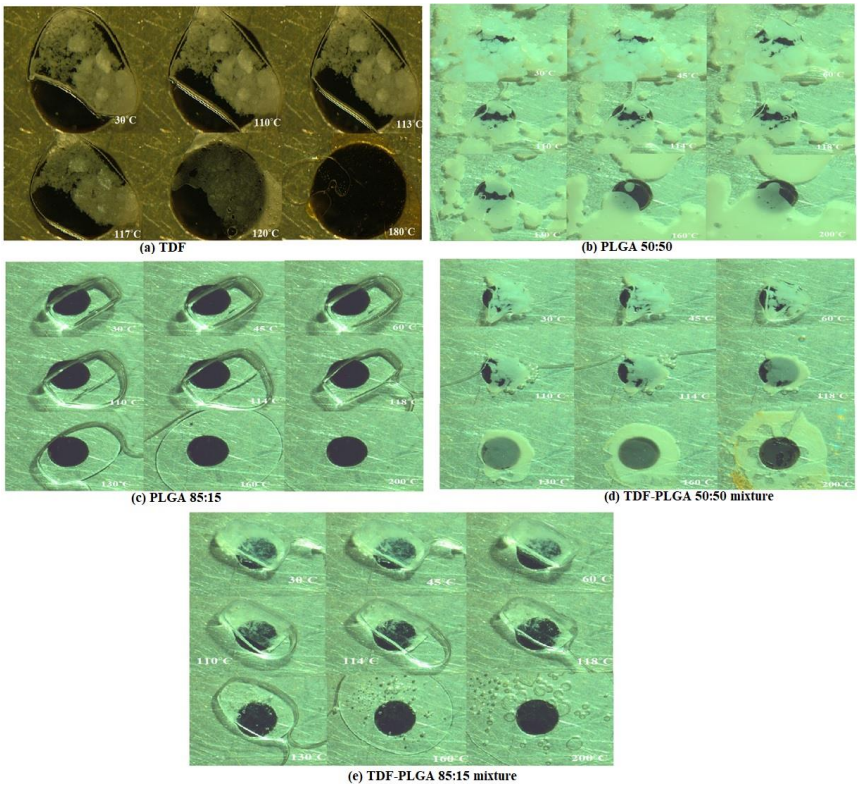


Figure 4.3: *HSM images of (a) TDF, (b) PLGA 50:50, (c) PLGA 85:15, (d) TDF-PLGA 50:50 physical mixture, and (e) TDF-PLGA 85:15 physical mixture*

The melting of PLGA 50:50 when analyzed using HSM is shown in Figure 4.3(b). Melting commenced at about 45°C; the sample gradually melted with no appearance of bubbles, an indication that no moisture was entraped in the samples. At temperatures above 60°C, the sample had passed its indicated glass transition

temperature, and appeared to be oily and viscous. There were however no visible signs of degradation (discolouration) even at temperatures up to 200°C.

Figure 4.3(c) presents HSM analysis of PLGA 85:15, with melting commencing at about 55°C. The sample gradually melted with no appearance of bubbles, like what was obtained with PLGA 50:50, also an indication that no moisture was entrapped in the samples. At temperatures above 60°C, the sample had passed its indicated glass transition temperature, and appeared to be oily and viscous. As happened with PLGA 50:50, the samples did not show any visible signs of degradation even at temperatures up to 200°C.

Figure 4.3(d) shows images from the HSM analysis of the polymer mixture (TDF-PLGA 50:50). Signs of melting were observed from temperatures around 56°C, with the appearance of bubbles at temperature changes between 110°C and 114°C. This was around the melting point of the API, confirming the presence of the API in the physical mixture. The appearance of the bubbles was also an indication of moisture entrapment between the slides covering the sample. The bubbles eventually disappeared, and signs of degradation such as browning of the sample appeared at a temperature of 160°C.

Figure 4.3(e) presents images from the HSM analysis of TDF-PLGA 85:15 physical mixture. Signs of sample melting were observed around 56°C, with the appearance of bubbles at temperatures between 110°C and 114°C. This was also around the melting point of TDF, confirming its presence in the physical mixture. The appearance of the bubbles was an indication of moisture being entrapped between the slides covering the sample, or fumes from the API melting. Unlike what was obtained with TDF-PLGA 50:50 physical mixture [Figure 4.3(d)] however, the bubbles did not disappear on

continued heating and instead grew bigger, indicating degradation. Another sign of degradation, browning of the sample, appeared at a temperature of 160°C. Given that the copolymers, PLGA 50:50 and PLGA 85:15, did not show any signs of degradation under HSM analyses [Figure 4.3 (b) and (c)] while TDF did, the presence of TDF in the physical mixture can be inferred from the degradation observed on HSM of TDF-PLGA 85:15.

### 4.2.3 Thermogravimetric analysis (TGA)

Changes in thermal stability, organic solvent evolution and the degradation of TDF, PLGA 50:50, PLGA 85:15, and a mixture(physical) of both polymers with TDF (mixed by grinding) was evaluated using TGA. Figure 4.4 shows the TGA curves obtained when the samples were analyzed. There was release of volatile substance from the samples and weight loss due to moisture was observed. The temperature at which mass loss began ($T_{onset}$°C) and ended ($T_{endset}$°C) as well as the temperature at which maximum mass loss occurred ($T_{deg.max.}$°C) were determined and are presented in Table C1.4 in appendix C.

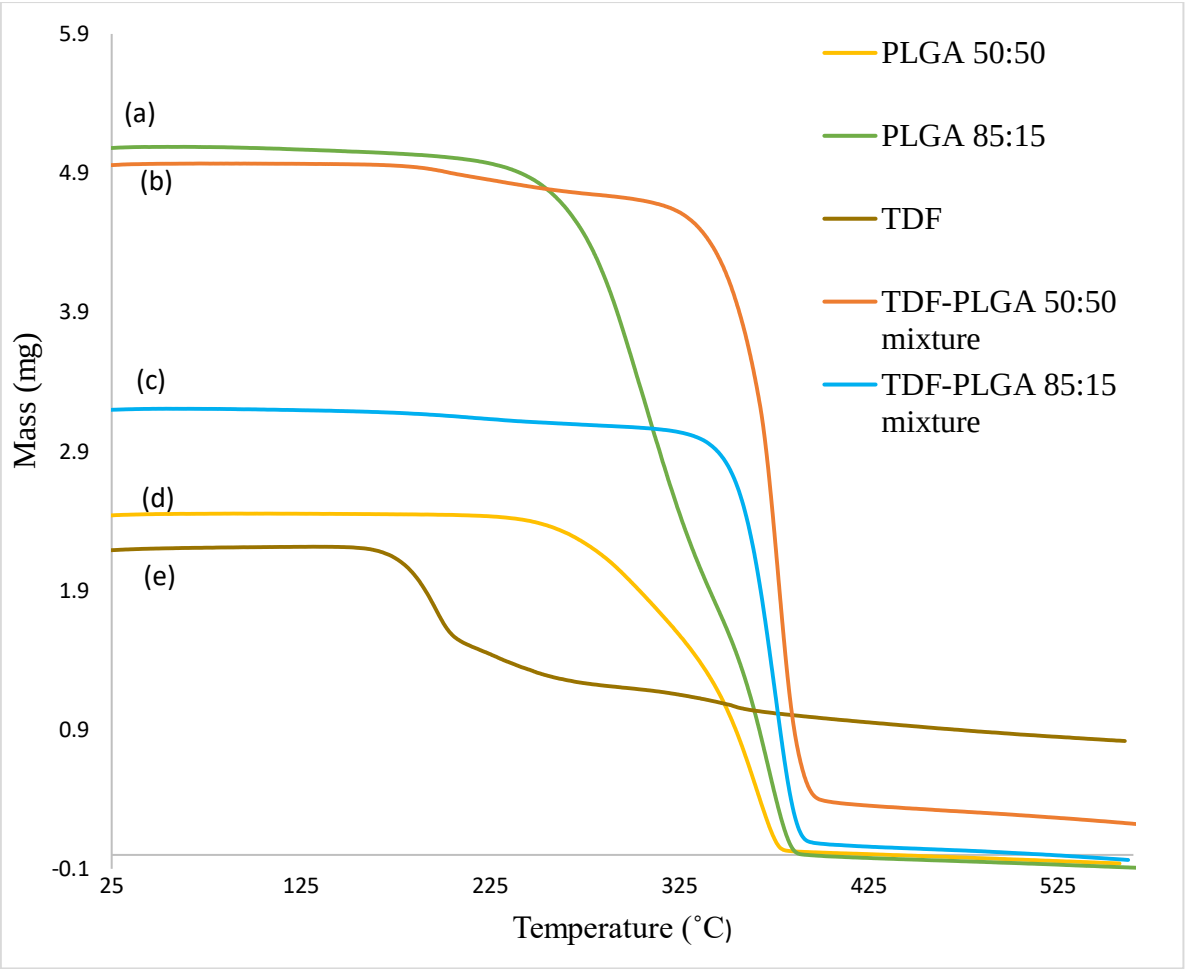


Figure 4.4: *TGA curves of (a) PLGA 85:15, (b) TDF-PLGA 50:50 physical mixture, (c) TDF-PLGA 85:15 physical mixture, (d) PLGA 50:50, and (e) TDF.*

Both polymers (PLGA 50:50 and 85:15) displayed two mass loss events associated with the degradation process of the polymer [Figure 4.4 (a) and (d)]. PLGA 50:50 had a first and second mass loss of about 30% and 68%, respectively, while PLGA 85:15 showed mass loss values of about 65% and 35%, respectively. When compared to each other, PLGA 50:50 did not obtain a 100% mass loss; it proceeded with a 2% inert residue. When the physical mixtures of TDF with PLGA 50:50 and TDF with PLGA 85:15 were analyzed, both samples showed a single mass loss event compared to the individual polymers and TDF [Figure 4.4 (b) and (c)]. The percentage mass loss for TDF-PLGA 50:50 and TDF-PLGA 85:15 were about 93% and 98%, respectively.

The $T_{onset}$ values for TDF-PLGA 50:50 and TDF-PLGA 85:15 were at a lower temperature when compared to that of both polymers and higher than that of TDF alone (Table C1.4) in appendix C. The physical mixture of TDF and PLGA showed an overall increase in thermal stability when compared to the individual polymers and TDF[1]. The differences in the mass loss percentages in the polymers could be attributed to their differences in molecular mass and composition since each polymer has a different ratio of lactic and glycolic acid.

### 4.2.4 Differential Scanning Calorimetry (DSC)

Prior to formulation of the nanoparticles, the melting points of the samples were determined using DSC. Figure 4.5a shows the thermograms of PLGA 50:50 and PLGA 85:15; both co-polymers showed a single endothermic peak, indicating that the melting points for both polymers were at about 55.41°C and 45.84°C, respectively.

Figure 4.5b shows the DSC thermogram of TDF. Two endothermic peaks were observed, within the range of temperatures, 111°C-118°C; these peaks corresponded to the melting points of two different polymorphic forms of TDF, according to literature there are about three different polymorphic forms (A, B and I).[2,3] The first endothermic peak was because of polymorphic form $I_{-1}$ melting, which was then followed by recrystallisation (an exothermic event) of the melted API into form I which presented with a melting peak of 118°C[2,4], thus both endothermic peaks can be attributed to the different forms of TDF.

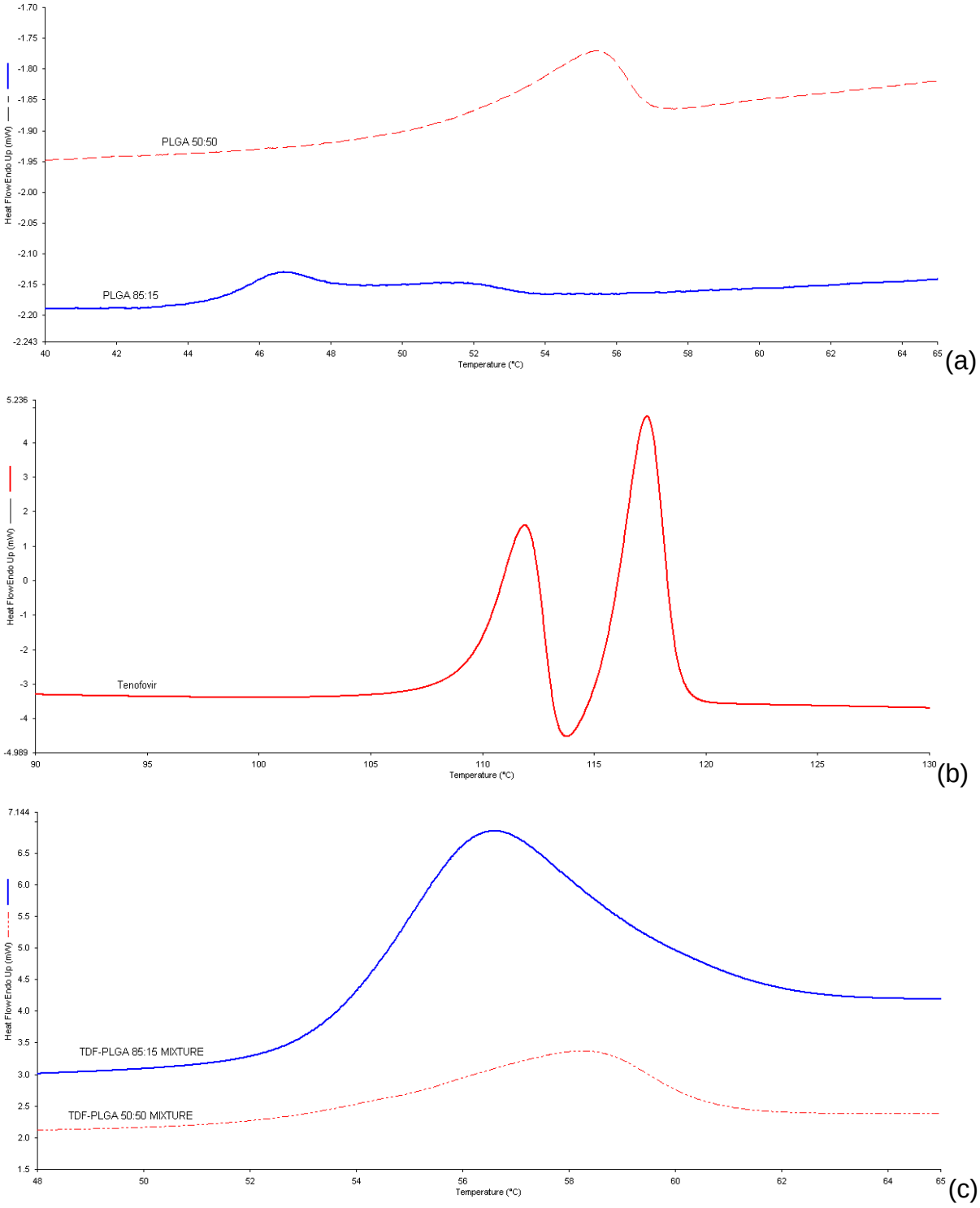


*Figure 4.5: DSC thermograms of (a) PLGA (50:50 and 85:15), (b) Tenofovir disoproxil fumarate, (c) TDF-PLGA 50:50 and TDF-PLGA 85:15 physical mixtures.*

Figure 4.5c presents thermograms of TDF when it was analyzed as a physical mixture by grinding separately with PLGA 50:50 and PLGA 85:15. A single endothermic event was observed for each sample, with highest peaks at 58.27°C and 56.51°C for TDF-

PLGA 50:50 and TDF PLGA 85:15 physical mixture, respectively. Comparing these peaks with PLGA alone, a slight shift of about 3-4°C can be observed. This indicates a slight increase in stability of the physical mixture, which might also indicate that there is some form of interaction taking place in the physical mixture.

## 4.3 Formulation and characterisation of TDF loaded nanoparticles

Figure 4.6 below shows diagrammatically each step in the formulation of TDF-loaded nanoparticles. Formulation was done using the water-in-oil-in-water double emulsion solvent evaporation and diffusion method by Liu *et al*., 2010 with modifications to decrease nanoparticle size and increase encapsulation efficiency.

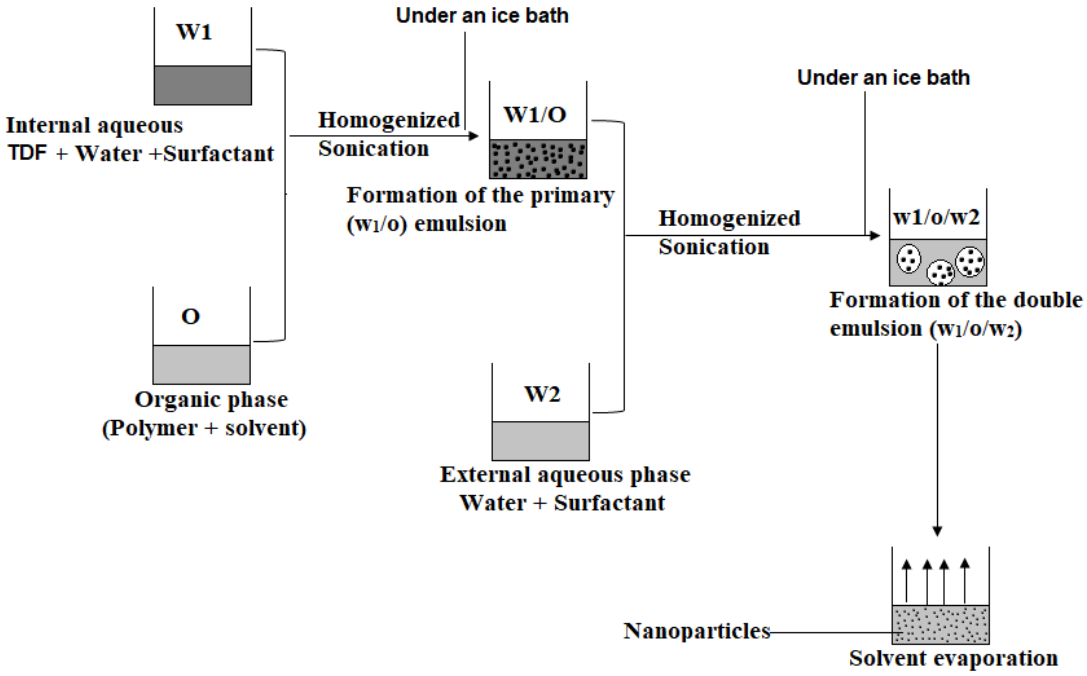


*Figure 4.6: Schematic presentation of TDF-loaded nanoparticle formulation process.*

After formulation, the loaded nanoparticles were freeze dried and characterized for particle size and distribution, surface morphology, zeta potential, percentage yield, drug entrapment and encapsulation efficiency.

### 4.3.1 Particle size and distribution (polydispersity index ) PDI

The particle size distribution of the TDF-PLGA (50:50 and 85:15) loaded nanoparticles was determined immediately after formulation and evaporation of the organic solvents from the sample, using dynamic light scattering in the Malvern particle-sizing system. The mean particle sizes for TDF-PLGA 50:50 and TDF-PLGA 85:15 were found to be 117.3 ± 0.45 nm and 103.0 ± 1.62 nm, respectively. There was an increase in particle sizes after the TDF-PLGA (50:50 and 85:15) loaded nanoparticles were washed three times with distilled water. The average sizes after washing for TDF-PLGA 50:50 and TDF-PLGA 85:15 were found to be 153.2 ± 4.3 nm and 127 ± 2.32 nm, respectively. The increase in particle size (Table 4.1) could have resulted from particle aggregation after the surfactants and emulsifiers had been removed by the washing process.

Table 4.1: *Particle size distribution of TDF-loaded nanoparticles.*

| **Formulated nanoparticle** | **Particle size (nm)** | |
|---|---|---|
| | Before wash | After wash |
| **TDF-PLGA 50: 50** | 117.3 ± 0.45 | 153.2 ± 4.3 |
| **TDF-PLGA 85: 15** | 103.0 ± 1.62 | 127.0 ± 2.32 |

The particle size of formulated nanoparticles plays an important role in their therapeutic efficacy. The smaller the particle size, the higher the rate of particle absorption from the intestine into the blood stream.[5,6] Therefore, a high uptake of particles is expected from the formulation prepared, given the particle sizes obtained. The postulated mechanisms to show how particles pass through the gastrointestinal and physiological barriers highlights endocytosis as one of the mechanisms, for particles < 500 nm. It can therefore be seen that the sizes of TDF-PLGA 50:50 and TDF-PLGA 85:15 nanoparticles immediately after formulation (117.2 ± 2.33 nm and 103.0 ± 1.62 nm, respectively) and immediately after washing (153.2 ± 4.3 nm and 127.0 ± 2.32 nm, respectively) favors uptake *via* endocytosis. As such, it may be

inferred that the formulated nanoparticles would easily permeate physiological barriers to promote absorption.

*Table 4.2: Polydispersity index of TDF-loaded nanoparticles.*

| **Formulated nanoparticle** | **Polydispersity index** | |
|---|---|---|
| | Before wash | After wash |
| **TDF-PLGA 50: 50** | 0.160 ± 0.01 | 0.303 ± 0.06 |
| **TDF-PLGA 85: 15** | 0.152 ± 0.04 | 0.355 ± 0.01 |

The polydispersity index (PDI) values (Table 4.2) for TDF-PLGA (50:50) and TDF-PLGA (85:15) after formulation were found to be an average of 0.160 ± 0.01 and 0.152 ±0.07, respectively. These PDI values increased to 0.303 ± 0.06 and 0.355 ± 0.01 (Table 4.2) for TDF-PLGA 50:50 and TDF-PLGA 85:15, respectively, after washing of the loaded nanoparticles. These values are indicative of a homogenous distribution of the nanoparticles. PDI values between 0.1 and 0.4 are indicative of monodisperse samples; the nanoparticles are relatively of the same size, width and/or shape while PDI value greater than 0.5 indicate a polydispersed sample.[7] The increase in the PDI after washing of the pellets could be due to such pellets aggregating or coalescing after removal (washing) of the surfactants and emulsifiers, hence making the distribution a bit more heterogeneous post washing.

### 4.3.2 Evaluation of surface morphology of the nanoparticles

The morphology (shape and properties) of the nanoparticles was determined using high resolution scanning electron microscopy (HR-SEM). Blank nanoparticles were prepared and the morphology (shape and properties) of the nanoparticles were determined. Figure 4.7 [(a) and (b)] shows images of blank PLGA 50:50 and blank PLGA 85:15 nanoparticles; the images showed that the particles were spherical in shape with smooth surfaces.

Figure 4.7c shows images of TDF-PLGA 85:15 loaded nanoparticles. The images showed spherical shaped particles with smooth surfaces. The average particle size was above 200 nm which was greater than the sizes provided by the zeta sizer (127 nm). As mentioned previously, the increase in size might be due to aggregation and coalescence of the nanoparticles. Such aggregation and coalescence may be attributed to the freeze-drying process, which may have caused irreversible fusion of the nanoparticles. The freeze-drying process can also cause mechanical stress on the nanoparticles leading to a change in particle morphology.[8] As shown by (Pirooznia *et al*., 2012), the addition of cryoprotectants in the final step before lyophilization can decrease the tendency for the nanoparticles to aggregate, thus preventing changes in particle morphology.

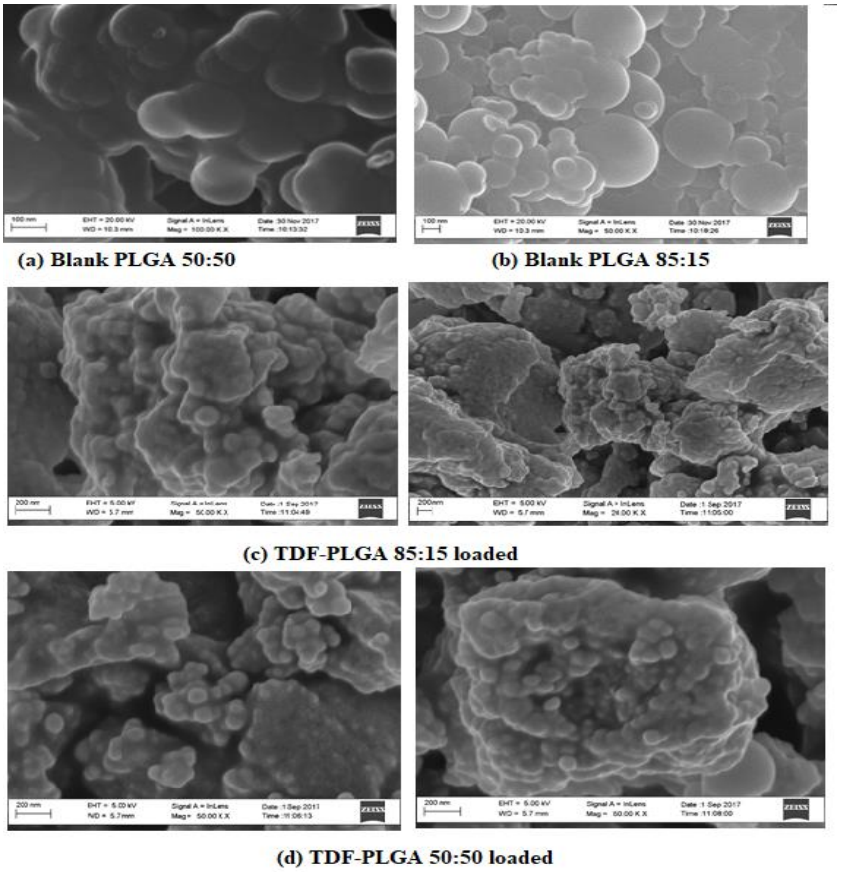


Figure 4.7: *HR-SEM of formulated nanoparticles: (a) Blank PLGA 50:50, (b) Blank PLGA 85:15, (c) TDF-PLGA 85:15 loaded, (d) TDF-PLGA 50:50 loaded*

Figure 4.7d shows images of TDF-PLGA 50:50 taken using the HR-SEM. Similar characteristics to those which were obtained with TDF-PLGA 85:15 were observed (Figure 4.7c); the nanoparticle surface was smooth and spherical, with signs of aggregation and coalescence.

When Figure 4.7a and Figure 4.7b were compared to Figure 4.7c and Figure 4.7d the latter appeared to be less smooth and more coagulated this might be as a result of the presence of TDF in the formulation.

### 4.3.3 Zeta potential

Following formulation of the TDF-PLGA 50:50 and TDF-PLGA 85:15 loaded nanoparticles, their zeta potentials were determined using the Malvern zeta-sizing system. The mean zeta potential values for TDF-PLGA 50:50 and TDF-PLGA 85:15 were found to be -8.84 ± 0.35 mV and -5.69 ± 0.6 mV, respectively (Table 4.3). These values decreased to -19.1 ± 0.91 mV and -5.72 ± 1 mV, respectively, after washing of the samples. The change in zeta potential for TDF-PLGA 85:15 was not significantly different. The negative charge on the nanoparticles directly affects the cellular uptake of the nanoparticles by inducing a positive charge on the cell membrane, resulting in attraction between the two surfaces. The decrease in the zeta potential values is also an indication of the increased stability of the nanoparticles. A high bioavailability may be obtained due to this increased stability, because the TDF loaded nanoparticles would possibly be able to permeate the cell membrane and be transported to endosomes found within the cell.[9]

Table 4.3: *Zeta potential of TDF-loaded nanoparticles*

| Drug Polymer ratio | Zeta potential | |
|---|---|---|
| | Before wash | After wash |
| **TDF-PLGA 50: 50** | -8.84 ± 0.35 mV | -19.1 ±0.91 mV |
| **TDF-PLGA 85: 15** | -5.69 ± 0.6 mV | -5.72 ± 1 mV |

### 4.3.4 Percentage yield

The percentage yield is the total amount of nanoparticles recovered after formulation expressed as a percentage of the total weight of products used for formulation, while drug entrapment efficiency is the ratio of the API amount expected to be loaded *versus* the actual amount of API loaded after formulation and encapsulation efficiency determines the actual amount of drug found in the formulated nanoparticles.

TDF-PLGA 50:50 and TDF-PLGA 85:15 loaded nanoparticles were recovered and weighed after freeze-drying. The values obtained after weighing were 71.2 mg and 61.0 mg, for TDF-PLGA 50:50 and TDF-PLGA 85:15 loaded nanoparticles, respectively (Table 4.4)**.** The percentage yield was calculated as per Equation 3.2

$$Percentage\ yield(\%) = \frac{mass\ of\ nanoparticles\ recovered}{mass\ of\ PLGA, drug\ and\ excipients\ used\ in\ formulation} x100$$

$$Percentage\ yield(\%) = \frac{71.2\ mg}{105\ mg} x100$$

= 67.82% for TDF-PLGA 50:50

$$Percentage\ yield(\%) = \frac{61\ mg}{105\ mg} x100$$

= 58.10% for TDF-PLGA 85:15

The percentage yield was calculated to be 67.82% and 58.10% for TDF-PLGA 50:50 and TDF-PLGA 85:15 loaded nanoparticles, respectively. The loss in mass could be

due to unbound polymer and drug discarded during collection of the formulated nanoparticles or washing process.

*Table 4.4:* Mass of TDF-loaded nanoparticles recovered (mg) and percentage yield.

| Drug polymer combination | Mass of TDF used in formulation(mg) | Mass of polymer used (mg) | Mass of nanoparticle recovered (mg) | Percentage yield (%) |
|---|---|---|---|---|
| **TDF-PLGA 50:50** | 5 | 100 | 71.2 | 67.82 |
| **TDF-PLGA 85:15** | 5 | 100 | 61 | 58.10 |

To determine the encapsulation efficiency and entrapment, we first needed to develop a method (HPLC-DAD and UV-spectrometry method) of which we used to determine the amount of TDF in the nanoparticles.

### 4.3.5 Standard calibration plot for determination of TDF (HPLC-DAD and UV-spectrometry method)

To determine linearity of the method, samples were analyzed at an absorbance frequency of 260 nm, at which TDF is reported to have its maximum absorbance.[10] A linear regression model was used to study the relationship between absorbance of TDF and its concentration, and a graph of mean TDF absorbance *versus* TDF concentration was plotted (Figure 4.8). This model enabled the prediction of TDF concentration in the prepared nano-formulations by measuring its absorbance in the sample; data obtained is featured in appendix C (Table C1.1 and Table C1.2).

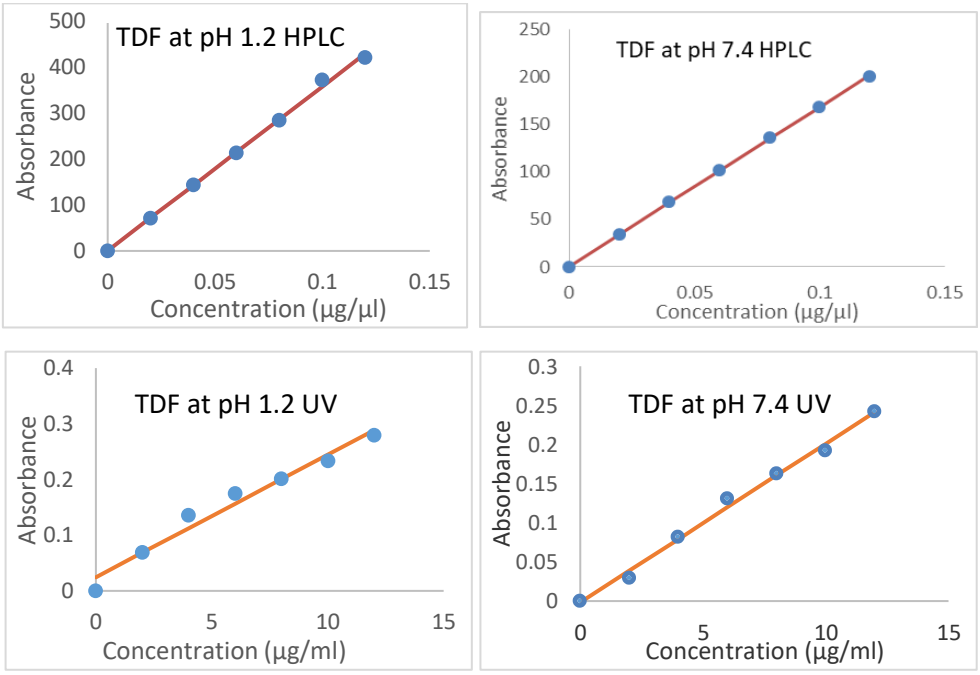


*Figure 4.8: Standard calibration graph of Tenofovir disoproxil fumarate (λmax=260nm).*

Stock solutions and working standards were prepared in phosphate buffer solution (PBS) at a pH of 1.2 and pH 7.4. Samples were analyzed at 25ºC. Data values were recorded in triplicate presented as mean ± SD (n=3).

Table 4.5 presents computed data derived from plotting the calibration curves for TDF. The $R^2$ values at pH 1.2 and pH 7.4 depicted linearity and showed how close the data was to the fitted regression line. The relationship between concentration and absorbance can be expressed by Equation 4.1 with substitutions from Table 4.5. From this, the amount of drug encapsulated within the nanoparticles was determined. Data obtained is featured in appendix C (Table C1.1 and Table C1.2).

$$y = intercept + slope(x)$$

*Equation 4.1*

where $y$ = TDF peak area

$x$ = the standard solution concentration in µg/ml

*Table 4.5:* Linearity data and quantification limits of Tenofovir disoproxil fumarate at pH 1.2 and 7.4 (*HPLC-DAD and UV-spectrometry methods*).

| **Validation parameters** | **HPLC-DAD** | | **UV-spectrometry** | |
|---|---|---|---|---|
| | pH 1.2 | pH 7.4 | pH 1.2 | pH 7.4 |
| **$R^2$** | 0.9781 | 0.9999 | 0.9702 | 0.9938 |
| **Slope ± SD** | 3578.54±69.44 | 1677.96±7.86 | 0.0220±0.002 | 0.02±0.001 |
| **Intercept ± SD** | 0.32±5.01 | 0.79±0.567 | 0.024±0.01 | -0.002±0.01 |
| **Concentration range (µg/ml)** | 0.02-0.12 | 0.02-0.12 | 200-1200 | 200-1200 |
| **LOD (µg/ml)** | 0.001 | 0.01 | 1.87 | 0.85 |
| **LOQ (µg/ml)** | 0.003 | 0.014 | 5.65 | 2.5 |

Analyses with HPLC-DAD presented better linearity values than those with UV-spectrometry, and linearity values obtained at pH 7.4 seemed better than values obtained at pH 1.2 (as shown by the $R^2$ values); however, it is not clear if these differences in values are statistically significant. The results obtained indicate that the two methods, HPLC-DAD and UV-spectrometry, were sensitive enough to determine the concentration of the API in the standard solutions. However, the concentration ranges, as well as the LOD and LOQ values are lower for the HPLC-DAD method than for the UV-spectrometry method, attesting to the increased sensitivity of the HPLC-DAD compared to the UV-spectrometry method.

The percentage recovery was calculated from the equation of the calibration curve and was found to be between 98% and 102% (Table 4.6). This was acceptable when viewed against the International Conference on Harmonisation (ICH) guidelines for assays using the HPLC-DAD method. The precision (repeatability) of the methods was determined by analyzing replicates of TDF standard solution, at three different concentrations (over the ranges, 0.02-0.12 µg/µl for the HPLC-DAD method and 2-12

µg/µl for the UV-spectrometry method) covering the standard calibration range (Table C1.1 and Table C1.2 in the appendix ). The values were expressed as % RSD and found to be less than 2% (Table 4.6); suggesting that the results provided by the methods are reproducible.

Table 4.6: Intra-day and inter-day assay precision and accuracy for Tenofovir disoproxil fumarate at pH 1.2 and 7.4 (HPLC-DAD method).

| | pH 1.2 | | | pH 7.4 | | |
|---|---|---|---|---|---|---|
| **TDF(µg/µl)** | 0.02 | 0.06 | 0.12 | 0.02 | 0.06 | 0.12 |
| | | | **Intra-day (n=3)** | | | |
| | | | **Day 1** | | | |
| **Mean** | 0.02 | 0.06 | 0.12 | 0.02 | 0.06 | 0.12 |
| **SD** | 0.0003 | 0.0009 | 0.0006 | 0.0003 | 0.0008 | 0.0007 |
| **Precision[1] (%)** | 1.51 | 1.51 | 0.51 | 2.01 | 1.32 | 0.59 |
| **Accuracy[2] (%)** | 99.50 | 99.30 | 97.92 | 99.50 | 100.80 | 99.40 |
| | | | **Day 2** | | | |
| **Mean** | 0.02 | 0.06 | 0.12 | 0.02 | 0.06 | 0.12 |
| **SD** | 0.0002 | 0.0007 | 0.0012 | 0.0002 | 0.0007 | 0.0005 |
| **Precision[1] (%)** | 1.00 | 1.17 | 1.02 | 1.00 | 1.13 | 0.42 |
| **Accuracy[2] (%)** | 100.00 | 99.83 | 98.00 | 99.50 | 101.80 | 99.10 |
| | | | **Day 3** | | | |
| **Mean** | 0.02 | 0.06 | 0.12 | 0.02 | 0.06 | 0.12 |
| **SD** | 0.0002 | 0.0006 | 0.0009 | 0.0003 | 0.0009 | 0.0009 |
| **Precision[1] (%)** | 1.00 | 1.00 | 0.77 | 1.47 | 1.50 | 0.75 |
| **Accuracy[2] (%)** | 100.50 | 99.50 | 97.83 | 99.50 | 99.50 | 99.50 |
| | | | **Inter-day (n=9)** | | | |
| **Mean[3]** | 0.02 | 0.06 | 0.12 | 0.02 | 0.06 | 0.12 |
| **SD** | 0.00008 | 0.0001 | 0.00008 | 0.0002 | 0.0008 | 0.0002 |
| **Precision[1] (%)** | 0.40 | 0.12 | 0.07 | 1.00 | 1.32 | 0.17 |
| **Accuracy[2] (%)** | 100.00 | 99.50 | 97.92 | 100.50 | 101.00 | 99.30 |

The accuracy of the method for assay purposes was determined by measuring the absorbance of TDF at three different concentrations (0.02, 0.06, 0.12 µg/ µl and 2, 6, 12 µg/ µl, for the HPLC-DAD and UV-spectrometry methods, respectively) covering the standard calibration range (Figure 4.8). The accuracy data from the UV-spectrometry method on the other hand provided values within the range, 99-116.7% (Table 4.7). The acceptable recovery range in assays for quality control and drug

registration is between 90 and 110%,[11] and so this method did not meet the requirements for quality control and drug registration. However, since this study is still preliminary and not for quality control or drug registration purposes, the UV spectrometry method was also utilized as a comparison to the HPLC-DAD method for determination of TDF in samples.

*Table 4.7: Intra-day and inter-day assay precision and accuracy for Tenofovir disoproxil fumarate at pH 1.2 and 7.4 (UV-spectrometry method).*

| | pH 1.2 | | | pH 7.4 | | |
|---|---|---|---|---|---|---|
| **TDF(µg/µl)** | 2 | 6 | 12 | 2 | 6 | 12 |
| | | | **Intra-day (n=3)** | | | |
| | | | **Day 1** | | | |
| **Mean** | 2.04 | 6.90 | 11.63 | 1.98 | 5.95 | 12.03 |
| **SD** | 0.0006 | 0.0008 | 0.0006 | 0.0002 | 0.0003 | 0.0007 |
| **Precision[1] (%)** | 0.03 | 0.01 | 0.005 | 0.08 | 0.005 | 0.006 |
| **Accuracy[2] (%)** | 102 | 115 | 96.9 | 99 | 99.2 | 100.3 |
| | | | **Day 2** | | | |
| **Mean** | 2.05 | 6.87 | 11.52 | 2.07 | 6.01 | 12.19 |
| **SD** | 0.0005 | 0.0013 | 0.0020 | 0.0003 | 0.0001 | 0.0002 |
| **Precision[1] (%)** | 0.02 | 0.02 | 0.02 | 0.01 | 0.002 | 0.002 |
| **Accuracy[2] (%)** | 102.5 | 114.5 | 96.0 | 103.5 | 100.1 | 101.6 |
| | | | **Day 3** | | | |
| **Mean** | 2.04 | 7.00 | 11.57 | 2.09 | 6.05 | 12.01 |
| **SD** | 0.0006 | 0.0006 | 0.0025 | 0.0002 | 0.0001 | 0.0002 |
| **Precision[1] (%)** | 0.030 | 0.009 | 0.020 | 0.010 | 0.002 | 0.002 |
| **Accuracy[2] (%)** | 100.1 | 116.7 | 96.4 | 104.5 | 100.8 | 102.0 |
| | | | **Inter-day (n=9)** | | | |
| **Mean[3]** | 2.04 | 6.92 | 11.68 | 2.07 | 6.00 | 12.15 |
| **SD** | 0.0002 | 0.0020 | 0.0010 | 0.0005 | 0.0010 | 0.0020 |
| **Precision[1] (%)** | 0.01 | 0.03 | 0.90 | 0.02 | 0.02 | 0.02 |
| **Accuracy[2] (%)** | 102.00 | 115.30 | 97.30 | 103.50 | 100.00 | 101.30 |

Values obtained in Table 4.6 and Table 4.7 were calculated as follows;

- [1]Expressed as % RSD = (SD/mean) × 100.
- [2]Calculated as (mean determined concentration/nominal concentration) × 100.
- [3]n = 3 days with three replicates per day

### 4.3.6 Encapsulation efficiency

The encapsulation efficiency was determined using Equation 3.6.

$$Encapsulation\ efficiency(\%) = \frac{total\ amount\ of\ drug\ in\ the\ yield}{amount\ of\ drug\ added\ during\ encapsulation} x100$$

$$Encapsulation\ efficiency(\%) = \frac{2.29}{5} x100$$

= 45.8% for TDF-PLGA 50:50

$$Encapsulation\ efficiency(\%) = \frac{2.49}{5} x100$$

= 49.8 for TDF-PLGA 85:15

The total amount of drug in the yield was determined by dissolving 5 mg of the TDF-loaded nanoparticles in 0.5 ml of ethyl acetate (in a 5 ml Eppendorf tube) with vortexing. The ethyl acetate was evaporated, and 3 ml of phosphate buffer solution (PBS) was added to the Eppendorf tube. The tube was vortexed, and the contents centrifuged at a speed of 10000 rpm for 15 minutes. Thereafter, the supernatant was collected, and the absorbance measured using the UV-spectrometer and HPLC-DAD system. The concentration of the drug in that sample was determined by extrapolating the absorbance value from the calibration plot of TDF in Figure 4.8.

The results obtained from using Equation 3.6 are presented in Table 4.8. The nano-formulations prepared with PLGA 85:15 showed about 4% increase in drug encapsulation when compared to those prepared with PLGA 50:50. The significance of this difference was however not calculated. A possible reason for this could be the high ratio of PLA (hydrophilic nature) in the PLGA 85:15 polymer. The encapsulation efficiency suggests that less than half the initial amount of TDF used during the formulation process was recovered after formulation. The amount of TDF lost might be because of un-encapsulated drug discarded during the washing process.

Table 4.8: *Total amount of drug in recovered TDF-loaded nanoparticles and encapsulation efficiency.*

| Drug polymer combination | Amount of drug in nano-formulation (mg) | Encapsulation efficiency (%) |
|---|---|---|
| **TDF-PLGA 50:50** | 2.29 | 45.8 |
| **TDF-PLGA 85:15** | 2.49 | 49.8 |

### 4.3.7 Drug entrapment efficiency

The theoretical drug loading, actual drug loading, and drug entrapment efficiency, were calculated using the following equations

Equation 3.3,

$$Theoretical\ drug\ loading\ (TDL)(\%) = \frac{weight\ of\ drug\ added}{weight\ of\ polymer\ and\ drug\ added}\ x\ 100$$

$$Theoretical\ drug\ loading\ (TDL)(\%) = \frac{5}{105}\ x\ 100$$

= 4.76% for both TDF-PLGA 50:50 and 85:15

Equation 3.4,

$$Actual\ drug\ loading\ (\%) = \frac{weight\ of\ drug\ in\ nanoparticles}{weight\ of\ nanoparticles} x100$$

$$Actual\ drug\ loading\ (\%) = \frac{2.29}{71.2} x100$$

= 3.23% for TDF for PLGA 50:50

$$Actual\ drug\ loading\ (\%) = \frac{2.49}{61} x100$$

= 4.08% for TDF for PLGA 85:15

and Equation 3.5;

$$Drug\ Entrapment\ efficiency(\%) = \frac{actual\ drug\ loading}{theoretical\ drug\ loading} x100$$

$$Drug\ Entrapment\ efficiency(\%) = \frac{3.23}{4.76} x100$$

= 67.86% for TDF-PLGA 50:50

$$Drug\ Entrapment\ efficiency(\%) = \frac{4.08}{4.76} x100$$

= 85.71% for TDF-PLGA 85:15

Table 4.9 presents the results of the calculations. The formulation with PLGA 50:50 had a higher entrapment efficiency of the drug (TDF) than the formulation with PLGA 85:15. The reasons for the difference in entrapment efficiency are yet unknown, our hypothesis is that this might be as a result of differences in the polymer ratios. The significance of this difference was however not calculated.

*Table 4.9: Actual and theoretical drug loading values, and drug entrapment efficiency of TDF-PLGA formulations*

| Drug/polymer combination | Theoretical drug loading (% w/w) | Actual drug loading (% w/w) | Drug entrapment efficiency (% w/w) |
|---|---|---|---|
| **TDF-PLGA 50:50** | 4.76 | 3.23 | 67.86 |
| **TDF-PLGA 85:15** | 4.76 | 4.08 | 85.71 |

### 4.3.8 Fourier Transform Infrared Spectroscopy (FT-IR)

Following drug loading, the nanoparticles were analyzed using FT-IR spectroscopy. Figure 4.9 presents the FT-IR spectra of TDF-PLGA (50:50) and TDF-PLGA (85:15) physical mixtures and loaded nanoparticles. When compared to the FT-IR spectra obtained during analysis of the parent compounds and the physical mixtures, the characteristic intensity bands, that is the peaks obtained with the loaded products mostly corresponded to the polymer (PLGA 50:50 or 85:15) Figure 4.2 a & c. From this, it can be inferred that TDF was encapsulated within the polymer. Comparison of both loaded polymers (loaded formulations of PLGA 50:50 and 85:15) showed the appearance of an extra intensity peak at 2945.29 $cm^{-1}$ (Figure 4.9d) for TDF-PLGA 85:15 loaded nanoparticles, which was not observed with the TDF-PLGA 50:50 loaded nanoparticles (Figure 4.9c) or the physical mixture of TDF-PLGA 85:15. TDF-PLGA

85:15 also presented with the disappearance of a peak at 1674.85 $cm^{-1}$ present in the physical mixture but absent in TDF-PLGA 85:15 loaded nanoparticles, indicating that there is some interaction taking place between the two components . This also further confirmed that TDF was indeed encapsulated within the polymer. Figure 4.10 below shows possible points of interactions between PLGA and TDF.

The differences shown in the FT-IR spectra of both polymers could be due to their ratios, that is, their composition and molecular weight. Comparing TDF-polymer physical mixture to TDF-PLGA loaded nanoparticles, it was noted that the frequency band values for TDF-PLGA loaded nanoparticles had increased; further confirming an interaction (hydrogen bonding) between TDF and PLGA (Table 4.10). This interaction is possibly an encapsulation of TDF within the polymer. It is known that the physicochemical properties of PLGA enable it to entrap drugs for onward delivery to the required site of action[12]. As such, evidence of TDF encapsulation within the polymer may infer a possible improvement in TDF delivery.

*Table 4.10: Selected FTIR data for TDF-PLGA 50:50 and TDF-PLGA 85:15 loaded nanoparticles compared with TDF-PLGA 50:50 physical mixture and TDF-PLGA 85:15 physical mixture.*

| Analyzed sample | Experimental frequency bands ($cm^{-1}$) | Standard frequency bands (cm-1) | Associated functional groups from IR bands |
|---|---|---|---|
| **TDF-PLGA 50:50 loaded** | 2949.09 | 3000 - 2500 | Chelated O-H stretching bridge |
| | 1748.08 | 1790 - 1740 | Strong C=O stretching of the carbonyl group |
| **TDF-PLGA 85:15 loaded** | 2995.67 | 3000 - 2500 | Chelated O-H stretching bridge |
| | 2945.29 | 3000 - 2500 | Chelated O-H stretching bridge |
| | 1748.18 | 1790 - 1740 | Strong C=O stretching of the carbonyl group |
| **TDF-PLGA 50:50 physical mixture** | 2993.81 | 3000 - 2500 | Chelated O-H stretching bridge |
| | 1750.07 | 1790 - 1740 | Strong C=O stretching of the carbonyl group |
| **TDF-PLGA 85:15 physical mixture** | 2985.88 | 3000 - 2500 | Chelated O-H stretching bridge |
| | 1754.32 | 1790 - 1740 | Strong C=O stretching of the carbonyl group |
| | 1674.85 | 1685 - 1665 | Strong C=0 stretching |

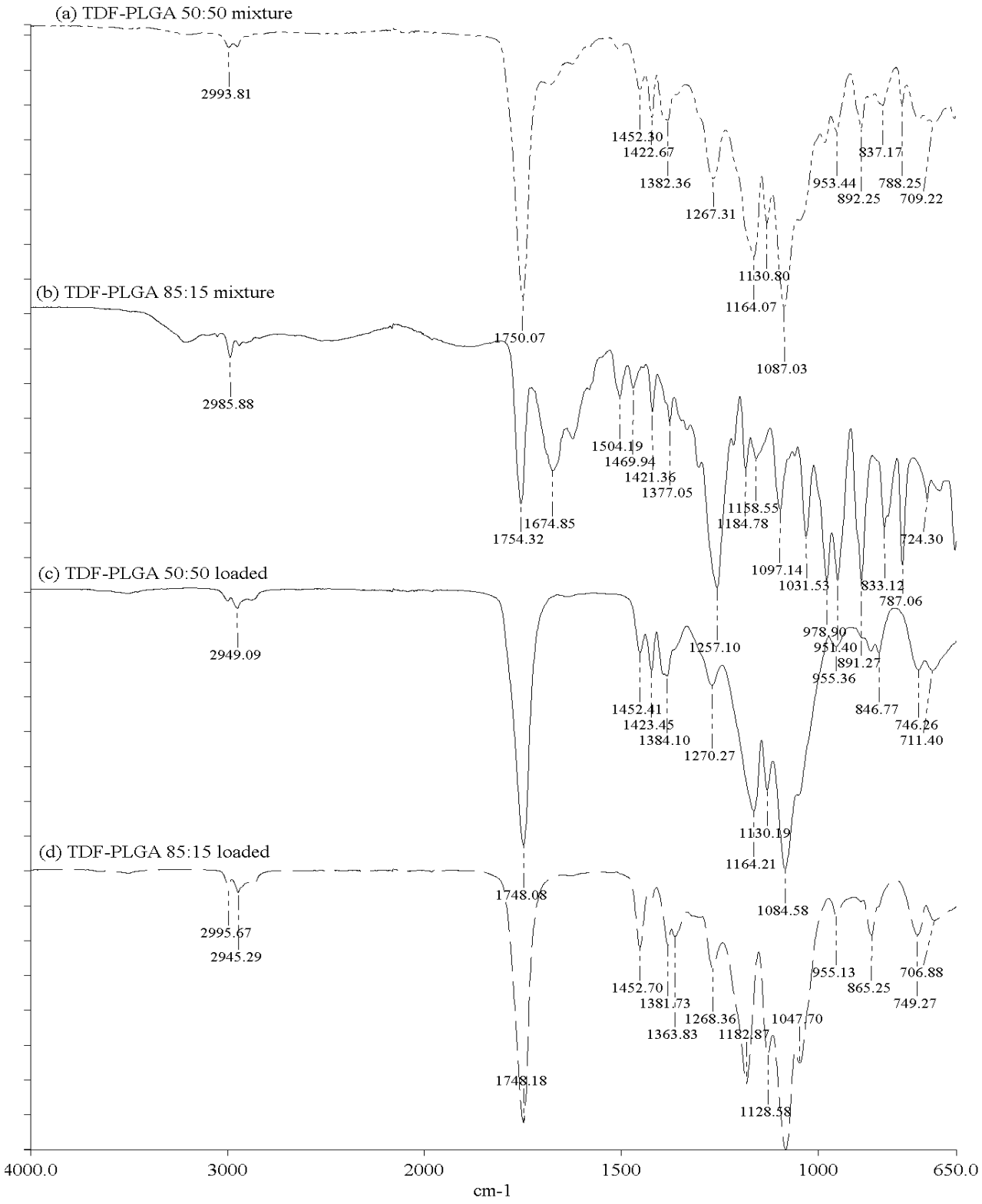


Figure 4.9: FT-IR spectra of (a): TDF-PLGA 50:50 physical mixture, (b): TDF-PLGA 85:15 physical mixture(c): TDF-PLGA 50:50 loaded and (d): TDF-PLGA 85:15 loaded nanoparticles.

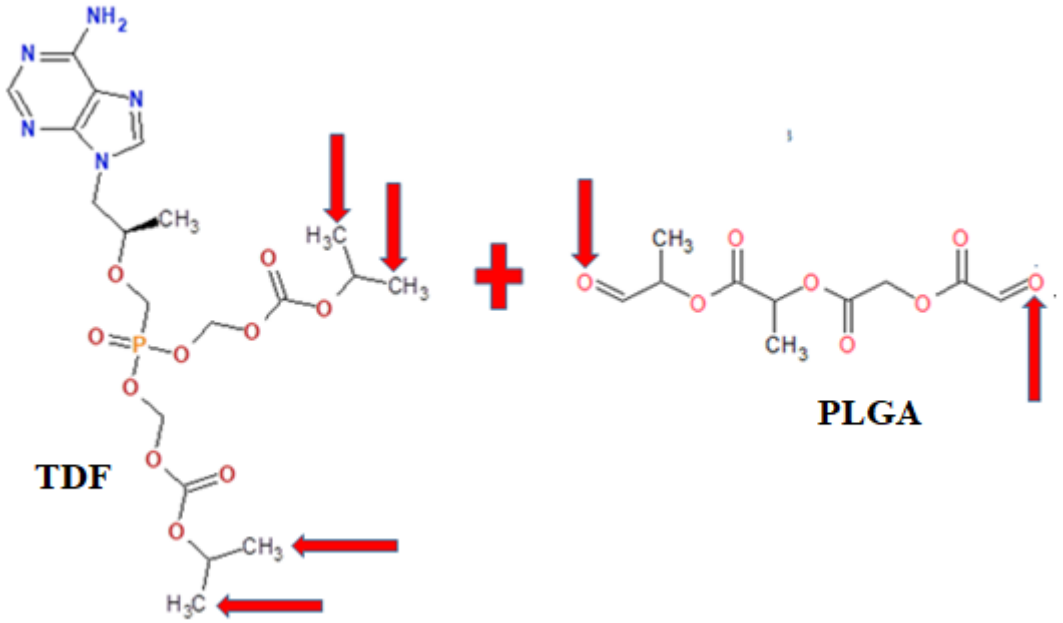


*Figure 4.10: Schematic representation of possible functional group interactions between TDF and PLGA.*

### 4.3.9 Hot Stage Microscopy (HSM)

Following collection of the freeze dried TDF-loaded nanoparticles, the samples were analyzed using HSM. Figure 4.11c shows images from the HSM analysis of TDF-PLGA 50:50 loaded nanoparticles.

Changes to the sample because of an increase in temperature were a bit difficult to visualize between 40°C and 60°C; however noticeable changes such as signs of melting were observed at temperatures above 110°C. No appearance of bubbles or visible degradation of the sample was observed. This could be explained by the rationale that the polymer completely encapsulated TDF and therefore protected it from degradation. It may also be because the amount of TDF in the formulation was too small for the degradation process to be visualized.

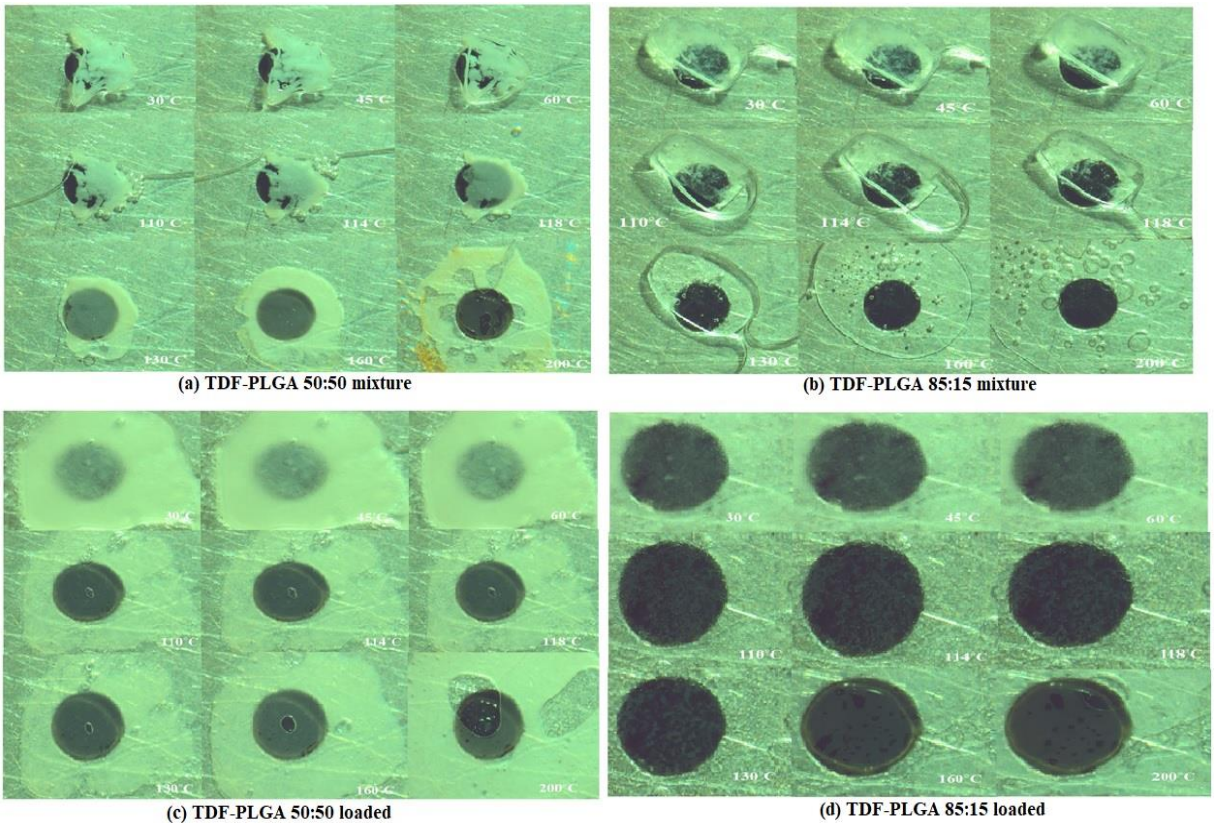


Figure 4.11: *HSM images of TDF-PLGA 50:50 physical mixture, TDF-PLGA 85:15 physical mixture, TDF-PLGA 50:50 loaded, and TDF-PLGA 85:15 loaded nanoparticles.*

Both TDF loaded nanoparticles and physical mixtures showed an increase in thermal stability (Figure 4.11) when compared to the parent compounds. A reference to Figure 4.11c shows that the HSM of TDF-PLGA 50:50 loaded nanoparticles did not show any evidence of being oily or viscous, but rather appeared to dry up at temperatures above 130°C. Figure 4.11d shows images from the HSM of TDF-PLGA 85:15 loaded nanoparticles. Changes to the sample with increase in temperature were a bit difficult to visualize at temperatures between 40°C and 60°C, as was the case with TDF-PLGA 50:50 loaded nanopartilces, with the sample showing signs of melting at temperatures above 110°C. unlike what was observed with Figure 4.11c, the TDF-PLGA 85:15 sample (Figure 4.11d) appeared to be oily and viscous at temperatures above 130°C. This may be because of the difference in polymer ratios used. No appearance of bubbles or visible degradation of the sample was observed on continued heating of

TDF-PLGA 85:15. As with TDF-PLGA 50:50, this could be explained by the rationale that the polymer completely encapsulated TDF and therefore protected it from degradation, or that the amount of TDF in the formulation was too small for the degradation process to be visualized. If the former is the case, then the oral delivery of TDF would likely be improved by its encapsulation within the polymer. **(NB melting point of TDF is in the range 114-118 °C).**

### 4.3.10 Thermogravimetric analysis (TGA)

Thermogravimetric data analysis of TDF-PLGA (50:50 and 85:15) loaded nanoparticles (Figure 4.12) shows the exhibition of two mass loss events. This was different when compared to the single mass loss event exhibited by the TDF-PLGA physical mixtures (Figure 4.4c). The differences in the TGA results between the physical mixture and the nano-formulation could perhaps be a result of change in thermal stability of the nano-formulation.

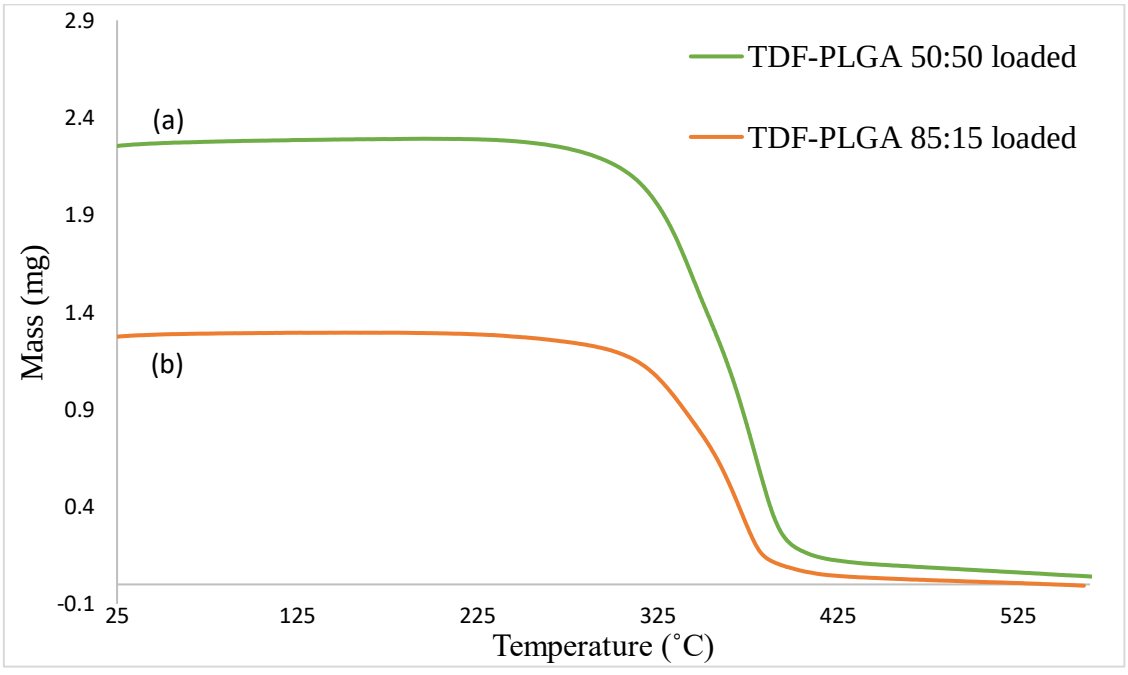


Figure 4.12: *TGA curve of (a) TDF-PLGA 50:50 loaded and (b) TDF-PLGA 85:15 loaded nanoparticles.*

Table C1.5 in the appendix presents data from the thermal analyses of TDF formulated nanoparticles. This shows the temperatures at which sample degradation started, and

when degradation ended. The results indicated that TDF-PLGA 50:50 and TDF-PLGA 85:15 exhibited a total mass loss of about 93 and 91%, with a 7% and 9% inert residue remaining, respectively.

### 4.3.11 Differential Scanning Calorimetry (DSC)

Figure 4.13 below shows thermograms of TDF-PLGA 50:50 and TDF-PLGA 85:15 loaded nanoparticles. No identifiable peaks of TDF could be found in the thermograms. This could indicate that no crystalline TDF was found in the nanoparticles. It may also indicate that TDF was molecularly dispersed in the polymer matrix, or that the amount of TDF present in the analyzed sample was too small to show any significant peaks. The loaded nanoparticles however showed peaks that agreed with TDF-PLGA physical mixtures (mentioned earlier); that is, it showed melting points of about 56.38°C and 58.88°C for TDF-PLGA 85:15 and TDF-PLGA 50:50. It is however not known if these differences in temperature are significant.

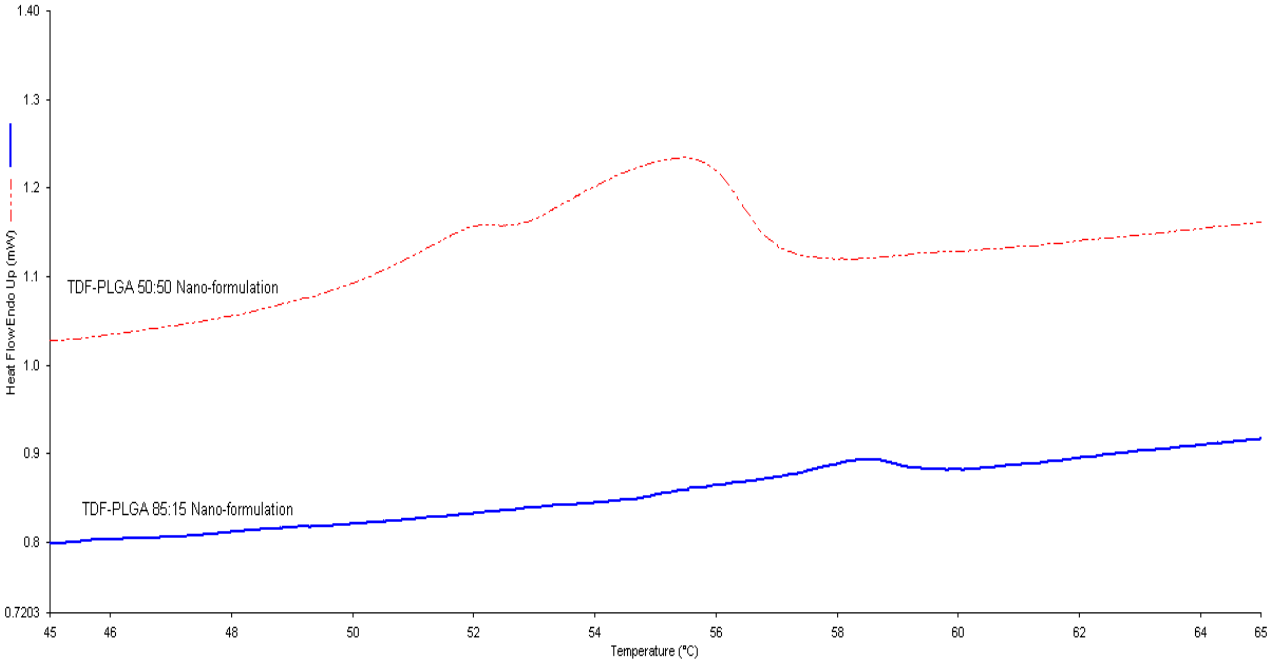


*Figure 4.13: DSC thermograms of TDF-PLGA 50:50 and TDF-PLGA 85:15 loaded nanoparticles*

### 4.3.12 Determination of TDF release from TDF-PLGA loaded nanoparticles

Figure 4.14 shows the cumulative percentage of drug released from TDF-loaded nanoparticles at pH 1.2 and pH 7.4 *versus* time. Samples were analyzed using HPLC-DAD and UV-spectrometry. The release profile displayed by both polymers was biphasic; an initial burst of TDF accompanied by a sustained release profile as is commonly seen in core-shell type nanoparticles[13]. This model also confirmed the presence of surface drug on the nanoparticles with the bulk of the TDF encapsulated within the nanoparticles. If this is the case, some level of extended release can be obtained from the nano-formulation without compromise of immediate release. This ensures that the surface drug can be immediately released and delivered to the site of action immediately. This will be followed by gradual release of TDF from the nano-formulation over time, ensuring extending TDF release.

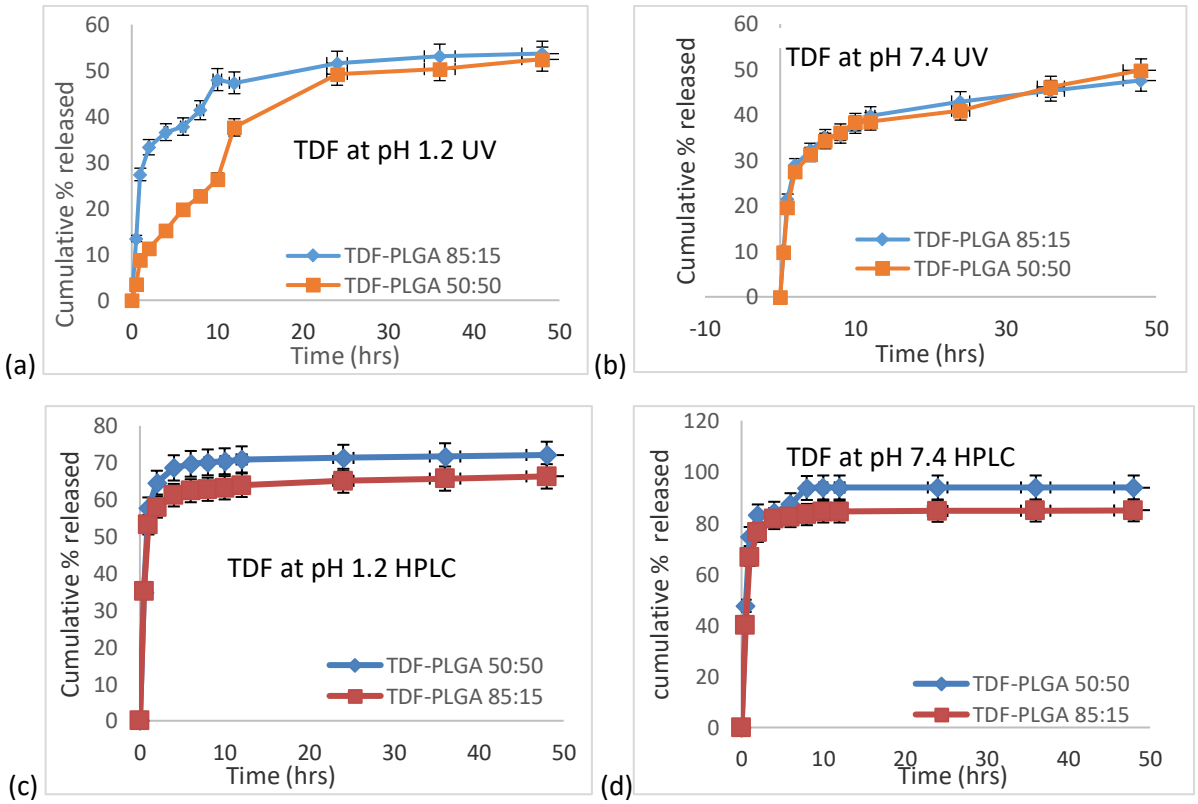

*Figure 4.14:* In-vitro release of TDF-PLGA 50:50 and TDF-PLGA 85:15 loaded nanoparticles

The release was done at pH 1.2 (Figure 4.14a & c) and pH 7.4 (*Figure* 4.14b & d) at 37˚C over a period of 48h, analyzed using UV-spectrometry (*Figure* 4.14a & b) and HPLC-DAD (*Figure* 4.14c & d). Data was collected in triplicates and is here presented as mean ± SD (n=3).

Table 4.11 shows the total percentage of TDF released in 12 hours from the formulations. The same sample was analyzed using two analytical methods (HPLC-DAD and UV-spectrometry). The results from HPLC-DAD analysis, compared to those from UV spectrometry, showed additional release of TDF from the formulations at both pH values. While human error may be a factor, the low values may very likely be due to the lower sensitivity of the UV-spectrometric method.

*Table 4.11: Percentage of TDF released from formulations after 12 hours analysis*

| **Formulation** | **Percentage of TDF released** | | | |
|---|---|---|---|---|
| | **HPLC-DAD** | | **UV-spectrometry** | |
| | pH 1.2 | pH 7.4 | pH 1.2 | pH 7.4 |
| **TDF-PLGA 50:50** | 63.9% | 84.4% | 39.82% | 47.3% |
| **TDF-PLGA 85:15** | 70.9% | 93.7% | 38.62% | 37.64% |

### 4.3.13 Mathematical modeling of drug release data

The mechanism of TDF release from TDF-PLGA formulated nanoparticles was evaluated by fitting the release data to four mathematical models namely; Gompertz model, Korsmeyer-Peppas model, Peppas-Sahlin model, and the Weibull model. DDsolver a peer-reviewed modelling program[14] was used for this analysis, the release data was fitted to the four mathematical models (named above) which are commonly used in literature.[15]

Best fit model was selected using the adjusted coefficient of determination ($R^2$ adj) and a model with the highest $R^2$ adj was deemed to be the best fit model. $R^2$ adj allows for better comparison of the models when compared to coefficient of determination ($R^2$).[14] The release data of TDF obtained at both pH 1.2 and 7.4 was fitted to the four models mentioned above. Of these four models, the Weibull model was adjudged the model of best fit according to the $R^2$ adj value obtained, as illustrated in Table 4.12.

In the Weibull models **α** is a parameter that represents the time scale, **Ti** is the lag time before onset of the dissolution and **β** describes the shape of the curve which can follow either one of the following:

- **β=1** the shape is exponential
- **β>1** the shape is S-shaped (sigmoid) with an upward curvature followed by a turning point.
- **β<1** the shape has a high initial slope followed by a consistent exponential curve.

The Weibull model has four different modifications that generally differ in terms of the absence or presence of the following parameters $\mathbf{F_{max}}$ and **Ti**. **β** according to literature which can be used as an indicator to describe the mechanism of drug release from a polymer matrix.[16]

Data collected from the different models can be seen in Table 4.12, the Weibull model as earlier mentioned was selected as best fit model for the four samples analyzed. The value of **β** was less than 0.75 for all four formulations thereby conforming that the release was Fickian diffusion which was in line with data from literature.[16]

Release mechanism from polymeric systems using Weibull model can be interpreted as follows:

| Time exponent | Release mechanism |
|---|---|
| **β≤0.75** | Fickian diffusion in fractal or Euclidian spaces |
| **0.75<β<1** | Combined release mechanism |
| **β>1** | Complex release mechanism |

Table 4.12: *Parameter values and $R^2$ adj values obtained from fitting drug release experimental data to four mathematical models*

| **pH** | | **1.2** | | **7.4** | |
|---|---|---|---|---|---|
| | **Parameters** | **TDF-PLGA50:50** | **TDF-PLGA85:15** | **TDF-PLGA50:50** | **TDF-PLGA85:15** |
| **Weibull_1** | β | 0.08 | 0.01 | 0.19 | 0.12 |
| | α | 1.01 | 1.19 | 0.63 | 0.75 |
| | Ti | 0.5 | 0.5 | 0.49 | 0.5 |
| | $R^2$adj | 0.993 | 0.998 | 0.994* | 0.991 |
| **Gompertz_1** | α | 0.64 | 0.71 | 0.39 | 0.50 |
| | β | 0.56 | 0.42 | 1.71 | 1.01 |
| | $R^2$adj | 0.931 | 0.951 | 0.983 | 0.952 |
| **Peppas-Sahlin_1** | K1 | 67.24 | 63.24 | 86.5 | 77.78 |
| | K2 | -15.20 | -14.94 | -19.3 | -17.01 |
| | m | 0.27 | 0.24 | 0.27 | 0.28 |
| | $R^2$adj | 0.950 | 0.964 | 0.965 | 0.951 |
| **Korsmeyer-Peppas with Tlag** | n | 0.04 | 0.04 | 0.04 | 0.04 |
| | k | 63.2 | 56.8 | 80.9 | 74.4 |
| | $R^2$adj | 0.992 | 0.997 | 0.989 | 0.988 |

### 4.3.14 Stability of TDF-PLGA loaded nanoparticles

The formulated nanoparticles were stored at temperatures between 2 and 8°C. They were evaluated for stability by measuring parameters such as the zeta potential, particle size and PDI, at the time of preparation and at different time intervals during storage over a period of 90 days.

**Particle size**

After formulation, the average size of the formulated TDF-PLGA 50:50 nanoparticles was measured to be 117.2 ± 2.33 nm while TDF-PLGA 85:15 was measured to be 111.1 ± 0.02 nm. These values increased to 161.2 ± 4.82 nm and 138.3 ± 0.02 nm after washing, then to 2074 ± 63.3 nm and 1824 ± 70.02 nm after freeze drying for TDF-PLGA 50:50 and TDF-PLGA 85:15 respectively, with no significant difference between the means ($p<0.0001$). Subsequently, the size increased steadily to about 4520 ± 93.1 nm and 5598 ± 82.7 nm after 90 days (Figure 4.15).

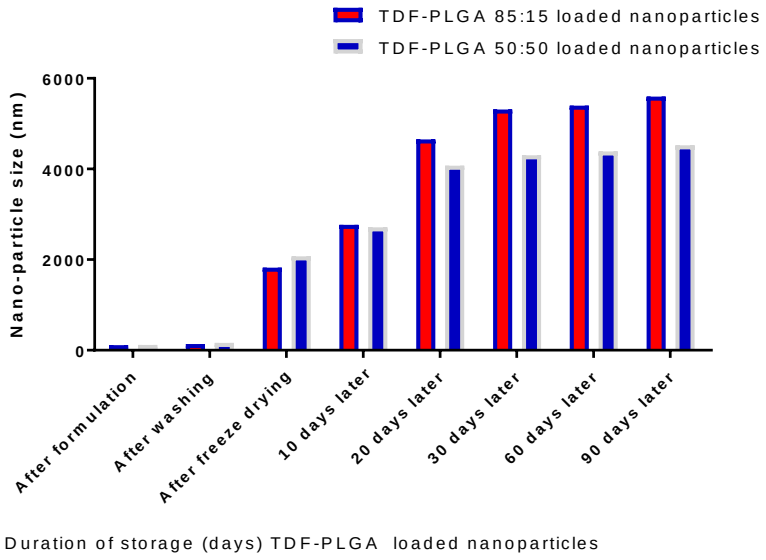


*Figure 4.15: Changes in nanoparticle size of TDF-PLGA 50:50 and 85:15 freeze dried loaded nanoparticles*

Comparing both formulations, the particles sizes of TDF-PLGA 50:50 formulations were less than those of TDF-PLGA 85:15, at every measurement. The two formulations showed the same trend, an increase in particle size that was proportional (perhaps not necessarily directly) to the duration of storage.

The postulated mechanisms to show how particles pass through the gastrointestinal and physiological barriers highlights endocytosis as one of the mechanisms, for particles < 500 nm. It can therefore be seen that the nanoparticle sizes immediately

after formulation and after washing favors uptake *via* endocytosis. Following the freeze-drying and 90-days storage processes however, the increase in particle size as mentioned above was such that endocytosis may not be favorable as an uptake mechanism. There may however be some success with uptake *via* lymphatic passage, with absorption by cells in Peyer's patches, especially for particles less than 5 μm. It can be seen that the nanoparticle size increased after the washing process, possibly due to agglomeration of these particles. We propose that more assessments can be carried out to assess ways to limit such agglomeration in the washing process, perhaps by the use of suitable surface-active agents. Such an intervention may slow / prevent agglomeration, ensuring that particle sizes remain close to the values obtained immediately after formulation. This will enhance penetration through physiological barriers and hence improve bioavailability.

**Zeta potential**

The average zeta potential of the formulated nanoparticles was also assessed and found to be -6.74 ± 0.02 mV and -5.32 ±4.1 mV for TDF-PLGA 50:50 and TDF-PLGA 85:15 respectively (Figure 4.16), the zeta potential values further decreased after washing and freeze drying, indicating an increase in stability. On assessing the samples after 10 days of storage, the zeta potential had increased, indicating a decrease in stability of the nano-formulation with increase in time. However, on day 30, the samples showed some discrepancy indicating an increase in stability. The zeta potential further increased from day 60 through 90 Figure 4.16, indicating a decrease in stability.

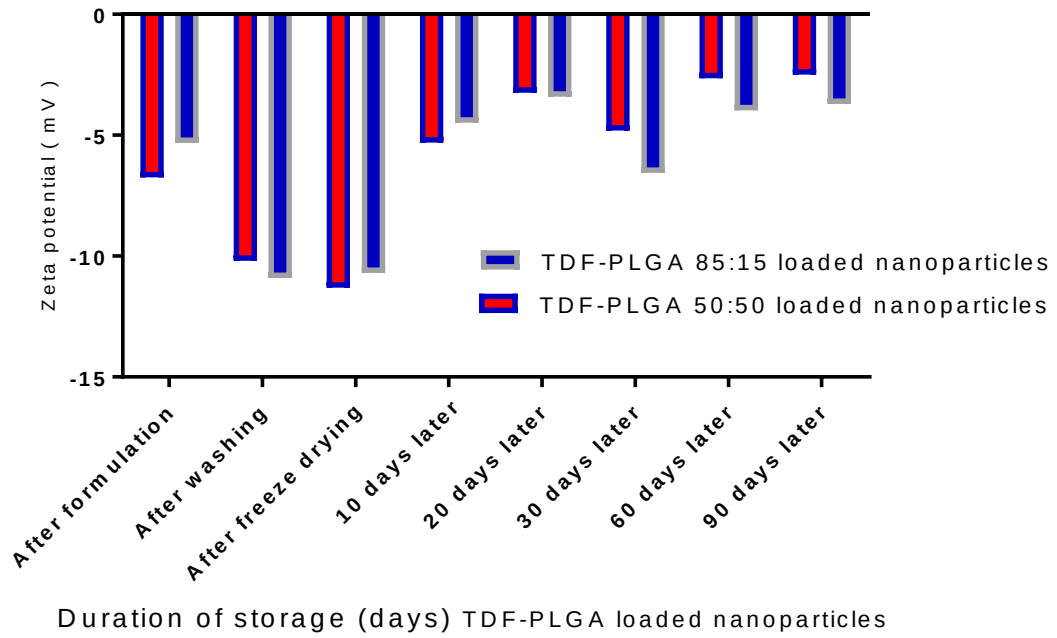


*Figure 4.16: Changes in zeta potential of TDF-PLGA 50:50 and 85:15 freeze dried loaded nanoparticles*

Comparing the stability of both formulations, the data indicated that TDF-PLGA 50:50 seemed more stable than TDF-PLGA 85:15, until day 20 when TDF-PLGA 85:15 seemed to be more stable than TDF-PLGA 50:50 until day 90. It may not be easy to tell at this point, without further studies, if these seeming differences in stability are significant – statistically, pharmaceutically, physiologically or therapeutically.

**Polydispersity index**

The PDI of the formulated nanoparticles were also assessed immediately and the values were 0.149 ± 1.3 and 0.191 ±3.1 for TDF-PLGA 50:50 and TDF-PLGA 85:15 respectively. The PDI value further increased which indicated coalescence of the nanoparticles after washing and freeze drying (Figure 4.17). The PDI value after day 10 of storage showed signs of increased coalescence of the nanoparticles. A steady increase in the PDI values was expected; however, on day 10, 20 and 30, and 90 for both formulations, a decrease in the PDI values was noticed, indicating less coalescence, and an increase was noticed in these values from day 60 to 90 (Figure

4.17). These changes could be due to more samples aggregating during this period of storage.

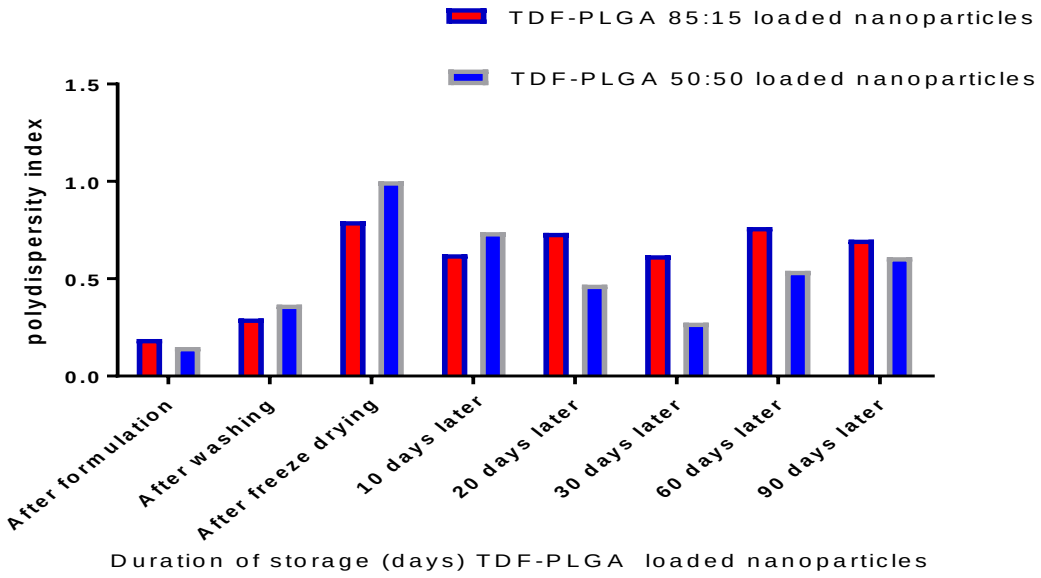


*Figure 4.17: Changes in PDI of TDF-PLGA 50:50 and 85:15 freeze dried loaded nanoparticles*

Comparing both formulations from the data presented, it could be inferred that TDF-PLGA 50:50 was more monodispersed than TDF-PLGA 85:15 after formulation until day 10 when TDF-PLGA 85:15 became more monodispersed. It is our hypothesis that the molecular weight and copolymer ratios may be a factor for these differences.

The overall changes in the nanoparticle size, zeta potential and PDI over the duration of storage were indicative of a decrease in stability of the formulated nanoparticles over time.

Comparing the results obtained from characterizing TDF-loaded nanoparticles with other studies we observed that the encapsulation efficiency was less than that obtained by Shailender *et al.,* 2017 and Destache *et al*., 2016 64% and 52.9%, respectively. However, the particle size range obtained for this study was less than that obtained by the aforementioned studies, with zeta potential higher than that

reported by Shailender *et al.,* 2017 (-4.8 mv) but less than what Destache *et al*., 2016 (-26.7 mv) reported. Shailender *et al.,* 2017 reported a biphasic release profile which was similar to what we obtained with this study. Shailender *et al.,* 2017 also reported that the nanoparticles were stable after 3 months of storage between 2 and 8°C, which was the opposite of what we obtained.

Chapter 5 will follow with the results obtained during formulation and characterization of nanoparticles formulated with AZT, PLGA 50:50 and PLGA 85:15.

## Bibliography

1. Wilkie, C. A., and Morgan, A. B., (2009). 'Thermal and fire performance of polymer nano composites and mechanisms. *In Fire retardancy of polymeric materials*', (2nd ed., pp. 279-285).
2. Gomes, E., Ercole de Carvalho, I., Fialho, S., Barbosa, J., Yoshida, M. and da Silva Cunha Júnior, A., (2017) 'Mixing method influence on compatibility and polymorphism studies by DSC and statistical analysis', *Journal of Thermal Analysis and Calorimetry*, 131(3), pp.2123-2128.
3. Lee, E., Smith, D., Fanwick, P., and Byrn, S., (2010) 'Characterization and Anisotropic Lattice Expansion/Contraction of Polymorphs of Tenofovir Disoproxil Fumarate', Crystal Growth & Design, 10(5), pp.2314-2322.
4. Gomes, E., Mussel, W., Resende, J., Fialho, S., Barbosa, J., Carignani, E., Geppi, M., and Yoshida, M., (2015) 'Characterization of Tenofovir Disoproxil Fumarate and Its Behavior under Heating', Crystal Growth & Design, 15(4), pp.1915-1922.
5. Jani, P.U., Halbert, G.W., Langridge, J., Florence, A.T., (1990) 'Nanoparticle uptake by the rat gastrointestinal mucosa: Quantitation and particle size dependency', *J. Pharm. Pharmacol*, 42(N/A), pp. 821–826.
6. Gref, R., Minamitake, Y., Peracchia, M.T., Trubetskoy, V., Torchilin, V., Langer, R., (1994) 'Biodegradable long-circulating polymeric nanospheres', *Science*, 263 (5153), pp.1600–1603.
7. Bhattacharjee, S., (2016) 'DLS and zeta potential – What they are and what they are not?', Journal of Controlled Release, 235, pp.337-351.

8. Fonte, P., Andrade, F., Azevedo, C., Pinto, J., Seabra, V., Van de Weert, M., Sarmento, B., (2016). 'Effect of the freezing step in the stability and bioactivity of protein-loaded PLGA nanoparticles upon lyophilization', *Pharmaceutical research*, *33*(11), pp. 2777-2793.
9. Cui, L., Liu, Z., Yu, D., Zhang, S., Bligh, S. and Zhao, N. (2014). Electrosprayed core-shell nanoparticles of PVP and shellac for furnishing biphasic controlled release of ferulic acid. *Colloid and Polymer Science*, 292(9), pp.2089-2096.
10. Abdelhay, M., Gazy, A., Shaalan, R., and Ashour, H., (2015). 'Selective RP-HPLC DAD method for determination of tenofovir fumarate and emtricitabine in bulk powder and in tablets', *Acta Chromatographica*, 27(1), pp.41-54.
11. Shabir G. A., (2005). 'Step-by-step analytical methods validation and protocol in the quality system compliance industry', *JVT* 10(N/A), pp. 314-325.
12. Makadia, H. K., and Siegel, S. J., (2011). 'Poly Lactic-co-Glycolic acid (PLGA) as biodegradable controlled drug delivery carrier', *Polymers*, 3(4), pp. 1377–1397.
13. Panyam, J., Labhasetwar, V., (2003). 'Biodegradable nanoparticles for drug and gene delivery to cells and tissue', *Adv Drug Deliv Rev*, 55(N/A), pp.329-347.
14. Zhang, Y., Huo, M., Zhou, J., Zou, A., Li, W., Yao, C. and Xie, S., (2010). 'DDSolver: An Add-In Program for Modeling and Comparison of Drug Dissolution Profiles', *The AAPS Journal*, 12(3), pp.263-271.
15. Maryam, J., Babak, K., 'Mathematical Kinetic Modeling on Isoniazid Release from Dex-HEMA-PNIPAAm Nanogels', *Nanomed research journal,* 1(2), pp.90-96.

16. Papadopoulou, V., Kosmidis, K., Vlachou, M. and Macheras, P., (2006). 'On the use of the Weibull function for the discernment of drug release mechanisms', *International Journal of Pharmaceutics*, 309(1-2), pp.44-50.
17. Pirooznia, N., Hasannia, S., Lotfi, A. and Ghanei, M., (2012). 'Encapsulation of Alpha-1 antitrypsin in PLGA nanoparticles: In Vitro characterization as an effective aerosol formulation in pulmonary diseases', *Journal of Nanobiotechnology*, 10(1), p.20.
18. Shailender, J., Ravi, P., Saha, P., Dalvi, A., and Myneni, S., (2017). 'Tenofovir disoproxil fumarate loaded PLGA nanoparticles for enhanced oral absorption: Effect of experimental variables and in vitro, ex vivo and in vivo evaluation', *Colloids and Surfaces B: Biointerfaces*, 158, pp.610-619.
19. Destache, C., Mandal, S., Yuan, Z., Kang, G., Date, A., Lu, W., Shibata, A., Pham, R., Bruck, P., Rezich, M., Zhou, Y., Vivekanandan, R., Fletcher, C. and Li, Q. (2016). 'Topical Tenofovir Disoproxil Fumarate Nanoparticles Prevent HIV-1 Vaginal Transmission in a Humanized Mouse Model', *Antimicrobial Agents and Chemotherapy*, 60(6), pp.3633-3639.

# CHAPTER 5: RESULTS AND DISCUSSION FOR ZIDOVUDINE LOADED NANOPARTICLES

*This chapter presents the results obtained and discussion following when Zidovudine (AZT) was analyzed. Emphasis is placed on the different ratios of poly-lactic-co-glycolic acid (PLGA 50:50 and 85:15) used in this study.*

## 5.1 Introduction

The objectives of this study were twofold of which the formulation of AZT as a nanoparticle presented the following specific sub-objectives:

- to characterize AZT and PLGA
- to formulate non-covalent complexes of AZT with PLGA of different ratios (50:50 and 85:15);
- to characterize and compare physicochemical properties of the formulated complexes using various analytical techniques;
- to compare the pharmaceutical properties (i.e. particle size, stability and *in-vitro* release) of both formulations (AZT-PLGA 50:50 and AZT-PLGA 85:15) as a means of addressing some of the limitations associated with optimal delivery of AZT (e.g., short plasma half-life and extensive first pass metabolism).

## 5.2 Characterization of AZT and PLGA (50:50 and 85:15)

Prior to formulation of the nanoparticle proper, AZT and two PLGA ratios (PLGA 50:50 and PLGA 85:15) were characterized individually, and in combination as a physical mixture (AZT-PLGA 50:50 and AZT-PLGA 85:15). The results of the characterization assessments were as follows;

### 5.2.1 Fourier-transform infra-red (FT-IR) spectroscopy

Figure 5.1 below shows the structure of AZT and PLGA while Figure 5.2 shows the FT-IR spectra of AZT, PLGA (50:50, and 85:15), and AZT-PLGA (50:50 and 85:15)

physical mixtures. The physical mixtures were prepared in a similar manner as discussed in chapter 4 section 4.2.1. The FTIR spectra of these physical mixtures were compared to those of the single component compounds (AZT, PLGA 50:50 and PLGA 85:15) to identify characteristic functional groups as a physical mixture, as well as the appearance of or disappearance of such functional groups in the combination (Figure 5.2 and Table 5.1).

*Table 5.1: Selected FTIR data for AZT, PLGA (50:50 and 85:15), AZT-PLGA 50:50 physical mixture, and AZT-PLGA 85:15 physical mixture*

| Analyzed sample | Experimental frequency bands ($cm^{-1}$) | Standard frequency bands (cm-1) | Associated functional groups from IR bands |
|---|---|---|---|
| **AZT** | 3458.92 | 3500 - 3300 | Medium N-H stretching bands |
| | 2974.83 | 3200 - 2500 | O-H stretching |
| | 2813.97 | | |
| | 2081.50 | 2160-2120 | Strong N=N=N stretching |
| | 1669.58 | 1685-1666 | Strong C=O stretching |
| **PLGA 50:50** | 2950.52 | 2960 - 2850 | Chelated O-H stretching bridge |
| | 1750.32 | 1800 – 1750 | C=O stretching of the carbonyl group |
| **PLGA 85:15** | 2996.25 | 3000 - 2500 | Chelated O-H stretching bridge |
| | 1746.64 | 1790 - 1740 | Strong C=O stretching of the carbonyl group |
| **AZT-PLGA 50:50 physical mixture** | 3461.12 | 3500 - 3300 | Medium N-H stretching bands |
| | 3023.15 | 3000 - 2500 | Chelated O-H stretching bridge |
| | 2814.57 | 3200 - 2500 | O-H stretching |
| | 2082.39 | 2160-2120 | Strong N=N=N stretching |
| | 1751.54 | 1770 - 1710 | Strong C=O stretching |
| | 1679.98 | 1685-1666 | Strong C=O stretching |
| **AZT-PLGA 85:15 physical mixture** | 3460.60 | 3500 - 3300 | Medium N-H stretching bands |
| | 3023.04 | 3000 - 2500 | Chelated O-H stretching bridge |
| | 2082.15 | 2160-2120 | Strong N=N=N stretching |
| | 1750.91 | 1770 - 1710 | Strong C=O stretching |
| | 1677.09 | 1685-1666 | Strong C=O stretching |

FT-IR spectra of pure PLGA 50:50 and PLGA 85:15 was the same as discussed in chapter 4 Figure 4.2 b & c. AZT on the other hand shared characteristic peaks similar to TDF (Figure 4.2a). Similarities such as N-H, and O-H groups at 3458.92 $cm^{-1}$ and

2974.83 $cm^{-1}$ stretching vibrations respectively, however AZT also presented with differences such as lack of the C=C (1752.31 $cm^{-1}$) found in TDF and the presence of $N_3$ group present at 2081.50 $cm^{-1}$ in AZT but absent in TDF. These unique stretching areas were expected given the respective structures below.

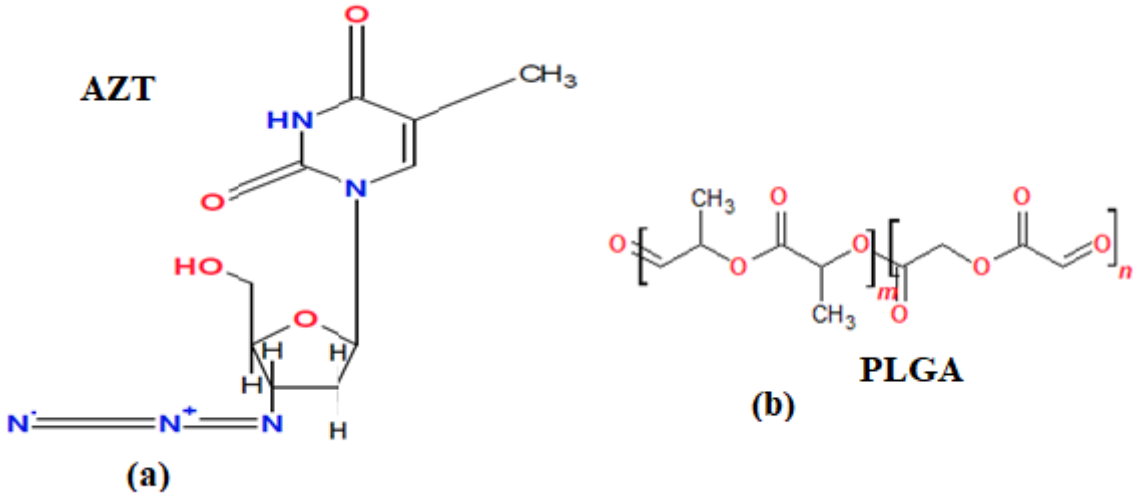


*Figure 5.1: Structure of (a) AZT and (b ) PLGA (**n** represents the number of lactic acid units while **m** represents the number of glycolic acid units)*

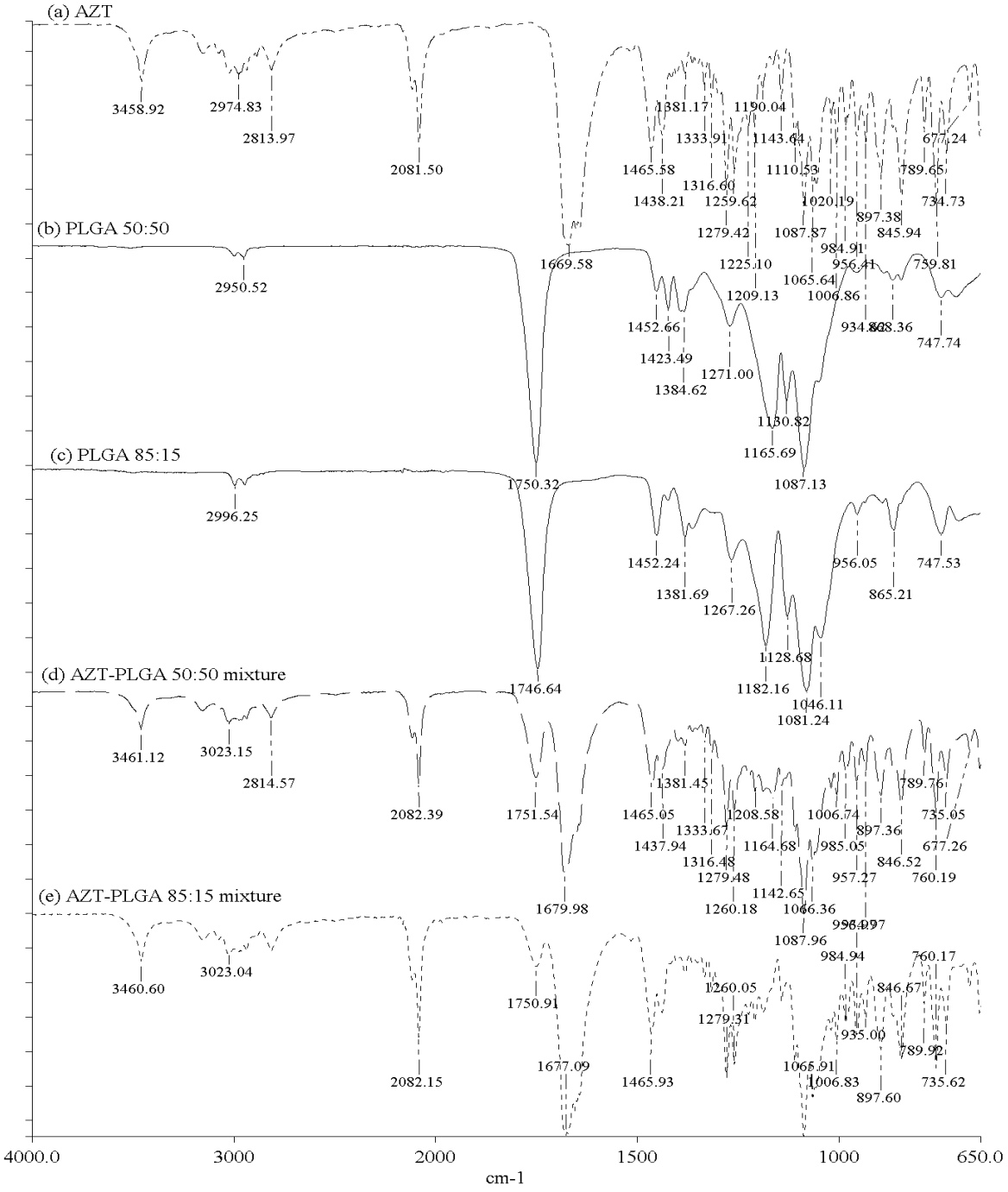


*Figure 5.2:* FT-IR spectra of (a) AZT, (b) PLGA 50:50, (c) PLGA 85:15, (d) AZT-PLGA 50:50 physical mixture, (e) AZT-PLGA 85:15 physical mixture

When compared to the FT-IR spectrum of either AZT or the polymer alone, the physical mixture of AZT-PLGA 50:50 and AZT-PLGA 85:15 (Figure 5.2(d) and (e), respectively) showed slight shifts in the bands of the resulting physical mixture as well as indicated some physiochemical interaction in the spectrum. AZT-PLGA 50:50

showed bands at 3461.12 $cm^{-1}$, attributed to OH stretching; at 3023.15 $cm^{-1}$ which were attributed to C-H stretching vibration; at 2814.57 $cm^{-1}$ which was attributed to strong $CH_3$ stretching vibration; at 2082.39 $cm^{-1}$, attributed to $N_3$ asymmetric stretching vibration; as well as at 1751.54 $cm^{-1}$ and 1679.98 $cm^{-1}$ which were attributed to C=O stretching vibrations. In Figure 5.2(e), AZT-PLGA 85:15 showed bands at 3460.60 $cm^{-1}$ attributed to OH stretching; at 3023.04 $cm^{-1}$ attributed to C-H stretching vibration; at 2082.15 $cm^{-1}$ attributed to $N_3$ asymmetric stretching vibration; and at 1750.91 $cm^{-1}$ and 1677.09 $cm^{-1}$ attributed to C=O stretching vibrations. AZT-PLGA 85:15 also presented with the disappearance of the O-H stretching vibration (2813.97 $cm^{-1}$) which is present in the AZT-PLGA 50:50 physical mixture these may be because of the differences in PLGA ratios. No new peaks were observed, but the intensity of certain characteristic peaks such as 2950.52 $cm^{-1}$ and 2996.25 $cm^{-1}$ increased while those at 1750.32 $cm^{-1}$ and 1746.64 $cm^{-1}$ decreased in the physical mixture for PLGA 50:50 and PLGA 85:15 respectively when compared to the parent compound further confirming an interaction taking place.

Overall, both physical mixtures showed slight shifts and disappearance of characteristic peaks when compared to the parent compounds, thus indicating an interaction between AZT and PLGA.

### 5.2.2 Hot stage microscopy

The results presented below were obtained during sample analysis using hot stage microscopy (HSM). The compounds were analyzed individually as AZT, PLGA 50:50, PLGA 85:15, and in combination that is as a physical mixture of the polymer with AZT (mixed by grinding). The samples were heated up to a maximum temperature of 200°C at a temperature increase rate of 10°C per min.

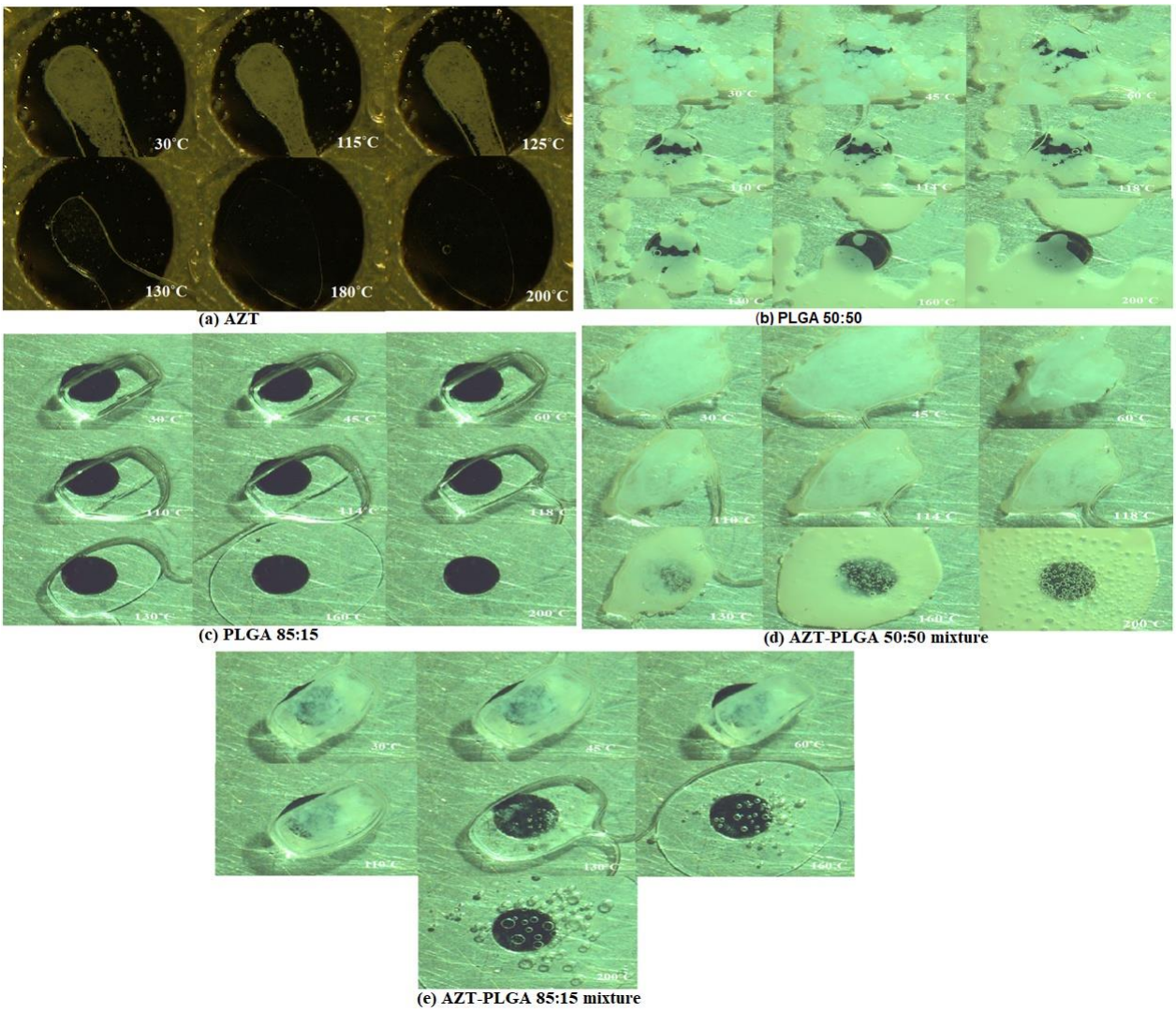


Figure 5.3: *HSM of (a)AZT, (b)PLGA 50:50, (c)PLGA 85:15, (d)AZT-PLGA 50:50 physical mixture, (e)AZT-PLGA 85:15 physical mixture*

Figure 5.3(a) shows images taken during HSM analysis of AZT. The melting of AZT commenced at 120°C and continued up till 125°C. No bubbles were observed during this process, indicating that no moisture was contained in the sample. At 130°C, the sample had completely melted. The degradation of AZT, observed by discoloration of the sample, started at about 180°C. The results obtained from this analysis were in line with the certificate of analysis which indicated that the melting point of AZT is between 120°C and 127°C. Figure 5.3b & c are HSM images of PLGA 50:50 and PLGA 85:15, which have been discussed in chapter 4, section 4.2.2.

Figure 5.3d shows HSM images of the copolymer and AZT physical mixture (AZT-PLGA 50:50). Melting commenced at about 30°C, with the appearance of bubbles observed at about 110°C. The appearance of bubbles was an indication of moisture being trapped under the slide covering the sample. Unlike the case with TDF-PLGA 50:50 physical mixture (Figure 4.3 d), the bubbles did not disappear, however; as noticed with TDF-PLGA 50:50 physical mixture, sign of degradation such as browning of the sample was noticed at a temperature of about 160°C.

Figure 5.3e shows images from HSM analysis of AZT and the polymer (AZT-PLGA 85:15 physical mixture). As with AZT-PLGA 50:50 physical mixture, melting commenced at about 30°C, with the appearance of bubbles, noticed at about 120°C. This temperature is around the melting point of AZT, thus confirming the presence of AZT in the physical mixture. The appearance of the bubble was an indication of moisture being trapped under the slide covering the sample. The bubbles did not disappear on continued heating but rather increased in size. Degradation, such as browning of the sample appeared at about 160°C. Since the initial polymer did not show any sign of degradation under HSM analysis (Figure 5.3c) whereas AZT degraded (Figure 5.3a), such degradation in AZT-PLGA 85:15 physical mixture could further infer the presence of AZT in the sample.

### 5.2.3 Thermogravimetric analysis (TGA)

Changes in thermal stability, organic solvent evolution and the degradation form of AZT, PLGA 50:50, PLGA 85:15, and a combination of both polymers with AZT (mixed by grinding) was evaluated using TGA. Figure 5.4 shows the curves obtained when the samples were analyzed. There was release of volatile species, and weight loss due to moisture was observed.

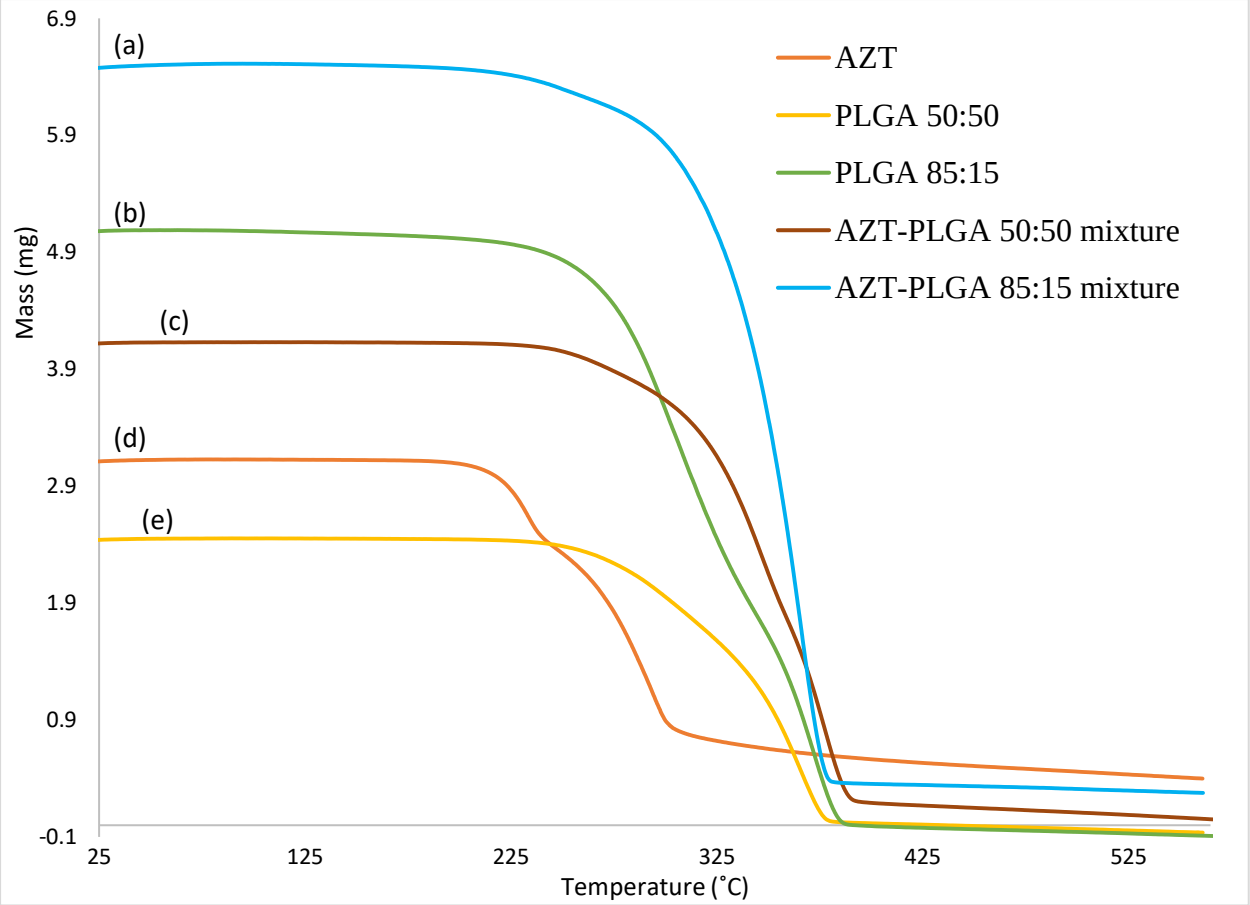


Figure 5.4*: TGA curves of (a) AZT-PLGA 85:15 physical mixture, (b) PLGA 85:15, (c) AZT-PLGA 50:50 physical mixture, (d) AZT, (e) PLGA 50:50*

Both polymers (PLGA 50:50 and PLGA 85:15) showed two mass loss events associated with the degradation process [Figure 5.4 (b) and (e)]. The first mass losses for PLGA 50:50 and PLGA 85:15 were about 30% and 65%, respectively. The second mass loss peak showed values of about 68% and 35% for PLGA 50:50 and PLGA 85:15, respectively. Unlike PLGA 85:15, PLGA 50:50 did not exhibit a 100% mass loss event; it had about 2% inert residue.

The drug-polymer physical mixtures (AZT-PLGA 50:50 and AZT-PLGA 85:15) were also analyzed via TGA [Figure 5.4 (a) and (c)]. The physical mixture with PLGA 50:50 showed two mass loss events while the physical mixture with PLGA 85:15 which showed a single mass loss event. The individual components (polymer and AZT)

showed two mass loss events. These differences in the TGA results between the individual components and the resulting physical mixture could be a result of differences in the polymer ratios and molecular weights (Appendix C, Table C1.8). The percentage weight loss for AZT-PLGA 50:50 and AZT-PLGA 85:15 were about 94% and 97%, respectively. The $T_{onset}$ values however were at a lower temperature when compared to that of either polymer or AZT alone.

### 5.2.4 Differential Scanning Calorimetry (DSC)

Figure 5.5a presents the thermogram of AZT; the peak indicated that the melting point of AZT was about 124.80°C which was in accordance with the melting point of AZT in literature.[1] The thermograms for PLGA 50:50 and 85:15 Figure 4.5a are discussed in chapter 4 section 4.2.4.

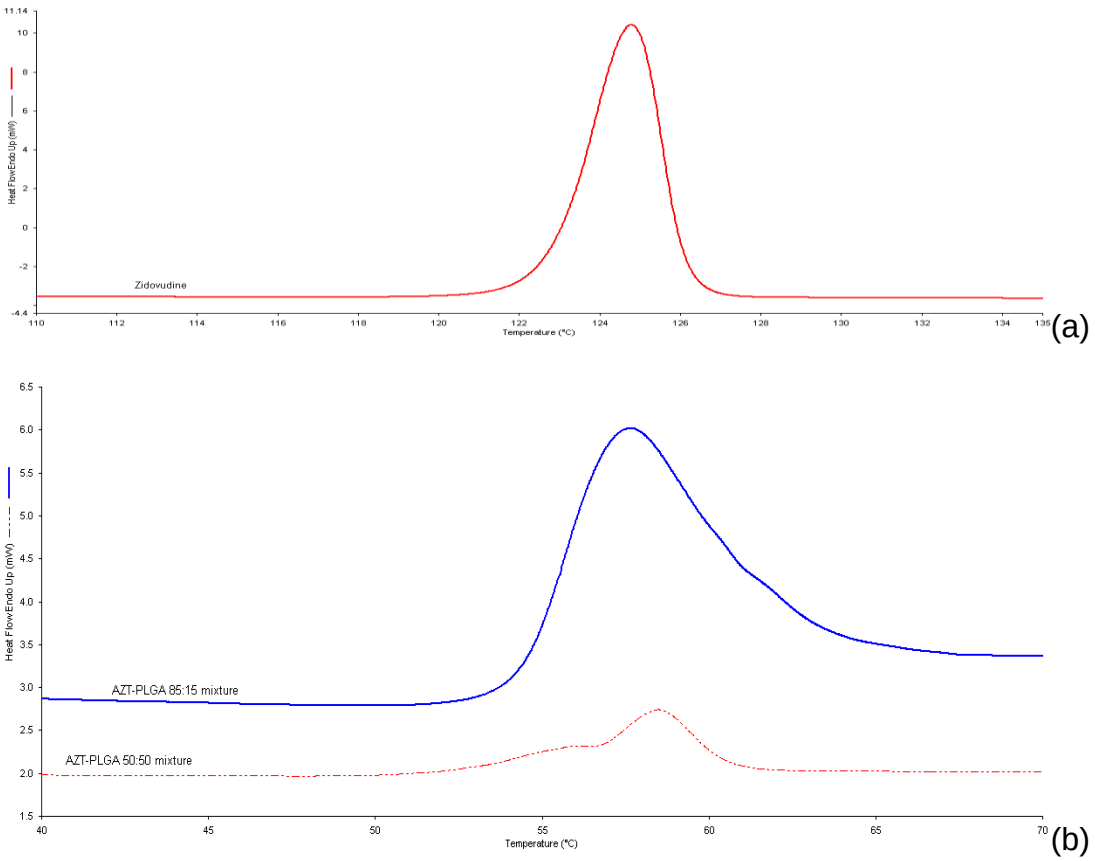


*Figure 5.5: DSC Thermograms of Zidovudine, AZT-PLGA 50:50 and AZT-PLGA 85:15 physical mixtures*

Figure 5.5b above presents thermograms of AZT when it was mixed and ground separately with PLGA 50:50 and PLGA 85:15. The thermograms indicated both physical mixtures had single peaks which indicated the melting point started from 57.48°C to 58.51°C for physical mixtures of AZT-PLGA 50:50 and AZT-PLGA 85:15 respectively. Comparing the physical mixture to PLGA alone (Figure 4.5), the plot indicated that the presence of AZT increased the stability of PLGA; however, a peak indicating the presence of AZT could not be seen. The lack of an AZT peak may perhaps be because too little of the AZT was used.

## 5.3 Formulation and characterization of AZT loaded nanoparticles

Figure 5.6 below shows diagrammatically each step in the formulation of AZT-loaded nanoparticles, formulation was done using the water-in-oil-in-water double emulsion solvent evaporation and diffusion method by Liu *et al*., 2010 with modifications to decrease nanoparticle size and increase encapsulation efficiency.

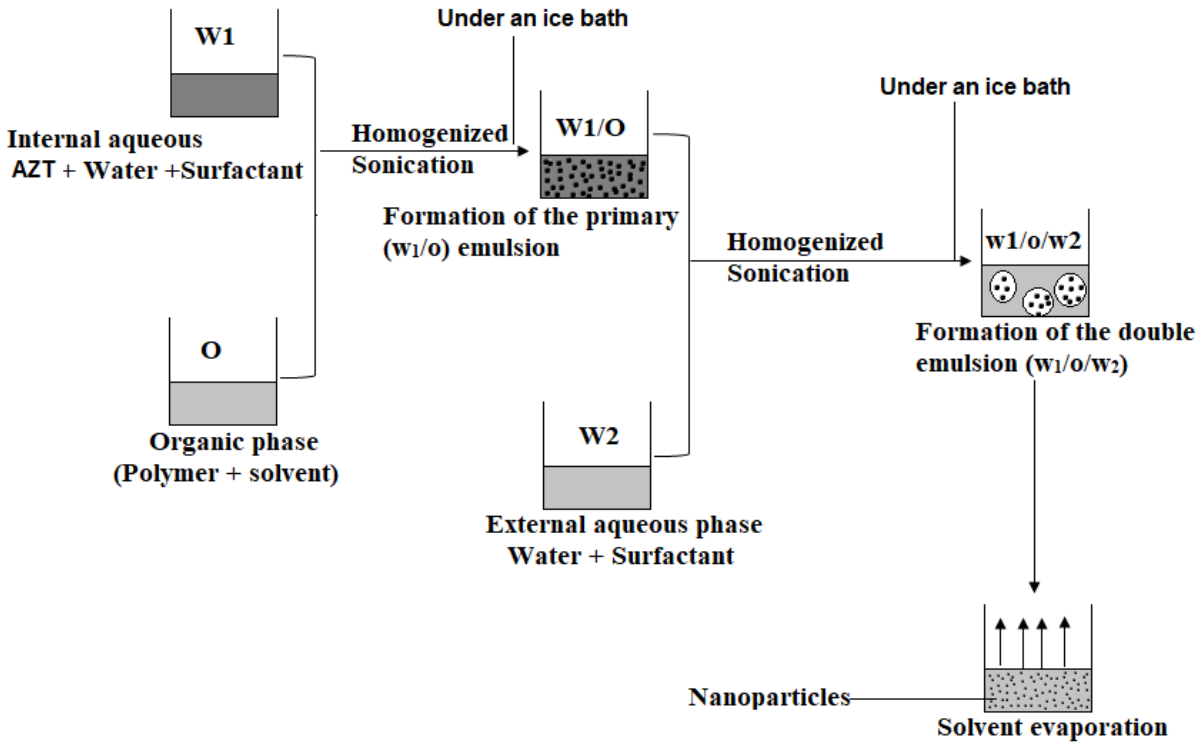


*Figure 5.6: Schematic presentation of AZT-loaded nanoparticle formulation process*

### 5.3.1 Particle size and distribution (polydispersity index, PDI)

The particle sizes of AZT-PLGA (50:50 and 85:15) loaded nanoparticles were measured, immediately after formulation and evaporation of the organic solvents from the sample, using dynamic light scattering (Malvern system). The mean particle sizes for AZT-PLGA 50:50 and AZT-PLGA 85:15 were found to be 110.6 ± 0.42 nm and 112.0 ± 2.43 nm, respectively (Table 5.2).

Table 5.2: *Particle size of AZT-loaded nanoparticles.*

| **Formulated nanoparticles** | **Particle size (nm)** | |
|---|---|---|
| | **Before wash** | **After wash** |
| **AZT-PLGA 50:50** | 110.6 ± 0.42 | 154.3 ± 3.1 |
| **AZT-PLGA 85:15** | 112.0 ± 2.43 | 160.4 ± 1.7 |

The postulated mechanisms to show how particles pass through the gastrointestinal and physiological barriers highlights endocytosis as one of the mechanisms, for particles < 500 nm. The particle sizes of the nanoparticles increased after they were washed three times with distilled water. The average size for AZT-PLGA 50:50 and AZT-PLGA 85:15 nanoparticles after washing was found to be 154.3 ± 3.1 nm and 160.4 ± 1.7 nm respectively (Table 5.2). The increase in particle size could be a result of the particle aggregation after surfactants and emulsifiers had been removed by the washing process. Particles size of formulated nanoparticles plays an important role in drug pharmacokinetics. The smaller the particle sizes of the drug / formulation, the higher the rate of particle absorption from the intestine into the blood stream.[1,2] A high uptake of particles can be expected because of the relatively small sizes of the nanoparticles formulated.

The polydispersity index (PDI) values for AZT-PLGA 50:50 and AZT-PLGA 85:15 after formulation were found to be an average of 0.165 ± 0.004 and 0.152 ± 0.015,

respectively. These values increased to 0.418 ± 0.004 and 0.376 ±0.17 for AZT-PLGA 50:50 and AZT-PLGA 85:15, respectively, after the washing process (Table 5.3).

*Table 5.3: Polydispersity index of AZT-loaded nanoparticles.*

| Formulated nanoparticles | Polydispersity index | |
|---|---|---|
| | Before wash | After wash |
| **AZT-PLGA 50:50** | 0.165 ± 0.004 | 0.418 ± 0.004 |
| **AZT-PLGA 85:15** | 0.152 ± 0.015 | 0.376 ± 0.17 |

The PDI values are indicative of a largely homogenous distribution of the nanoparticles.[3] Values of PDI closer to one (1) indicate a heterogeneous distribution of nanoparticles while values closer to zero (0) indicate a homogenous distribution of nanoparticles[4] The increase in PDI value could be as a result of formulated pellets fusing together after removal (washing off) of the surfactants and emulsifiers, hence making the distribution more heterogeneous when compared to the characteristic prior to the washing process.

### 5.3.2 Evaluation of surface morphology of the nanoparticle

The morphology (shape and properties) of the nanoparticles was determined using a high-resolution scanning electron microscopy (HR-SEM). Figure 5.7 shows images of blank nanoparticles of PLGA 50:50 and PLGA 85:15, AZT-PLGA 85:15 and AZT-PLGA 50:50 loaded nanoparticles. [Figure 5.7 (a) and (b)] are blank HR-SEM images of blank nanoparticles of PLGA 50:50 and PLGA 85:15, respectively; the images showed the particles were spherical in shape with smooth surfaces.

Figure 5.7(c) shows HR-SEM images of AZT-PLGA 85:15 loaded nanoparticles. From the image, it was observed that the particles were spherical in shape with smooth surfaces, with an average particle size above 200 nm (which was greater than the maximum size observed with the zeta sizer (160 nm). The increase in size might be a result of aggregation and coalescence of the small nanoparticles. Such aggregating

and coalescing behavior may be a consequence of the freeze-drying process, which may cause the nanoparticles to irreversibly fuse, hence increasing the particle size. Freezing of the samples can also cause mechanical stress on the nanoparticles leading to a change in particle morphology. As earlier mentioned, (Section 4.3.2), aggregation of formulated nanoparticles may be minimized (Pirooznia *et al*., 2012).

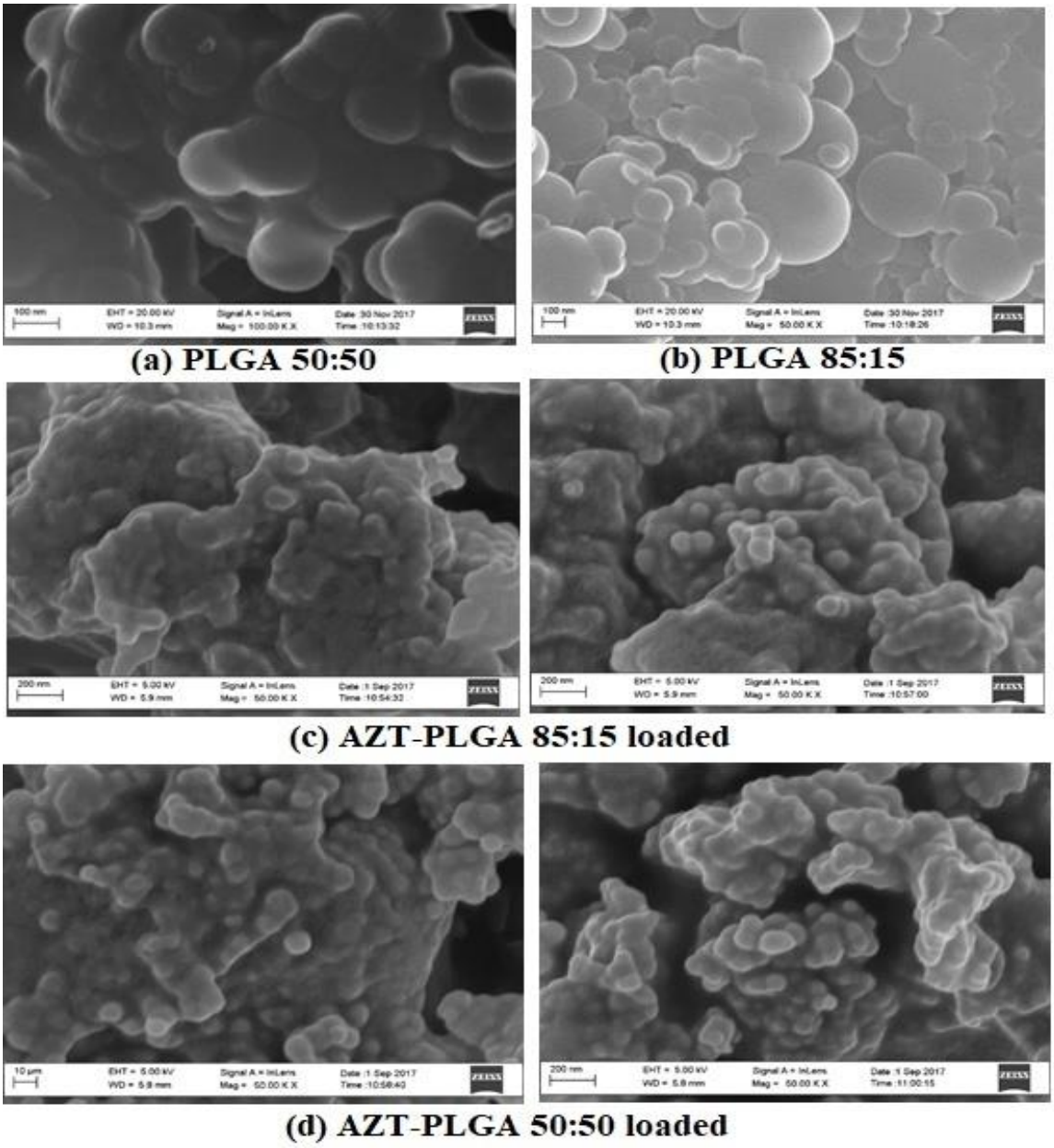


Figure 5.7: *HR-SEM of formulated nanoparticles (a) Blank PLGA 50:50, (b) Blank PLGA 85:15, (c) AZT-PLGA 85:15 loaded, and (d) AZT-PLGA loaded nanoparticles*

Figure 5.7d shows images of AZT-PLGA 50:50 loaded nanoparticles taken with HR-SEM. Similar characteristics to those of AZT-PLGA 85:15 (Figure 5.7c) were observed; the nanoparticle surface was smooth and spherical, with signs of aggregation and coalescence.

When Figure 5.7 (a) and (b) were compared to Figure *5.7*c and Figure 5.7d, the latter appeared to be less smooth and more coagulated; this might be as a result of the presence of AZT in the formulation.

### 5.3.3 Zeta potential

The zeta potential after formulation of the AZT-PLGA 50:50 and AZT-PLGA 85:15 loaded nanoparticles (Table 5.4) was determined using the Malvern system. The mean zeta potential for AZT-PLGA 50:50 and AZT-PLGA 85:15 were found to be -4.82 ± 0.62 mV and -5.41 ± 0.02 mV, respectively. These values had decreased to -15.3 ± 0.5 mV and -12.2 ± 0.6 mV, respectively, after washing of the samples, an indication that the stability of the nanoparticles had increased. The negative charge on the nanoparticles directly affects the cellular uptake of the nanoparticles by inducing a positive charge on the cell membrane, resulting in attraction between the two surfaces. This may result in higher bioavailability of AZT, as the drug-loaded nanoparticles may be better able to permeate the cell membrane and be transported to endosomes found within the cell.[6]

Table 5.4: *Zeta potential of AZT-loaded nanoparticles.*

| **Drug Polymer ratio** | **Zeta potential** | |
|---|---|---|
| | **Before wash** | **After wash** |
| **AZT-PLGA 50: 50** | -4.82 ± 0.62 mV | -15.3 ± 0.5 mV |
| **AZT-PLGA 85: 15** | -5.41 ± 0.02 mV | -12.2 ± 0.6 mV |

### 5.3.4 Percentage yield

After freeze drying, the AZT-PLGA 50:50 and AZT-PLGA 85:15 loaded nanoparticles were recovered and weighed. The values obtained after weighing were 83.1 mg and 67.02 mg, respectively (Table 5.5). The percentage yield, calculated as detailed in Equation 3.2,

$$Percentage\ yield(\%) = \frac{mass\ of\ nanoparticles\ recovered}{mass\ of\ PLGA, drug\ and\ excipients\ used\ in\ formulation} x100$$

$$Percentage\ yield(\%) = \frac{83.1}{105\ mg} x100$$

= 79.14% for AZT-PLGA 50:50

$$Percentage\ yield(\%) = \frac{67.02}{105\ mg} x100$$

= 63.83% for AZT-PLGA 85:15

The percentage yield was calculated to be 79.14% and 63.83%, respectively. The unbound polymer and drug could have been washed out and discarded during the washing process, resulting in the observed mass loss.

Table 5.5: *Mass of AZT-loaded nanoparticles recovered (mg) and percentage yield.*

| Drug polymer combination | Mass of AZT used in formulation (mg) | Mass of polymer used (mg) | Mass of nanoparticle recovered (mg) | Percentage yield (%) |
|---|---|---|---|---|
| **AZT-PLGA 50:50** | 5 | 100 | 83.1 | 79.14 |
| **AZT-PLGA 85:15** | 5 | 100 | 67.02 | 63.83 |

### 5.3.5 Standard calibration plot for determination of AZT (HPLC-DAD and UV-spectrometry method)

The linearity of the methods was determined by analyzing the samples at an absorbance frequency of 266 nm, at which AZT had been proven to have its maximum absorbance.[7] A linear regression model was used to study the relationship between

absorbance of AZT and its concentration, and a graph of mean AZT absorbance *versus* AZT concentration was plotted (Figure 5.8). This model enabled the prediction of AZT concentration in the prepared nano-formulations by measuring its absorbance in the sample; data obtained is featured in appendix C (Table C1.6 and Table C1.7)

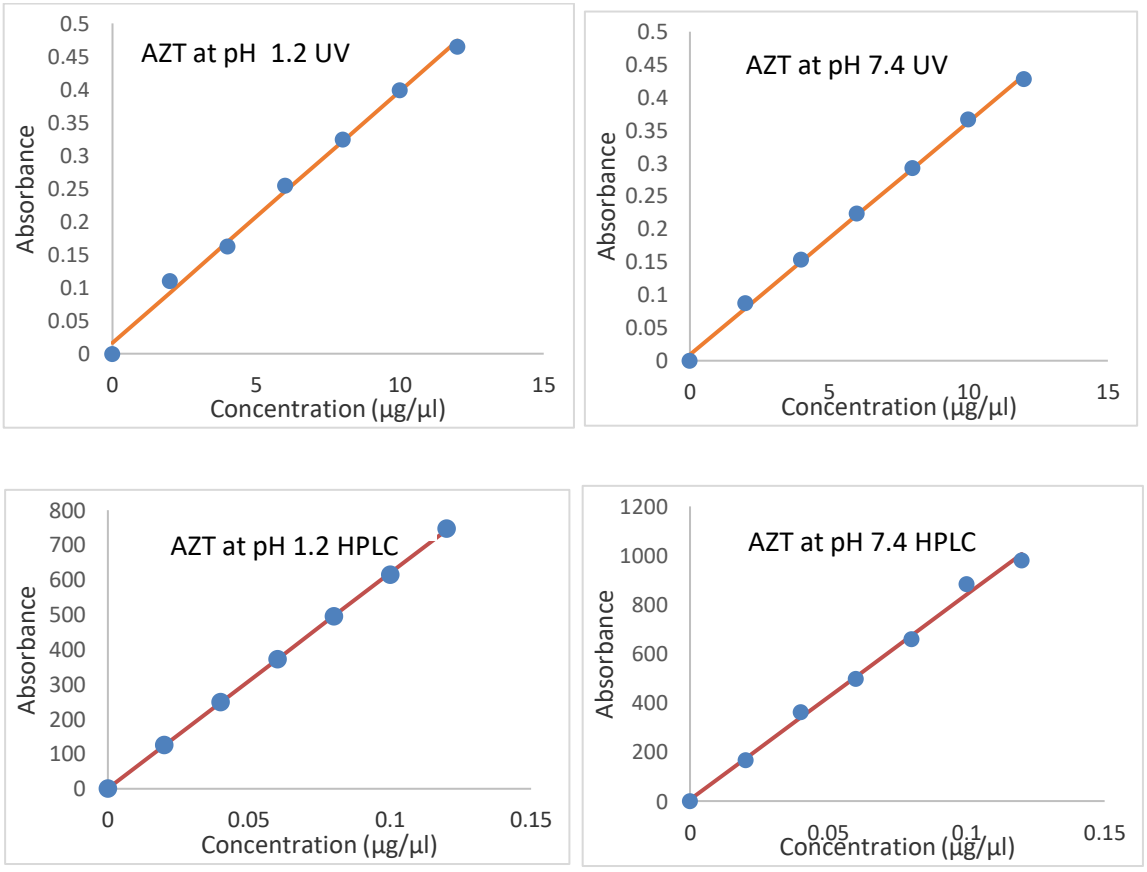


*Figure 5.8: Standard calibration graph of Zidovudine ($\lambda_{max}$=266nm).*

Stock solutions and working standards were prepared in PBS at a pH of 1.2 and pH 7.4. Samples were analyzed at 25ºC. Data values were recorded in triplicate and are presented as mean ± SD (n=3).

Table 5.6 presents computed data derived from plotting the calibration curves for AZT. The $R^2$ values at pH 1.2 and pH 7.4 depicted linearity and showed how close the data was to the fitted regression line. The relationship between concentration and absorbance can be expressed using Equation 5.1 with substitutions from Table 5.6

the amount of drug encapsulated within the nanoparticles was determined. Data obtained is featured in appendix C (Table C1.6 and Table C1.7).

$$y = intercept + slope(x)$$

*Equation 5.1*

*Where y* = AZT peak area

*x = the standard solution concentration in µg/ml*

*Table 5.6: Linearity data and quantification limits of AZT at pH 7.4 and 1.2 (HPLC-DAD and UV-spectrometry methods).*

| **Validation parameters** | **HPLC-DAD** | | **UV-spectrometry** | |
|---|---|---|---|---|
| | pH 1.2 | pH 7.4 | pH 1.2 | pH 7.4 |
| $R^2$ | 0.9999 | 0.9979 | 0.9951 | 0.9986 |
| Slope ± SD | 6181.304±27.59 | 8334.304±241.78 | 0.0381±0.0012 | 0.0654±0.00058 |
| Intercept ± SD | 0.8246±1.99 | 6.1803±17.44 | 0.0164±0.0086 | 0.00921±0.0042 |
| Concentration range (µg/ml) | 0.02-0.12 | 0.02-0.12 | 200-1200 | 200-1200 |
| LOD (µg/ml) | 0.001 | 0.007 | 0.75 | 0.40 |
| LOQ (µg/ml) | 0.001 | 0.021 | 2.26 | 1.19 |

Unlike what was obtained with the calibration plot for TDF, HPLC-DAD did not necessarily present better linearity values than analyses done with UV-spectrometry. The values obtained at pH 7.4 were also not necessarily better than those obtained at pH 1.2. It seems the HPLC-DAD method was more precise than the UV-spectrometry method at pH 1.2, while the UV-spectrometry method was more precise than the HPLC-DAD method at pH 7.4. However, the concentration ranges, as well as the LOD and LOQ values are lower for the HPLC-DAD method than for the UV-spectrometry

method (as was obtained with TDF analyses), attesting to the increased sensitivity of the HPLC-DAD compared to the UV-spectrometry method.

Repeatability, precision and accuracy of the methods (HPLC-DAD and UV-spectrometry methods) were assessed by analyzing replicates of AZT standard solution over a period of three days. Three different concentrations (0.02,0.06, 0.12 and 2, 6 and 12 µg/ µl ) covering the standard calibration range of AZT were selected and analyzed to determine the inter-day and intra-day variability as shown in Table 5.7 and Table 5.8. The intermediate precision and precision of the method at both pH 1.2 and 7.4 were expressed as % RSD and found to be less than 2% for both HPLC-DAD and UV-spectrometry which suggested that the above methods were reproducible.

*Table 5.7: Intra-day and inter-day assay precision and accuracy for Zidovudine at pH 1.2 and 7.4 (HPLC-DAD method)*

| | **pH 1.2** | | | **pH 7.4** | | |
|---|---|---|---|---|---|---|
| **AZT (µg/ µl)** | 0.02 | 0.06 | 0.12 | 0.02 | 0.06 | 0.12 |
| | | | **Intra-day (n=3)** | | | |
| | | | **Day 1** | | | |
| **Mean** | 0.0203 | 0.0599 | 0.1207 | 0.0192 | 0.0591 | 0.1167 |
| **SD** | 0.0002 | 0.0010 | 0.0012 | 0.0001 | 0.0008 | 0.0020 |
| **Precision[1] (%)** | 0.99 | 1.67 | 0.99 | 0.52 | 1.40 | 1.70 |
| **Accuracy[2] (%)** | 101.5 | 99.8 | 100.58 | 96 | 98.5 | 97.25 |
| | | | **Day 2** | | | |
| **Mean** | 0.0204 | 0.0600 | 0.1205 | 0.0193 | 0.0591 | 0.1167 |
| **SD** | 0.0004 | 0.0010 | 0.0020 | 0.00012 | 0.0008 | 0.0005 |
| **Precision[1] (%)** | 1.96 | 1.67 | 1.66 | 0.62 | 1.35 | 0.43 |
| **Accuracy[2] (%)** | 102.00 | 100.00 | 100.4 | 96.5 | 98.5 | 97.3 |
| | | | **Day 3** | | | |
| **Mean** | 0.0201 | 0.0597 | 0.1207 | 0.0190 | 0.0588 | 0.1166 |
| **SD** | 0.0001 | 0.0009 | 0.0018 | 0.0002 | 0.0003 | 0.0007 |
| **Precision[1] (%)** | 0.50 | 1.51 | 1.49 | 1.05 | 0.50 | 0.60 |
| **Accuracy[2] (%)** | 100.5 | 99.5 | 100.6 | 95 | 98 | 97.2 |
| | | | **Inter-day (n=9)** | | | |
| **Mean[3]** | 0.0203 | 0.0599 | 0.1206 | 0.0192 | 0.059 | 0.1167 |
| **SD** | 0.00012 | 0.00012 | 0.000094 | 0.00012 | 0.00014 | 0.000047 |
| **Precision[1] (%)** | 0.59 | 0.20 | 0.08 | 0.63 | 0.24 | 0.04 |
| **Accuracy[2] (%)** | 101.5 | 99.83 | 100.5 | 96 | 98.33 | 97.25 |

The results for accuracy (expressed as percentage of the mean determined concentration / nominal concentration) fell within the range, 95-102%. The acceptable mean recovery range in assays for quality control and drug registration is between 90

and 110%.[7] Thus, the accuracy and validity of the HPLC-DAD and UV-spectrometry method for AZT analyses was proven.

*Table 5.8: Intra-day and inter-day assay precision and accuracy for Zidovudine at pH 1.2 and 7.4 (UV-spectrometry method).*

| | **pH 1.2** | | | **pH 7.4** | | |
|---|---|---|---|---|---|---|
| **AZT (µg/ µl)** | 2 | 6 | 12 | 2 | 6 | 12 |
| | | | **Intra-day (n=3)** | | | |
| | | | **Day 1** | | | |
| **Mean** | 0.0920 | 0.2547 | 0.4644 | 0.0820 | 0.2303 | 0.4630 |
| **SD** | 0.0007 | 0.0001 | 0.0007 | 0.0001 | 0.0001 | 0.0002 |
| **Precision[1] (%)** | 0.76 | 0.04 | 0.15 | 0.14 | 0.04 | 0.05 |
| **Accuracy[2] (%)** | 99.12 | 104.1 | 97.9 | 102.8 | 104.1 | 106.8 |
| | | | **Day 2** | | | |
| **Mean** | 0.0923 | 0.2546 | 0.4656 | 0.0779 | 0.2185 | 0.44697 |
| **SD** | 0.0018 | 0.0002 | 0.0002 | 0.0002 | 0.0002 | 0.0003 |
| **Precision[1] (%)** | 1.95 | 0.08 | 0.04 | 0.26 | 0.10 | 0.07 |
| **Accuracy[2] (%)** | 99.52 | 104.1 | 98.16 | 97.0 | 98.5 | 103.1 |
| | | | **Day 3** | | | |
| **Mean** | 0.0924 | 0.2543 | 0.4637 | 0.0804 | 0.2193 | 0.4391 |
| **SD** | 0.0015 | 0.0003 | 0.0029 | 0.000006 | 0.0001 | 0.00064 |
| **Precision[1] (%)** | 1.62 | 0.12 | 0.63 | 0.07 | 0.05 | 0.15 |
| **Accuracy[2] (%)** | 99.65 | 104.0 | 97.75 | 100.6 | 99.0 | 103.1 |
| | | | **Inter-day (n=9)** | | | |
| **Mean[3]** | 0.0922 | 0.2545 | 0.4646 | 0.080121 | 0.22271 | 0.449701 |
| **SD** | 0.0002 | 0.0002 | 0.0010 | 0.002083 | 0.006584 | 0.012198 |
| **Precision[1] (%)** | 0.22 | 0.08 | 0.22 | 2.60 | 2.96 | 2.71 |
| **Accuracy[2] (%)** | 99.39 | 104.06 | 97.94 | 100.2 | 100.5 | 103.7 |

The values in Table 5.7 and Table 5.8 was calculated as follows;

- [1]Expressed as % RSD = (SD/mean) × 100.

- [2]Calculated as (mean determined concentration/nominal concentration) × 100.
- [3]n = 3 days with three replicates per day

### 5.3.6 Encapsulation efficiency

The encapsulation efficiency was determined using Equation 3.6,

$$Encapsulation\ efficiency(\%) = \frac{total\ amount\ of\ drug\ in\ the\ yield}{amount\ of\ drug\ added\ during\ encapsulation} x100$$

$$Encapsulation\ efficiency(\%) = \frac{3.69}{5} x100$$

= 73.82% for AZT-PLGA 50:50

$$Encapsulation\ efficiency(\%) = \frac{2.38}{5} x100$$

= 47.6% for AZT-PLGA 85:15

Table 5.9 below presents the encapsulation efficiency and the total amount of drug in the yield. This was determined by dissolving 5 mg of the AZT-loaded nanoparticles in 0.5 ml of ethyl acetate (in a 5 ml Eppendorf tube) with vortexing. The ethyl acetate was evaporated, and 3 ml of phosphate buffer solution (PBS) was added to the Eppendorf tube. The tube was vortexed, and the contents centrifuged at a speed of 10000 rpm for 15 minutes. Thereafter, the supernatant was collected, and the absorbance measured using the UV-spectrometer and HPLC-DAD system. The concentration of the drug in that sample was determined by extrapolating the absorbance value from the calibration plot of AZT in Figure 5.8.

Table 5.9: *Total amount of AZT in recovered nanoparticles and encapsulation efficiency*

| Drug polymer combination | Amount of drug in nano-formulation (mg) | Encapsulation efficiency (%) |
|---|---|---|
| **AZT-PLGA 50:50** | 3.69 | 73.82 |
| **AZT-PLGA 85:15** | 2.38 | 47.6 |

the above results indicated that formulation with PLGA 50:50 showed about 26.22% increase in encapsulation efficiency of AZT when compared to formulation with PLGA 85:15. Possible reasons for this could be the differences in the molecular weights and polymer ratios of PLGA 50:50 and PLGA 85:15. The encapsulation efficiency of AZT-PLGA 85:15 suggested that less than half the initial amount of AZT used during the formulation process was recovered after formulation. The amount of AZT lost might be because of un-encapsulated drug discarded during the washing process.

### 5.3.7 Drug entrapment efficiency

The theoretical, actual loading and drug entrapment efficiency were calculated using the following equations;

Equation 3.3,

$$Theoretical\ drug\ loading\ (TDL)(\%) = \frac{weight\ of\ drug\ added}{weight\ of\ polymer\ and\ drug\ added}\ x\ 100$$

$$Theoretical\ drug\ loading\ (TDL)(\%) = \frac{5}{105}\ x\ 100$$

= 4.76% for both AZT-PLGA 50:50 and 85:15

Equation 3.4

$$Actual\ drug\ loading\ (\%) = \frac{weight\ of\ drug\ in\ nanoparticles}{weight\ of\ nanoparticles} x100$$

$$Actual\ drug\ loading\ (\%) = \frac{3.69}{83.1} x100$$

= 4.44% for AZT for PLGA 50:50

$$Actual\ drug\ loading\ (\%) = \frac{weight\ of\ drug\ in\ nanoparticles}{weight\ of\ nanoparticles} x100$$

$$Actual\ drug\ loading\ (\%) = \frac{2.38}{67.02} x100$$

= 3.57% for AZT-PLGA 85:15

and Equation 3.5,

$$Drug\ Entrapment\ efficiency(\%) = \frac{actual\ drug\ loading}{theoretical\ drug\ loading} x100$$

$$Drug\ Entrapment\ efficiency(\%) = \frac{4.44}{4.76} x100$$

= 93.23% for AZT-PLGA 50:50

$$Drug\ Entrapment\ efficiency(\%) = \frac{3.57}{4.76} x100$$

= 75% for AZT-PLGA 85:15

Table 5.10 below presents data derived from the above calculations. The formulation with PLGA 50:50 showed higher encapsulation of the drug compared to the formulation with PLGA 85:15. The reasons for the difference in entrapment efficiency are yet unknown, our hypothesis (similar to that with the TDF formulations) is that this might be as a result of differences in the polymer ratios. The significance of this difference was however not calculated.

Table 5.10: *Actual and theoretical drug loading values, and drug entrapment efficiency of TDF-PLGA formulations.*

| Drug polymer combination | Theoretical drug loading (% w/w) | Actual drug loading (% w/w) | Drug entrapment efficiency (% w/w) |
|---|---|---|---|
| **AZT-PLGA 50:50** | 4.76 | 4.44 | 93.23 |
| **AZT-PLGA 85:15** | 4.76 | 3.57 | 75 |

### 5.3.8 Fourier Transform Infrared Spectroscopy (FT-IR)

Figure 5.9 (c) and (d) present data from the FT-IR analysis of AZT-PLGA 50:50 and AZT-PLGA 85:15 loaded nanoparticles, respectively. The different intensity peaks showed that AZT was encapsulated within the polymer because, when compared to the FT-IR data obtained prior to formulation (Figure 5.9a and b), the characteristic intensity bands mostly corresponded to the polymer. The loaded AZT-PLGA 50:50 and AZT-PLGA 85:15 nanoparticles (Figure 5.9c & d) produced significantly less pronounced spectra. In the FT-IR spectra of the nano-formulation several peaks once

again shifted (compared to the parent compound), disappeared and even new peaks appeared (comparatively to the physical mixtures). What this suggests is a clear indication of a more pronounced interaction between AZT and the polymers as well as that the polymer is indeed loaded with AZT.

Figure 5.9d showed the appearance of an extra intensity peak at 2995.93 $cm^{-1}$. This peak was not present in Figure 5.9c and may be because of differences in the polymers used. The loaded nanoparticles also indicated the disappearance of certain peaks such as at 3461.12 $cm^{-1}$ and 3460.60 $cm^{-1}$ (N-H stretching vibration), 2814.57 $cm^{-1}$ (O-H stretching) as well as 1751.54 $cm^{-1}$ and 1750.91 $cm^{-1}$ (C=O stretching) for AZT-PLGA 50:50 and AZT-PLGA 85:15 respectively. Figure 5.10 indicates the possible functional groups that may interact between AZT and PLGA based on the FTIR analysis obtained below.

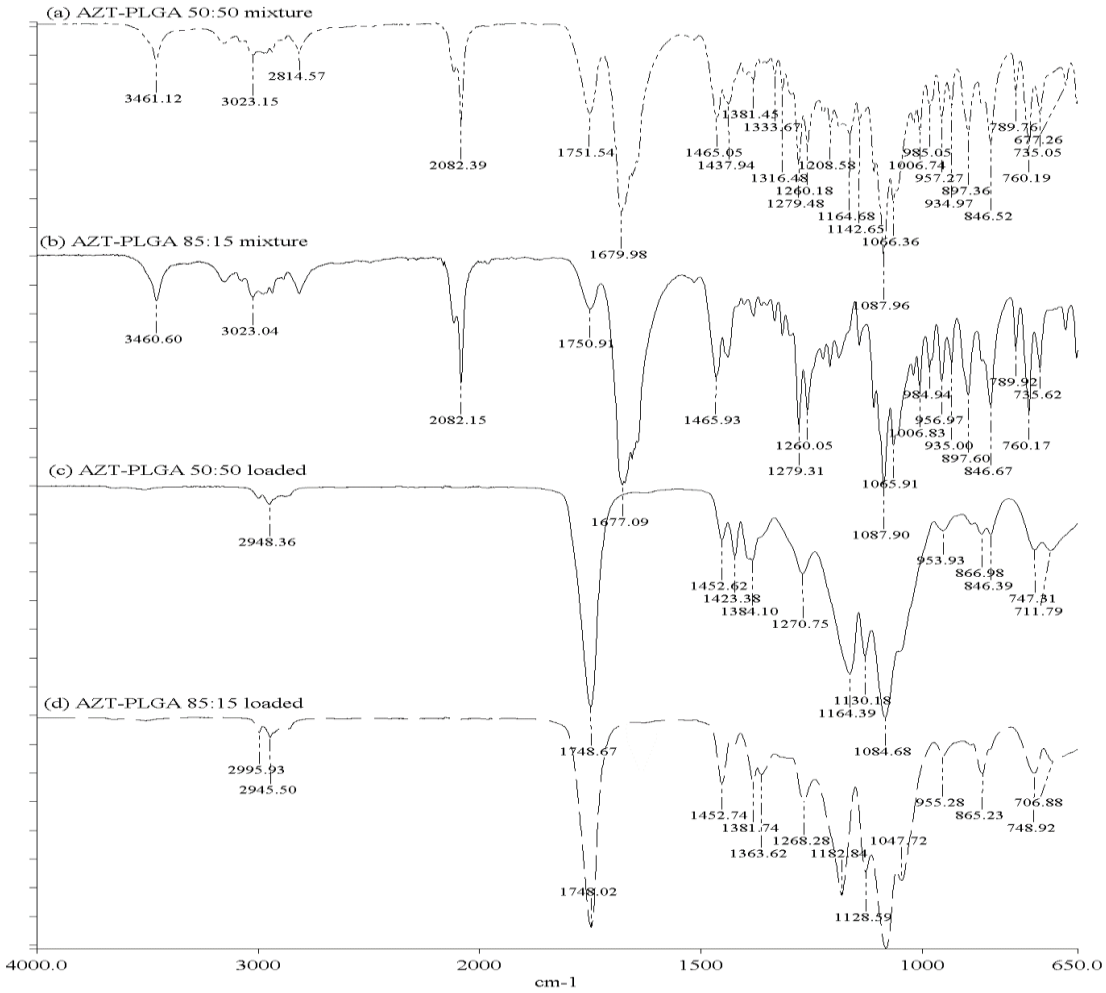


Figure 5.9**:** *FT-IR spectra of (a) AZT-PLGA 50:50 physical mixture, (b) AZT-PLGA 85:15 physical mixture, (c) AZT-PLGA 50:50 loaded, and (d) AZT-PLGA 85:15 loaded nanoparticles*

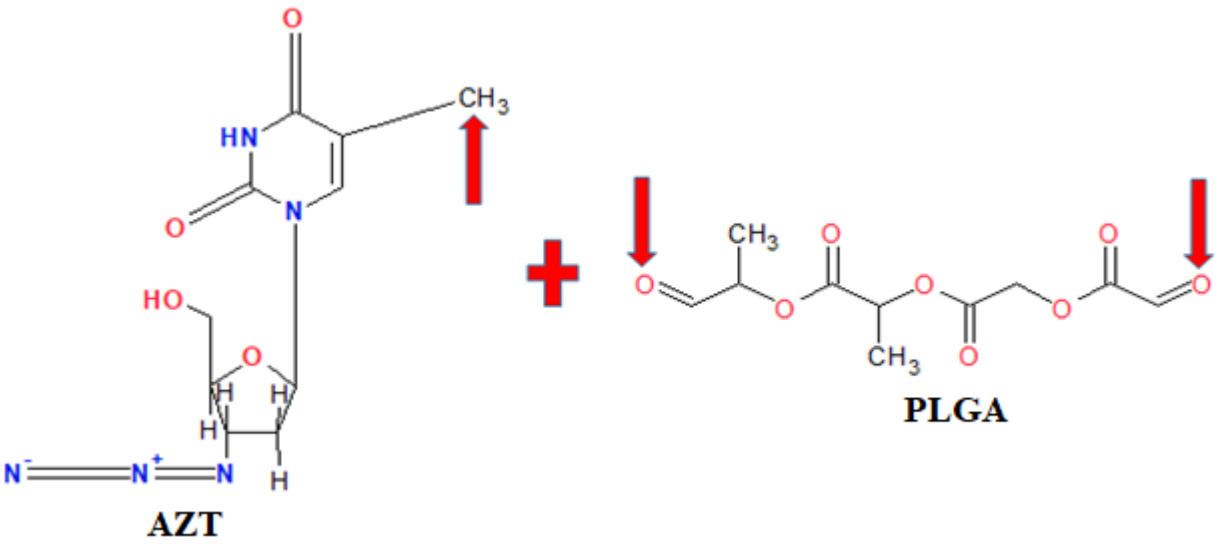


Figure 5.10: *Schematic representation of possible functional group interactions between AZT and PLGA*

### 5.3.9 Hot stage microscopy

Following collection of the freeze-dried AZT-loaded nanoparticles, the samples were analyzed using HSM. Figure 5.11a & b (AZT-PLGA 50:50 and AZT-PLGA 85:15 physical mixtures) are as discussed in section 5.2.2 (Figure 5.3 d and e), respectively. Figure 5.11c shows images from the HSM analysis of AZT-PLGA 50:50 loaded nanoparticles. Melting of the sample with increase in temperature was noticeable around 45°C; however, sample melting was challenging to visualize. At 110°C, clear change such as melting of the sample was observed. There was no appearance of bubbles or visible degradation of the sample; this may be explained by the inference that the polymer completely encapsulated AZT and therefore protected it from degradation. It could also be because the amount of AZT in the formulation was too small for the degradation process to be visualized. At temperatures above 130°C, the sample appeared oily and viscous with no further changes observed with increase in temperature.

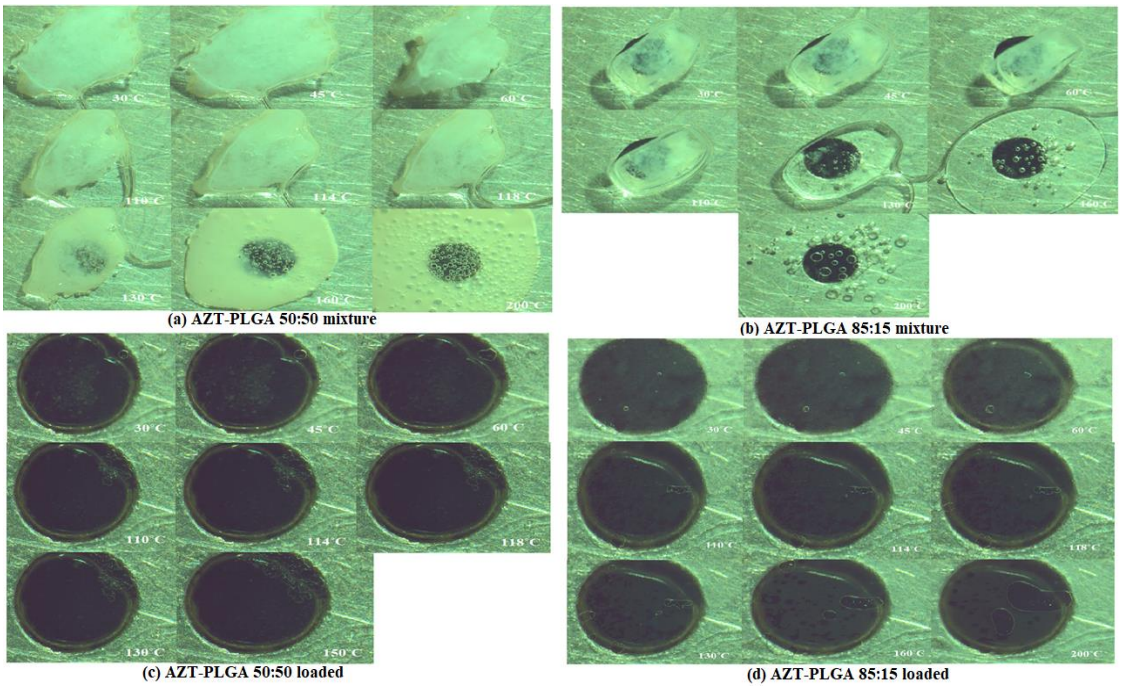


*Figure 5.11: HSM images of (a) AZT-PLGA 50:50 physical mixture, (b) AZT-PLGA 85:15 physical mixture, (c) AZT-PLGA 50:50 loaded and (d) AZT-PLGA 85:15 loaded*

Figure 5.11d above presents images from the HSM analysis of AZT-PLGA 85:15 loaded nanoparticles. Melting of the sample with increase in temperature was a bit difficult to visualize at temperature changes between 30°C and 60°C; however, noticeable change such as melting of the sample was observed at temperatures above 110°C. There was no appearance of bubbles, and no visible degradation of the sample was observed. This could possibly be explained by the fact that the polymer completely encapsulated AZT and therefore protected it from degradation. It may also be that the amount of AZT in the formulation was too small for the degradation process to be visualized. Unlike the case with AZT-PLGA 50:50 nano-formulation, the sample appeared to dry up when the temperature increased above 130°C.

### 5.3.10 Thermogravimetric analysis (TGA)

In Figure 5.12, data from the TGA of AZT-PLGA 50:50 and AZT-PLGA 85:15 loaded nanoparticles are presented. The AZT-PLGA 50:50 loaded nanoparticles exhibited a single mass loss event unlike AZT-PLGA 85:15 loaded nanoparticles which exhibited two mass loss events. This can be attributed to differences in polymer ratios and their molecular weights. During pre-formulation analysis however, the reverse was the case; the physical mixture of AZT-PLGA 50:50 exhibited two mass loss events while AZT-PLGA 85:15 exhibited a single mass loss event.

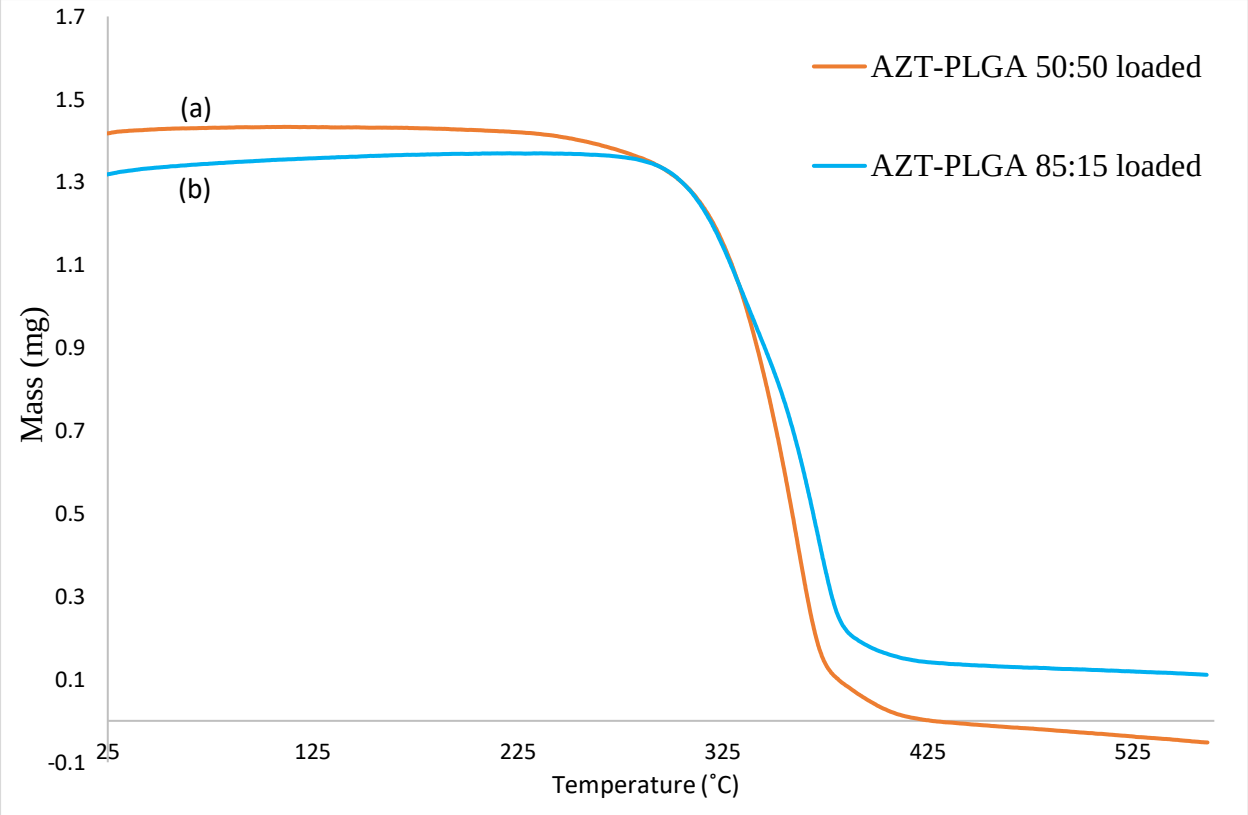


*Figure 5.12: TGA curve of (a) AZT-PLGA 50:50 loaded and (b) AZT-PLGA 85:15 loaded nanoparticles.*

These differences could perhaps be a result of insufficient trituration of the physical mixture and its components. It may also be due to a change in thermal stability of the products. These are only hypothetical currently; hence, may require further investigation.

Table C1.10 appendix C presents data from the thermal analyses of AZT formulated nanoparticles.

### 5.3.11 Differential Scanning Calorimetry (DSC)

Figure 5.13 shows thermograms of AZT-PLGA 50:50 and AZT-PLGA 85:15 loaded nanoparticles. As was the case with TDF, no identifiable peaks of AZT could be seen in the thermograms. The reason for this could be that no crystalline AZT was found in the nanoparticles. It may also indicate that the amount of AZT present in the sample was too small to show any peaks, or that AZT is molecularly dispersed in the polymer

matrix. The loaded nanoparticles showed peaks that were present when AZT physical mixtures were analyzed (Figure 5.5b), with melting points of 55.25°C and 56.09°C for AZT-PLGA 85:15 and AZT-PLGA 50:50 respectively. It is however not known if these differences in temperature are significant.

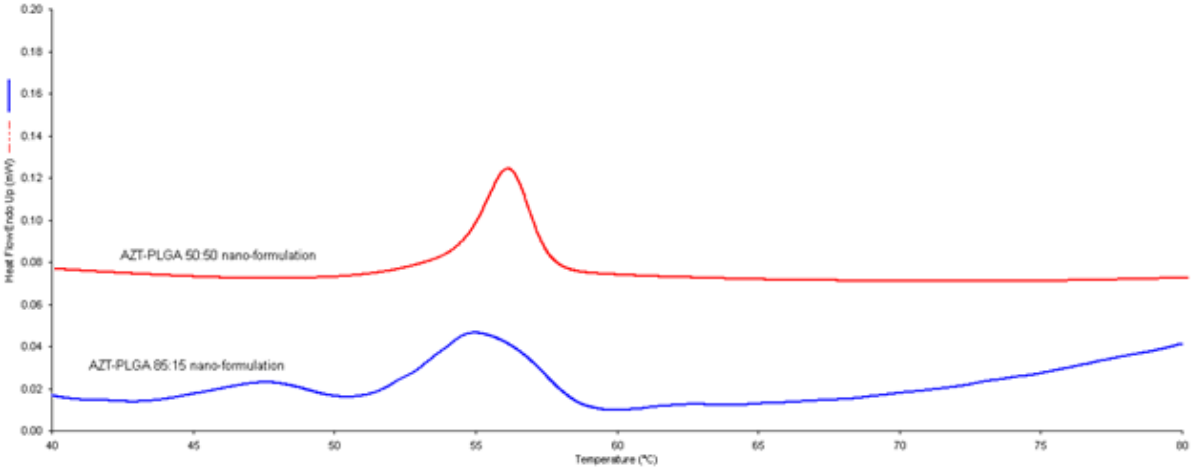


*Figure 5.13: DSC thermograms of AZT-PLGA 50:50 and AZT-PLGA 85:15 loaded nanoparticles*

### 5.3.12 Determination of AZT release from AZT-PLGA loaded nanoparticles

Figure 5.14 shows the cumulative percentage of AZT released from AZT-PLGA loaded nanoparticles at a pH 1.2 and pH 7.4 *versus* time. Samples were analyzed using two analytical methods, HPLC-DAD and UV-spectrometry. The release profiles from both analytical methods showed a biphasic release model with an initial burst of AZT followed by sustained release. This is typical of core-shell type nanoparticles.[8] The release profile also confirmed the presence of surface drug present on the nanoparticles, with the bulk of the AZT encapsulated within the nanoparticles. With such release kinetics, some level of extended release may possibly be obtained from the AZT-PLGA formulations. If this is the case, there may be no need for twice daily

dosing of AZT, thus making a formulation with once daily dosing, which can improve patient compliance and adherence to therapy.

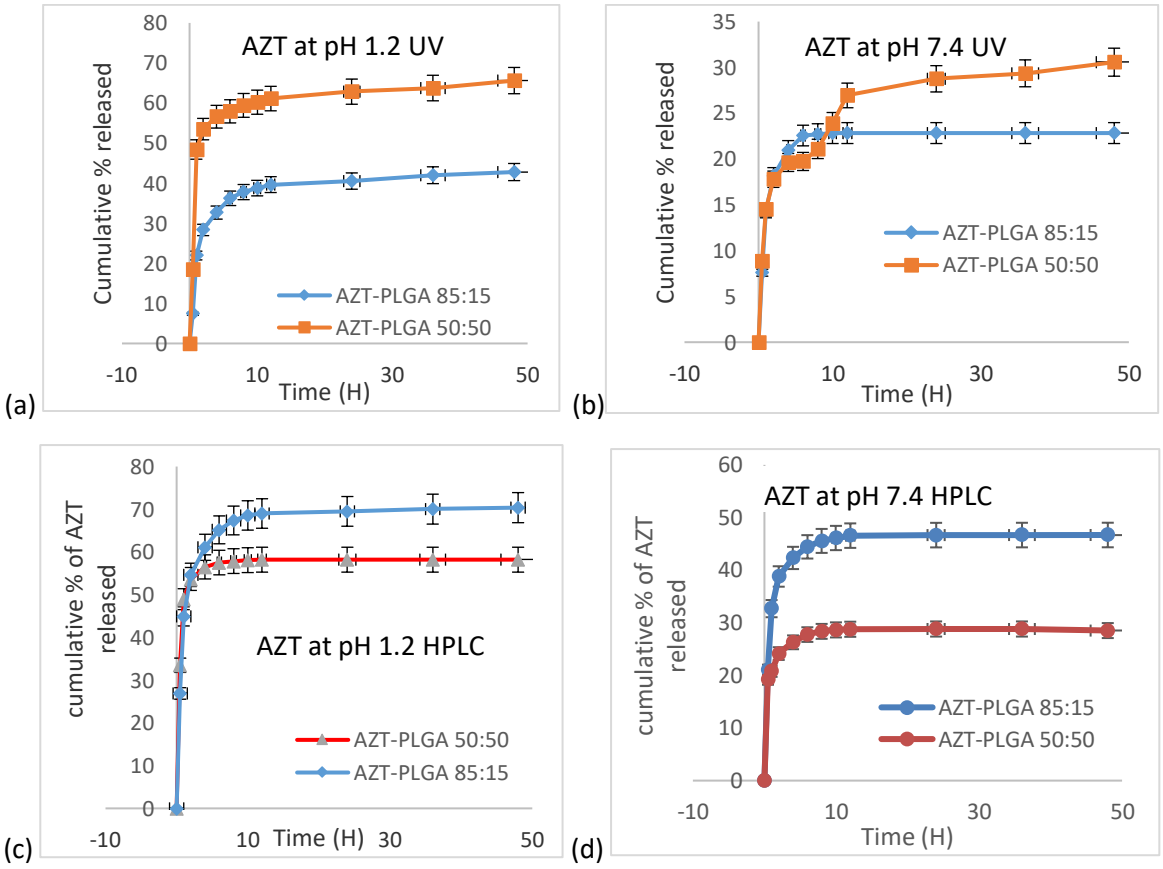


*Figure 5.14: In-vitro release of AZT-PLGA 50:50 and AZT-PLGA 85:15 loaded nanoparticles*

The release studies were done at pH 1.2 (Figure 5.14 a & c) and pH 7.4 (Figure 5.14 b & d) at 37˚C over a period of 48h, using the UV-spectrometry (Figure 5.14 a & b) and HPLC-DAD (Figure 5.14 c & d) analytical methods. Data was collected in triplicates and presented as mean ± SD (n=3).

Table 5.11 indicates an approximation of the total percentage of AZT released within 12 hours. Drug release from the same sample was quantified using two analytical equipment's. Some differences were observed when the release curves from one

method were compared to the other method. Could this be a result of human error, or some other reason not yet fully understood?

*Table 5.11: Percentage of AZT released (12 hours analysis)*

| **AZT** | **HPLC-DAD** | | **UV-spectrometry** | |
|---|---|---|---|---|
| | pH 7.4 | pH 1.2 | pH 7.4 | pH 1.2 |
| **PLGA 50:50** | 28.7 % | 58% | 27% | 61% |
| **PLGA 85:15** | 46.1% | 68% | 23% | 39% |

After the initial burst, more of AZT was released from the nano-formulations over a period of time before a constant release was attained. The release profiles of both formulations indicated that more of AZT was released from the AZT-PLGA 85:15 formulation when compared to the AZT-PLGA 50:50 formulation at pH 1.2 and pH 7.4 when analyzed using the HPLC-DAD method; however, the reverse was the case when the sample was analyzed using UV-spectrometry. This difference may be due to differences in the different polymers with respect to molecular weight, ratio and composition.

### 5.3.13 Mathematical modeling of drug release data

The release mechanism of AZT from AZT-PLGA formulated nanoparticles was evaluated by fitting the release data to four mathematical models, namely; Gompertz model, Korsmeyer-Peppas model, Peppas-Sahlin model, and Weibull model. DDsolver, a peer-reviewed modelling program [9], was used for this analysis. The release data was fitted to each of the four mathematical models listed above; these models are the ones commonly used in literature.[10]

The best fit model was selected by using the adjusted coefficient of determination ($R^2$ adj) and a model with the highest $R^2$ adj was deemed to be the best fitting model. $R^2$ adj allows for better comparison of the models when compared to the coefficient of

determination ($R^2$).[11] The release data of AZT obtained at both pH 1.2 and 7.4 was fitted to the four models mentioned above and it was determined that a majority of the formulations (3 out of 4) were best fit by the Weibull model. The exception was AZT-PLGA 50:50 at pH 7.4 whose best fit model (according to the $R^2$ adj value) was the Peppas-Sahlin model (Table 5.12).

Table 5.12 below presents parameter values and $R^2$adj values obtained from fitting drug release experimental data to the four mathematical models. The asterisked values correspond to the highest value of $R^2$adj obtained when the four models were compared, for each sample.

Parameters explaining the Weibull model are as discussed in chapter 4 section 4.3.13, The following samples were best fitted by Weibull model AZT-PLGA 85:15 at pH 7.4, AZT-PLGA 50:50 and AZT-PLGA 85:15 at pH 1.2, All three sample models displayed a **β** value less than 0.75, which implied that the release mechanism was by Fickian diffusion.

Parameters in Peppas-Sahlin can be described as follows **K1** is the constant that is related to Fickian kinetics (Fickian diffusion), **K2** is the constant that is related to case-II relaxation kinetics (matrix relaxation/erosion) and **m** is the diffusional exponent (ranges between 0 and 1).

As mentioned earlier, AZT-PLGA 50:50 at pH 7.4 did not fit with the other release data for Weibull model; its model of best fit was the Peppas-Sahlin model (Table 5.12). The release parameters for AZT-PLGA 50:50 under the Peppas-Sahlin model showed that the **k2** values were all negative. This indicates that **k1** was the only mechanism of release, which inferred that AZT release from the formulation was by Fickian diffusion.

*Table 5.12: Parameter values and $R^2$adj values obtained from fitting drug release experimental data to four mathematical models*

| **pH** | | **1.2** | | **7.4** | |
|---|---|---|---|---|---|
| | **Parameters** | **AZT-PLGA50:50** | **AZT-PLGA85:15** | **AZT-PLGA50:50** | **AZT-PLGA85:15** |
| **Weibull_1** | B | 0.15 | 0.05 | 0.07 | 0.07 |
| | A | 1.32 | 1.22 | 3.67 | 3.67 |
| | Ti | 0.49 | 0.5 | 0.47 | 0.47 |
| | $R^2$adj | 0.982* | 0.993* | 0.977 | 0.981* |
| **Gompertz_1** | A | 0.84 | 0.77 | 1.50 | 1.13 |
| | B | 0.70 | 0.30 | 0.14 | 0.32 |
| | $R^2$adj | 0.957 | 0.937 | 0.969 | 0.930 |
| **Peppas-Sahlin_1** | K1 | 51.42 | 59.9 | 28.19 | 38.33 |
| | K2 | -9.03 | -14.88 | -6.75 | -7.54 |
| | M | 0.33 | 0.24 | 0.24 | 0.30 |
| | $R^2$adj | 0.971 | 0.968 | 0.998* | 0.978 |
| **Korsmeyer-Peppas with Tlag** | N | 0.08 | 0.03 | 0.06 | 0.07 |
| | K | 53.9 | 53.0 | 23.9 | 38.0 |
| | $R^2$adj | 0.976 | 0.992 | 0.976 | 0.980 |

### 5.3.14 Stability of AZT-PLGA loaded nanoparticles

The formulated nanoparticles were stored at temperatures between 2 and 8°C. They were subsequently evaluated for stability by measuring parameters such as the particle size, zeta potential and PDI at the time of preparation and at different time intervals over a duration of 90 days.

**Particle size**

The average nanoparticle size after formulation was determined to be 122.4 ±1.48 nm and 110.4 ± 0.02 which increased to 155.3 ± 0.8 nm and 182.7 ± 3.7 nm after washing. These values further increased to 1941.3 ±32.21 nm and 1600 ± 74.8 nm after freeze

drying of the nanoparticles for AZT-PLGA 50:50 AZT-PLGA 85:15, respectively. During storage, the nanoparticles showed a steady pattern of increasing nanoparticle size with time (Figure 5.15). This was indicative of an increase in coalescence of the nanoparticles, and as such a decrease in stability with time.

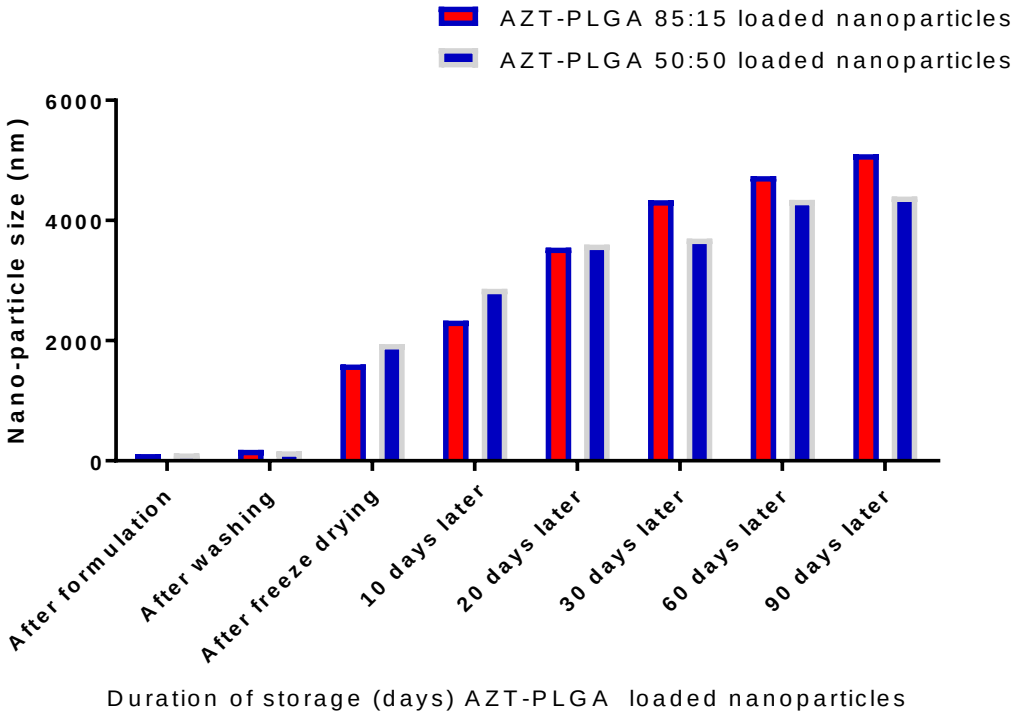


*Figure 5.15: Changes in nanoparticle size of TDF-PLGA 50:50 and 85:15 freeze dried loaded nanoparticles*

Upon comparison of the particle sizes, AZT-PLGA 85:15 showed a steady increase in particle over time, This was similar to the observation made with TDF-PLGA 85:15 (Figure 4.15) As noted with TDF-PLGA 50:50, the particle sizes of AZT-PLGA 50:50 also increased with time, albeit at a seemingly slower rate than was observed with AZT-PLGA 85:15. These differences in the rate of particle size increase may be due to differences in the copolymer ratios and their molecular weights.

The postulated mechanisms to show how particles pass through the gastrointestinal and physiological barriers highlights endocytosis as one of the mechanisms, for

particles < 500 nm. It can therefore be seen that the nanoparticle sizes immediately after formulation and after washing favors uptake *via* endocytosis. Following the freeze-drying and 90-days storage processes however, the increase in particle size as mentioned above was such that endocytosis may not be favorable as an uptake mechanism. There may however be some success with uptake *via* lymphatic passage, with absorption by cells in Peyer's patches, especially for particles less than 5 µm. It can be seen that the nanoparticle size increased after the washing process, possibly due to agglomeration of these particles. As with the TDF formulations a proposal may be made for more assessments of to limit such agglomeration after the washing process, perhaps by making use of suitable surface-active agents. Such an intervention may slow / prevent agglomeration, ensuring that particle sizes remain close to the values obtained immediately after formulation. This will enhance penetration through physiological barriers and hence improve bioavailability.

**Zeta potential**

The average zeta potential after formulation was determined to be -9.94 ± 0.02 mV and -5.11 ± 2.1 mV for AZT-PLGA 50:50 and AZT-PLGA 85:15, respectively. These values further decreased after washing, indicating an increase in stability. During storage, the zeta potential showed a steady increase in value, which is an indication of a decrease in stability of the nano-formulation with increase in time; however, on day 30, the sample showed some discrepancy indicating an increase in stability. The zeta potential further decreased from day 60 through day 90 (Figure 5.16).

The same trend was also noticed with the TDF formulations (section 4.3.14 and Figure 4.16). Was there perhaps some condition that improved stability on day 30, only to compromise such stability afterwards? This may be the subject of further studies.

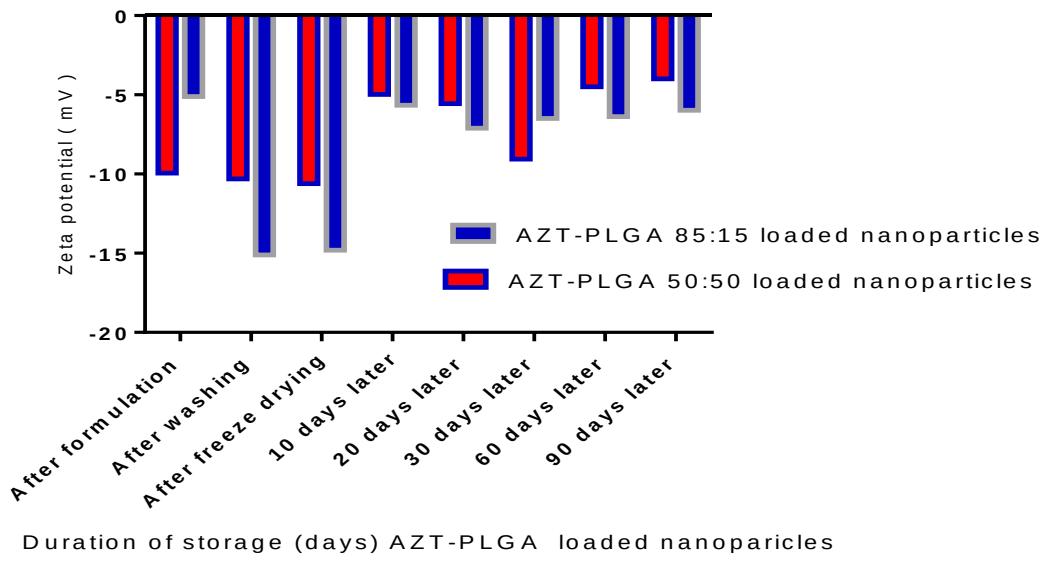


Figure 5.16: *Changes in zeta potential of AZT-PLGA 50:50 and AZT-PLGA 85:15 freeze dried loaded nanoparticles.*

**Polydispersity index**

The PDI values of the formulated nanoparticles were also assessed immediately after formulation. The values were 0.193 ±1.2 and 0.159 ± 0.02 for AZT-PLGA 50:50 and AZT-PLGA 85:15 respectively. The PDI values after day 10 of storage showed signs of increased coalescence of the nanoparticles. A steady increase in the PDI values was expected over time, however, on days 20, 30, 60 and 90, a drop was noticed in the PDI values, indicating less coalescence. It is our hypothesis that the molecular weight and copolymer ratios may be a factor responsible for these differences. (Figure 5.17).

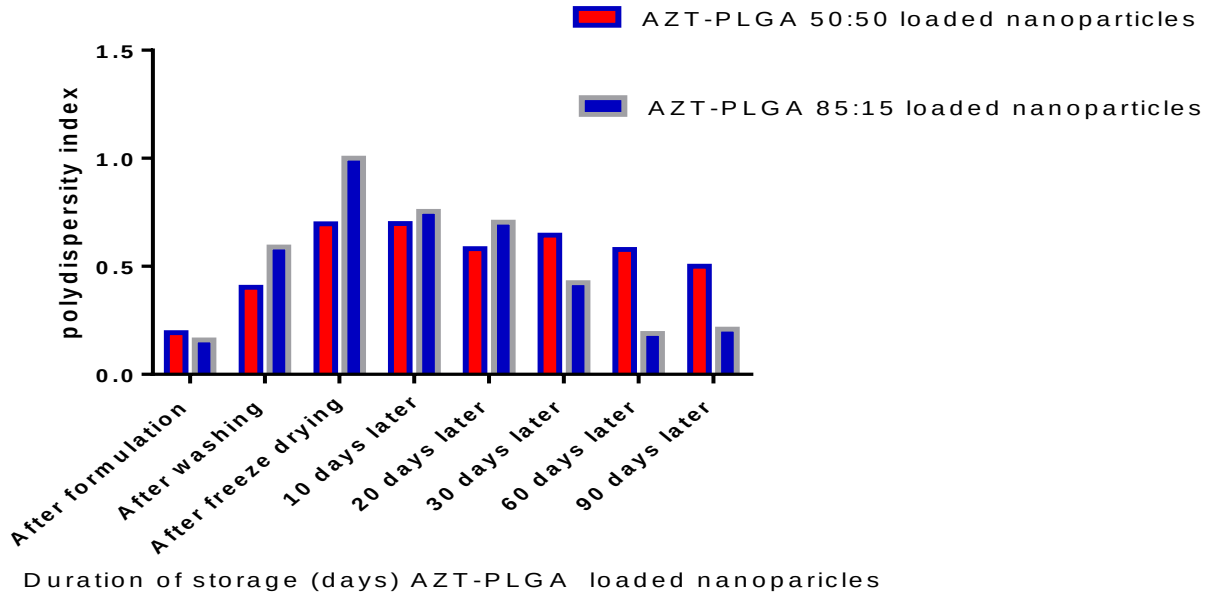


Figure 5.17*: Changes in PDI of AZT-PLGA 85:15 and AZT-PLGA 50:50 freeze dried loaded.*

The overall changes in the nanoparticle size, zeta potential and PDI over the duration of storage were indicative of a decrease in stability of the formulated nanoparticles over time.

Comparing the results obtained from characterizing AZT-loaded nanoparticles with the work done by Peter Christoper *et al.,* 2014 it could be determined that the author formulated nanoparticles which were less than 100 nm in size as opposed to the values obtained in the preset study (particle sizes greater than 100 nm). The present formulation with AZT-PLGA 50:50 yielded a higher encapsulation efficiency (73.8%) when compared to the value (59.50%) obtained by Peter Christoper *et al.,* 2014. Peter Christoper *et al.,* 2014 also modeled the drug release profile and found it to fit the Higuchi model while for this study, the release profile fit best to the Weibull and Peppas-Sahlin models.

Chapter 6 will follow with an overall conclusion of the study**.**

## Bibliography

1. Peter, C. G., Vijaya R. C., Siddharth, K., Siva S. K. M., and Hari, P. R., (2014). 'Formulation and optimization of coated PLGA – Zidovudine nanoparticles using factorial design and in vitro in vivo evaluations to determine brain targeting efficiency', *Saudi Pharmaceutical Journal*, *22*(2), pp 133-140.
2. Jani, P.U., Halbert, G.W., Langridge, J., Florence, A.T., (1990) 'Nanoparticle uptake by the rat gastrointestinal mucosa: Quantitation and particle size dependency', *J. Pharm. Pharmacol*, 42(N/A), pp. 821–826.
3. Gref, R., Minamitake, Y., Peracchia, M.T., Trubetskoy, V., Torchilin, V., Langer, R., (1994) 'Biodegradable long-circulating polymeric nanospheres', *Science*, 263 (5153), pp.1600–1603.
4. Bhattacharjee, S., (2016) 'DLS and zeta potential – What they are and what they are not?', *Journal of Controlled Release*, 235, pp.337-351.
5. Masarudin, M. J., Cutts, S. M., Evison, B. J., Phillips, D. R., Pigram, P. J., (2015). 'Factors determining the stability, size distribution, and cellular accumulation of small, monodisperse chitosan nanoparticles as candidate vectors for anticancer drug delivery: application to the passive encapsulation of [14C]-doxorubicin', *Nanotechnology, Science and Applications*, 8(N/A), pp. 67-80
6. Panyam, J., Labhasetwar, V., (2003). 'Biodegradable nanoparticles for drug and gene delivery to cells and tissue', *Adv Drug Deliv Rev*, 55(N/A), pp.329-347.
7. Shabir G. A., (2005). 'Step-by-step analytical methods validation and protocol in the quality system compliance industry', *JVT* 10(N/A), pp. 314-325.

8. Cui, L., Liu, Z., Yu, D., Zhang, S., Bligh, S. and Zhao, N. (2014). Electrosprayed core-shell nanoparticles of PVP and shellac for furnishing biphasic controlled release of ferulic acid. *Colloid and Polymer Science*, 292(9), pp.2089-2096.
9. Zhang, Y., Huo, M., Zhou, J., Zou, A., Li, W., Yao, C. and Xie, S., (2010). 'DDSolver: An Add-In Program for Modeling and Comparison of Drug Dissolution Profiles', *The AAPS Journal*, 12(3), pp.263-271.
10. Maryam, J., Babak, K., 'Mathematical Kinetic Modeling on Isoniazid Release from Dex-HEMA-PNIPAAm Nanogels', *Nanomed research journal,* 1(2), pp.90-96.
11. Papadopoulou, V., Kosmidis, K., Vlachou, M. and Macheras, P. (2006). 'On the use of the Weibull function for the discernment of drug release mechanisms', *International Journal of Pharmaceutics*, 309(1-2), pp.44-50.
12. Pirooznia, N., Hasannia, S., Lotfi, A. and Ghanei, M., (2012). 'Encapsulation of Alpha-1 antitrypsin in PLGA nanoparticles: In Vitro characterization as an effective aerosol formulation in pulmonary diseases', *Journal of Nanobiotechnology*, 10(1), p.20.

# CHAPTER 6: CONCLUSION AND RECOMMENDATIONS

Co-formulation of TDF and AZT with PLGA to produce TDF-PLGA and AZT-PLGA nanoparticles, respectively, was the overall aim of this study. Producing these nanoparticles would in turn improve absorption and reduce the dose of drug required to attain therapeutic concentrations, thereby improving bioavailability and reducing the adverse effects associated with the use of these APIs when administered orally.

The overall objectives of the study were:

- to characterize AZT, TDF and PLGA
- to formulate non-covalent complexes of TDF and AZT with PLGA of different ratios (50:50 and 85:15);
- to characterize and compare physicochemical properties of the formulated complexes using various analytical techniques;
- to compare the pharmaceutical properties (i.e. particle size, stability and *in-vitro* re*lease st*udies) of the formulated complexes as a means of addressing some of the limitations associated with the optimal delivery of TDF and AZT (e.g. low permeability, low bioavailability).

The above objectives were achieved by formulating nanoparticles using a modified water in oil in water (w/o/w) double emulsion solvent evaporation and diffusion method which had been proven to be efficient in encapsulating hydrophilic drugs.[1] Part of the hypothesis was successfully achieved when AZT and TDF were successfully co-formulated to produce AZT-loaded and TDF-loaded nanoparticles.

Nanoparticles of relatively small sizes in the range of 103 to 160 nm were successfully formulated, with PDI and zeta potential values indicating good homogeneity (PDI of less than 0.4) and good stability of the formulated nanoparticles (zeta potential of up to -19 mV). These smaller particle sizes play an important role as they are likely to be absorbed from the small intestine in greater proportions than the larger nanoparticles.

Analysis on FTIR provided spectra which were indicative of TDF and AZT encapsulation within the formulated nanoparticles. This was characterized by shifts, disappearance, appearance, increase or decrease in the intensity of the characteristic peaks when both formulations where compared to the parent compounds and physical mixtures of TDF and AZT with the polymers.

A significant visual difference was noticed when the nanoparticles where analyzed using SEM; the blank nanoparticles showed surfaces that were smother than the loaded nanoparticles. This difference was explained by the APIs presence in the nanoparticles. This study recommends both TEM and SEM analysis be performed on the APIs and physical mixtures with PLGA based on the absence of such data in previous studies and comparative analysis with loaded samples.

TEM on the loaded nanoparticles based on magnification of microscopic image may provide physical image of the loaded PLGA with the API visible in the micelle. Further structural elucidation could be determined using X-ray diffraction.

Both formulated nanoparticles of TDF and AZT showed high percentage yields greater than 50%, with high entrapment values (67-85% for TDF and 75-93% for AZT) and low encapsulation efficiency of less than 50%. An exception was the AZT-PLGA 50:50 formulation which presented with an encapsulation efficiency as high as 73.82%, a value which is 24.02% more than the second highest encapsulation efficiency obtained from the four formulations (TDF-PLGA 85:15). It is uncertain at this stage if this difference is significant. The limitations to this value are highlighted in chapters 4 and 5.

The developed method of formulation was sound and the API to polymer ratio should be reviewed for a possible increase in concentration of API to be included in subsequent studies.

The *in vitro* release profile of both formulations (TDF and AZT) suggested that the release profile was biphasic; firstly, there was an initial burst of the API which confirmed the presence of surface API in the formulated nanoparticles, followed by a sustained release. Overall, the release profile revealed that more of the API was released at pH 1.2 when compared to the release profile of the same formulation at pH 7.4 (Table 4.11 and Table 5.11). This was confirmed by both HPLC-DAD and UV-spectrometry analyses and it agreed with studies by Pamula and Menaszek *et la*, 2007 who stipulated that the surrounding medium influences the degradation process.

The total percentage of API released proposed that not all of the encapsulated drug was released within the 48-hour period. Hence, 48 hours is not sufficient time to achieve complete polymer swelling and degradation to facilitate drug diffusion from the nanoparticles.

Chapters 4 and 5 release data fit well to four Mathematical models, i.e. with the Peppas-Sahlin (only for AZT-PLGA 50:50 at pH 7.4) and the Weibull models (for all other formulations) as the best fit models. This also confirmed that the main mechanism of drug release from the formulated nanoparticles was by Fickian diffusion of the drug molecule from the nanoparticle core. Dissolution is a kinetic process and is quantified by the drug's rate of solubility in solution. Solubility quantifies the dynamic equilibrium state achieved when the rate of dissolution equals the rate of precipitation. Since release studies were not performed for the free drugs, the nanoparticle release profile was compared to the free drug release profile performed by Shailender *et al*., 2017 and Uronnachi *et al*., 2014 for TDF and AZT, respectively and to the calibration curve used to analyse the HPLC data. Shailender *et al*., 2017 and Uronnachi *et al*., 2014 established that the free drugs were completely released in less than four hours of testing. This confirmed that sustained release was achieved which can led to an

improvement in bioavailability and reduction of adverse effects associated with the use of these APIs thereby proving the hypothesis. *In-vivo* studies are however recommended to further test this hypothesis.

All drug formulations have to be tested for stability. The shelf-life of the product is dependent on such studies. Gradual changes in the stability of the nanoparticles was noticed after just 10 days of storage (2°C to 8°C). The sample showed a decrease in stability; however, these changes were not drastic, therefore the samples were not stable for a duration of 90 days at temperatures between 2°C to 8°C. It is our recommendation that the stability of samples be evaluated at room temperature at well.

According to literature, there are several factors and different mechanisms of polymer degradation to release encapsulated drugs.[2] (mentioned in chapter 2). Firstly, PLGA containing both *D*- and *L*- forms of PLA was purchased, a combination of both forms prevents concerns of prolong or fast degradation. In 1999 Tracy *et la*, stated that PLGA with acid terminated ends showed a 2-3-fold increase in degradation rate when compared to ester terminated PLGA. Thus, this influenced the purchase of ester terminated PLGA for this study which has been proven to degrade slower.[3] .

Finally, the results obtained showed that non-covalent nanoparticles were successfully formulated. Evaluation of the formulated nanoparticles revealed that future studies are needed to improve encapsulation efficiency, i.e., further work is needed to minimized wastage to improve the overall yield and stability, which can translate to a high percentage yield. Further work on *in vivo* analysis could also be performed to assess the ability of the nano-formulations to attenuate the limitations of the APIs.

## Bibliography

1. Liu, J., Qiu, Z., Wang, S., Zhou, L., and Zhang, S., (2010). 'A modified double-emulsion method for the preparation of daunorubicin-loaded polymeric nanoparticle with enhancedin vitroanti-tumor activity', *Biomedical Materials*, 5(6), pp. 065002.
2. Lanao, R. P. F., Jonker, A. M., Wolke, J. G. C., Jansen, J. A., van Hest, J. C. M., and Leeuwenburgh, S. C. G., (2013). 'Physicochemical properties and applications of Poly(lactic-co-glycolic acid) for use in bone regeneration', *Tissue Engineering Part B: Reviews*, 19(4), pp. 380–390.
3. Tracy, M., (1999). Factors affecting the degradation rate of poly(lactide-co-glycolide) microspheres in vivo and in vitro. *Biomaterials*, 20(11), pp.1057-1062.
4. Shailender, J., Ravi, P., Saha, P., Dalvi, A., and Myneni, S., (2017). 'Tenofovir disoproxil fumarate loaded PLGA nanoparticles for enhanced oral absorption: Effect of experimental variables and in vitro, ex vivo and in vivo evaluation', *Colloids and Surfaces B: Biointerfaces*, 158, pp.610-619.
5. Uronnachi, E., Ogbonna, J., Kenechukwu, F., Chime, S., Attama, A., and Okore, V., (2014). 'Formulation and Release Characteristics of Zidovudine-Loaded Solidified Lipid Microparticles', *Tropical Journal of Pharmaceutical Research*, 13(2), p.199.

# Appendices

## Appendix A: Method development for formulation of TDF and AZT loaded nanoparticles

Appendix A presents the different methods assessed to achieve the desired method for formulation of TDF and AZT loaded nanoparticles utilized in this study. The following general method was applied to prepare the nanoparticles, NP (methods A-F).

### The general method

1. 100 mg of polymer was weighed and dissolved in 10 ml of ethyl acetate: acetone (4:1 ratio) containing 5% v/v tween 80 in a beaker.
2. 5 mg of API was dissolved in 1 ml of distilled water in a separate beaker.
3. (2) was **sonicated** in (1) at a speed of 5000 rpm for 30 seconds, in an ice bath. The mixture was then **homogenized** at 87 kHz for 2 minutes in the ice bath to form the primary emulsion (w/o).
4. (3) was added dropwise into 40 ml of water and **sonicated** at a speed of 12000 rpm for a further 2 minutes to form the secondary emulsion (w/o/w). Thereafter, the mixture was **homogenized** at 87 kHz for 3 minutes.
5. The w/o/w double emulsion was then poured gradually into a beaker containing 0.05% w/v gelatin dissolved in water while stirring with a magnetic stirrer at 400 rpm.
6. The solution (5) was then continuously stirred at 400 rpm at a temperature of 30 degrees centigrade for 6 hrs. This served to evaporate the organic solvents i.e. ethyl acetate and acetone completely, leaving a white cloudy emulsion (the formed nanoparticles).

7. The nanoparticles where spun in a centrifuge at a speed of 16000 rpm for 30 min to collect the pellets (loaded nanoparticles).
8. The pellets where washed three times with distilled water.

**ORGANIC SOLVENT**

The first organic solvents (dichloromethane and acetone) used were selected because of its ready availability in the laboratory. However, neither of the two solvents could dissolve the polymer, and when used in combination, the polymer precipitated after homogenization (Appendix, Figure A1.1). The goal at this stage was to select an organic solvent that could solubilize the polymer to continue the study.

**A. Organic solvent: Dichloromethane / Acetone**

Dichloromethane and acetone were used alone and in combination (ratio 4:1), (Figure A1.1a). The organic solvents ( was able to dissolve the polymer completely; however, the polymer precipitated upon addition of the aqueous phase during homogenization/ sonication (Figure A1.1 b). Thus, the sample and the method with selected solvent mixture used was rejected.


(a)

(b)

Figure A1.1: *Result of polymer dissolution in the organic solvents (dichloromethane and acetone)*

### B. Organic solvent: chloroform

Chloroform was used alone as the organic solvent at this stage of experimentation, because the goal was to select a suitable organic solvent with a low boiling point thus capable of evaporating quickly. NPs were successfully produced but were not subjected to washing because the particle sizes obtained were larger than the expected value of less than 150 nm (Table A1.1). Chloroform had proven to solve the issue (precipitation of the polymer after homogenization) encountered with dichloromethane and acetone; however, it still presented its own shortcomings as particle size obtained was larger than required.

*Table A1.1: Particle size, polydispersity index and zeta potential of formulated AZT or TDF nanoparticle obtained with chloroform as the organic solvent.*

| **Solvent** | **Particle size (nm)** | | **Polydispersity index** | | **Zeta potential** | |
|---|---|---|---|---|---|---|
| | Before wash | After wash | Before wash | After wash | Before wash | After wash |
| **Chloroform** | 354.1 | - | 0.198 | - | -0.361 | - |

### C. Organic solvent: Ethyl acetate

Ethyl acetate was also tested as an organic solvent. The results are presented in Table A1. 2.

*Table A1. 2*: *Particle size, polydispersity index and zeta potential of formulated nanoparticles obtained with ethyl acetate and changes in gelatin concentration.*

| **Solvent Ethyl acetate** | **Gelatin (%) w/v** | **Particle size (nm)** | | **Polydispersity index** | | **Zeta potential** | |
|---|---|---|---|---|---|---|---|
| | | **Before wash** | **After wash** | **Before wash** | **After wash** | **Before wash** | **After wash** |
| **Sample 1 (TDF)** | 0.5 | 1859 | - | 1 | - | - | - |
| **Sample 2 (TDF)** | 0.5 sonicated | 185 | - | 1 | - | 4 | |
| **Sample 3 (TDF)** | 0.2 | 392.4 | - | 0.371 | - | 3.01 | - |
| **Sample 4 (TDF)** | 0.1 | 1603 | - | 0.274 | - | - | - |
| **Sample 5 (TDF)** | 0.05 | 312 | - | 1 | - | 2.91 | |
| **Sample 6 (TDF)** | 0.05 sonicated | 237.1 | - | 1 | - | 3.94 | - |
| **Sample 7 (AZT)** | 0.05 | 400 | - | 1 | - | -2 | |
| **Sample 8 (AZT)** | 0.05 sonicated | 93 | - | 0.98 | - | 6 | |
| **Sample 9 (AZT)** | 0.1 | 839 | - | 1 | - | -3.5 | |
| **Sample 10 (AZT)** | 0.2 | 501.2 | - | 0.917 | - | -2.91 | - |
| **Sample 11 (AZT)** | 0.5 sonicated | 117.1 | - | 0.528 | - | 5.61 | - |
| **Sample 12 (AZT)** | 0.5 | 1890 | - | 1 | - | -8 | |

Ethyl acetate was preferred over chloroform because it is less toxic than the latter. Further experimentation was carried out with ethyl acetate as the organic solvent. Changes were made to the concentration of gelatin in this exercise. Some gelatin samples were sonicated to aid with solubility before use because it was apparent that the size of the formulated NPs were affected by concentration and effects of sonication as seen in Table A1.3. When gelatin was sonicated before use, the nanoparticle sizes were of a lower value compared to the same concentration when gelatin was not sonicated. The concentration of gelatin was also varied and its effect on particle size investigated.

### D. Organic solvent: ethyl acetate/acetone ratio 4:1

Samples in this category were homogenized before sonication, unlike the samples previously prepared which were homogenized after sonication, to determine which sequence will yield the smallest particles sizes. The concentration of gelatin was kept constant at 0.05% w/v and the gelatin stock solution was sonicated before use. An exception was sample 3 which was not sonicated, this was to determine if there would be any difference in particle size, PDI and zeta potential when there is sonication and when there is no sonication (Table A1.3).

Table A1.3: *Particle size, polydispersity index and zeta potential of formulated nanoparticles obtained when samples were homogenized before sonication.*

| **Solvent** | **Particle size (nm)** | | **Polydispersity index** | | **Zeta potential** | |
|---|---|---|---|---|---|---|
| **Ethyl acetate / Acetone (4:1)** | Before wash | After wash | Before wash | After wash | Before wash | After wash |
| **Sample 1** | 99.66 | 360 | 0.412 | 3.12 | 3.12 | -8.63 |
| **Sample 2** | 126.9 | 278 | 0.385 | 0.365 | 2.85 | -9.05 |
| **Sample 3*** | 1895 | 1688 | 1 | 1 | - | - |

*samples not sonicated

### E. Reduction of sample size

Organic solvent: ethyl acetate/acetone ratio 4:1

The sample was prepared using the general method earlier reported with the exception that the w/o/w double emulsion prepared was not poured into 200 ml of water containing 0.05% gelatin but instead was directly transferred to the rotavapor for solvent evaporation at 400 rpm for 4 hrs. This step did not yield much difference in the particle size because the NPs were still not within the desired particle size range of 100-200 nm (Table A1.4).

Table A1.4: *Particle size, polydispersity index and zeta potential of formulated nanoparticles obtained when sample size was reduced.*

| **Solvent** | **Particle size (nm)** | | **Polydispersity index** | | **Zeta potential** | |
|---|---|---|---|---|---|---|
| | Before wash | After wash | Before wash | After wash | Before wash | After wash |
| **Ethyl acetate / Acetone (4:1)** | 1237 | - | 1 | - | - | - |

### F. Organic solvent less than 10ml i.e. ethyl acetate and acetone (4:1)

The emulsion was prepared with the general method reported above, with slight modification in the total volume of organic solvent (ethyl acetate and acetone) used. Instead of using a total volume of 10 ml, we tested 5 ml and 6 ml of the organic solvent in the same combination and ratio as above. The organic solvents were used individually as well to dissolve the polymer. A portion of the polymer precipitated during the process (Figure A1.2); and the sample was therefore discarded.

Figure A1.2: *Precipitation of sample (AZT and TDF) when less than 10ml of the organic solvent (ethyl acetate and acetone) was used.*

## Appendix B

### Reduction of total sample size from 251 ml to 91 ml using d-*α*-tocopheryl polyethylene glycol 1000 succinate (TPGS) and tween 80.

The general method previously described (appendix A) produced a total sample volume of 251 ml and this was very cumbersome and time consuming to centrifuge. In addition, some of the sample was lost during this process. There was thus a need to reduce the total sample size. The gelatin which was used as a surfactant affected the particle sizes of the NPs hence the change to TPGS. The general method below was used to accommodate these changes.

### Method

1) 100 mg of polymer was weighed and dissolved in 10 ml of a mixture of 4:1 ethyl acetate/acetone and vortexed to ensure that it was completely dissolved.
2) 5 mg of the API was dissolved in (1) ml of water containing 0.2% w/v tween 80.
3) (2) was homogenized in 1 at a speed of 5000 rpm for 2 min and sonicated at 87 kHz for 30 seconds under an ice bath to produce the primary emulsion.
4) (3) was added dropwise into 40 ml of external water containing 0.12% TPGS and homogenized for 3 min at a speed of 12000 rpm. The mixture was then sonicated at 87 kHz for 2 min.
5) The w/o/w double emulsion was poured gradually into a beaker containing 40 ml of 0.2% tween 80 while stirring with a magnetic stirrer at 800 rpm.
6) The solution was evaporated using the rotavapor at a speed of 400 rpm and temperature between 30-35 degrees for 6 hrs to completely evaporate the organic solvents.

7) The nanoparticles where spun at a speed of 16500 rpm for 60 min to collect the pellets which settled at the bottom.
8) The pellets where washed three times with distilled water.

### G. Sample preparation without TPGS

The sample was prepared using the method described above, however only with tween 80 (and no TPGS) as follows: The TPGS in step 4 was replaced with tween 80 thus in the final stage no surfactant was used. However, following centrifugation at a temperature of 4˚C and speed of 16500 rpm for 30 mins, the nanoparticles could not be collected. A possible reason for this might have been that the particle sizes were too small, and a higher centrifugation speed was needed for the nanoparticles formed to settle and be collected from the sample. This sample was rejected (Table B1.1).

Table B1.1: *Particle size, polydispersity index and zeta potential of formulated nanoparticles obtained when sample size was reduced and preparation was without TPGS.*

| **Solvent** | **Particle size (nm)** | | **Polydispersity index** | | **Zeta potential** | |
|---|---|---|---|---|---|---|
| | Before wash | After wash | Before wash | After wash | Before wash | After wash |
| **Ethyl acetate / Acetone (4:1)** | 89.92 | - | 0.232 | - | -4.94 | - |

### H. Sample preparation with TPGS

The sample was prepared as described previously by the general method in appendix B. Formulation data from this activity are presented in Table B1.2. Following preparation, the samples were spun at a speed of 26000 rpm for 30 mins. In the process, the Eppendorf tubes containing the samples were broken, leading to loss of samples. A possible reason proffered for this was the centrifuge speed, which may have been too high for the tubes used.

Table B1.2: *Particle size, polydispersity index and zeta potential of formulated nanoparticles obtained when sample size was reduced and preparation was with TPGS.*

| Solvent | Particle size (nm) | | Polydispersity index | | Zeta potential | |
|---|---|---|---|---|---|---|
| | Before wash | After wash | Before wash | After wash | Before wash | After wash |
| **Ethyl acetate / Acetone (4:1)** | 107.7 | - | 0.161 | - | -5.71 | - |

### I. Sample prepared with TPGS

The samples prepared in section H above confirmed the method to be used. The prepared sample was collected by centrifuging at a lower speed of 16500 rpm for one hour. The collected pellets were washed and freeze-dried. Data obtained from this activity is presented in Table B1.3.

Table B1.3: *Particle size, polydispersity index and zeta potential of formulated nanoparticles obtained when sample size was reduced, reduced collection speed (16500) and preparation was with TPGS.*

| Solvent Ethyl acetate / Acetone (4:1) | Particle size (nm) | | Polydispersity index | | Zeta potential | |
|---|---|---|---|---|---|---|
| | Before wash | After wash | Before wash | After wash | Before wash | After wash |
| **Sample 1** | 111.5 | 156.9 | 0.128 | 0.317 | -10.9 | -16.6 |
| **Sample 2** | 117.3 | 153.2 | 0.160 | 0.303 | -8.84 | -19.1 |

## Appendix C : Validation of UV-VIS assay method for tenofovir disoproxil fumarate and zidovudine in PBS at pH 1.2 and pH 7.4.

The tables presented by appendix C are computational data used for a standard callibration curve for both AZT and TDF. It also provides data used to prove the accuracy and precission of the of HPLC-DAD and UV-spectrometry method used for the prediction of TDF and AZT.

*Table C1.1: Calibration plot of TDF at pH 7.4 and pH 1.2 (HPLC-DAD analyses).*

| Concentration (µg/ml) | Mean Absorbance | | %RSD | |
|---|---|---|---|---|
| | pH 7.4 | pH 1.2 | pH 7.4 | pH 1.2 |
| 0.02 | 34.15 | 71.40 | 0.42 | 1.2 |
| 0.04 | 68.27 | 143.55 | 2.06 | 2.0 |
| 0.06 | 102.31 | 213.44 | 0.28 | 3.0 |
| 0.08 | 135.92 | 284.22 | 0.86 | 1.7 |
| 0.10 | 168.55 | 371.71 | 0.39 | 3.0 |
| 0.12 | 201.07 | 420.0 | 0.96 | 0.5 |

*Table C1.2: Calibration plot of TDF at pH 7.4 and pH 1.2 (UV-spectrometry analyses)*

| **Concentration (µg/ml)** | **Mean Absorbance** | | **%RSD** | |
|---|---|---|---|---|
| | pH 7.4 | pH 1.2 | pH 7.4 | pH 1.2 |
| 2 | 0.0295 | 0.0696 | 0.71 | 4.9 |
| 4 | 0.0817 | 0.1358 | 1.22 | 0.13 |
| 6 | 0.1306 | 0.1745 | 0.27 | 0.10 |
| 8 | 0.1630 | 0.2018 | 0.18 | 0.05 |
| 10 | 0.1927 | 0.2337 | 0.05 | 0.04 |
| 12 | 0.2424 | 0.2794 | 0.04 | 0.14 |

*Table C1.3: Selected FTIR data for TDF, PLGA 50:50, PLGA 85:15, TDF-PLGA 50:50 physical mixture, and TDF-PLGA 85:15 physical mixture*

| Analyzed sample | Experimental frequency bands ($cm^{-1}$) | Standard frequency bands (cm-1) | Associated functional groups from IR bands |
|---|---|---|---|
| **TDF** | 3459.12 | 3400-3500 | Medium N-H stretching |
| | 2981.38 | 2300-3300 | Strong broad O-H stretching |
| | 2814.22 | 2850 - 2810 | Medium $–OCH_3$ stretching |
| | 2018.44 | 2140 - 1990 | Strong and broad –N=C=S stretching |
| | 1752.31 | 1800 - 1750 | Strong C=0 stretching |
| | 1671.87 | 1685 - 1665 | |
| **PLGA 50:50** | 2950.52 | 2960 - 2850 | Chelated O-H stretching bridge |
| | 1750.32 | 1800 – 1750 | C=O stretching of the carbonyl group |
| **PLGA 85:15** | 2996.25 | 3000 - 2500 | Chelated O-H stretching bridge |
| | 1745.64 | 1790 - 1740 | Strong C=O stretching of the carbonyl group |
| **TDF-PLGA 50:50 physical mixture** | 2993.81 | 3000 - 2500 | Chelated O-H stretching bridge |
| | 1750.07 | 1790 - 1740 | Strong C=O stretching of the carbonyl group |
| **TDF-PLGA 85:15 physical mixture** | 2985.88 | 3000 - 2500 | Chelated O-H stretching bridge |
| | 1754.32 | 1790 - 1740 | Strong C=O stretching of the carbonyl group |
| | 1674.85 | 1685 - 1665 | Strong C=0 stretching |

*Table C1.4: Thermogravimetric analysis of data for TDF, polymers and TDF-polymer physical mixture*

| Sample | Mass loss events | $T_{onset}$ ± 1 (°C) | $T_{deg.max.}$ ±1 (°C) | $T_{endset}$ ± 1 (°C) | Total mass loss (%) |
|---|---|---|---|---|---|
| **PLGA 50:50** | 1st | 236 | 322 | 324 | 98 |
| | 2nd | 335 | 376 | 378 | |
| **PLGA 85:15** | 1st | 221 | 311 | 313 | 100 |
| | 2nd | 318 | 389 | 390 | |
| **TDF-PLGA 50:50** | | 215 | 399 | 400 | 93 |
| **TDF-PLGA 85:15** | | 217 | 396 | 397 | 98 |
| **TDF** | 1st | 135 | 199 | 201 | 87 |
| | 2nd | 203 | 275 | 276 | |

*Table C1.5: Thermal properties of TDF-PLGA loaded nanoparticles*

| Drug polymer combination | Mass loss events | $T_{onset}$ (°C) | $T_{deg.max.}$ (°C) | $T_{endset}$ (°C) | Total mass loss (%) |
|---|---|---|---|---|---|
| **TDF-PLGA 50:50 loaded** | 1st | 206 | 355 | 356 | 93 |
| | 2nd | 356 | 424 | 425 | |
| **TDF-PLGA 85:15 loaded** | 1st | 234 | 340 | 341 | 91 |
| | 2nd | 343 | 396 | 397 | |

*Table C1.6: Calibration plot of AZT at pH 7.4 and pH 1.2, (HPLC-DAD analyses)*

| Concentration (µg/ml) | Mean Absorbance | | %RSD | |
|---|---|---|---|---|
| | pH 7.4 | pH 1.2 | pH 7.4 | pH 1.2 |
| 0.02 | 165.83 | 124.97 | 0.72 | 0.85 |
| 0.04 | 330.59 | 249.14 | 0.17 | 0.99 |
| 0.06 | 495.44 | 391.12 | 0.28 | 0.19 |
| 0.08 | 656.09 | 494.27 | 0.02 | 0.4 |
| 0.10 | 824.70 | 614.31 | 0.13 | 0.32 |
| 0.12 | 976.90 | 745.93 | 0.2 | 0.2 |

*Table C1.7: Calibration plot of AZT at pH 7.4 and pH 1.2 (UV-spectrometry analyses)*

| Concentration (µg/ml) | Mean Absorbance | | %RSD | |
|---|---|---|---|---|
| | pH 7.4 | pH 1.2 | pH 7.4 | pH 1.2 |
| 2 | 0.0869 | 0.1100 | 0.24 | 0.18 |
| 4 | 0.1539 | 0.1625 | 0.10 | 0.06 |
| 6 | 0.2231 | 0.2539 | 0.09 | 0.37 |
| 8 | 0.2927 | 0.3248 | 0.07 | 0.06 |
| 10 | 0.3666 | 0.3993 | 0.27 | 0.09 |
| 12 | 0.428 | 0.4649 | 0.19 | 0.08 |

*Table C1.8: Thermal properties of AZT, polymers and AZT-polymer physical mixture*

| Sample | Mass loss events | $T_{onset}$ (°C) | $T_{deg.max.}$ (°C) | $T_{endset}$ (°C) | Total mass loss (%) |
|---|---|---|---|---|---|
| **AZT-PLGA 50:50** | 1st | 218 | 353 | 355 | 94 |
| | 2nd | 357 | 398 | 399 | |
| **AZT-PLGA 85:15** | | 220 | 386 | 387 | 97 |
| **AZT** | 1st | 172 | 247 | 257 | 76 |
| | 2nd | 249 | 317 | 318 | |

*Table C1.9: Selected FTIR data for AZT-PLGA 50:50 loaded nanoparticles, AZT-PLGA 85:15 loaded nanoparticles, AZT-PLGA 50:50 physical mixture, and AZT-PLGA 85:15 physical mixture*

| Compound | Experimental frequency bands ($cm^{-1}$) | Standard frequency bands (cm-1) | Associated functional groups from IR bands |
|---|---|---|---|
| **AZT-PLGA 50:50 loaded** | 2948.36 | 3000 - 2500 | Chelated O-H stretching bridge |
| | 1748.67 | 1770 - 1710 | Strong C=O stretching |
| **AZT-PLGA 85:15 loaded** | 2995.93 | 2960 - 2850 | Strong C-H bending |
| | 2945.50 | 3000 - 2500 | Chelated O-H stretching bridge |
| | 1748.02 | 1770 - 1710 | Strong C=O stretching |
| **AZT-PLGA 50:50 physical mixture** | 3461.12 | 3500 - 3300 | Medium N-H stretching bands |
| | 3023.15 | 3000 - 2500 | Chelated O-H stretching bridge |
| | 2814.57 | 3200 - 2500 | O-H stretching |
| | 2082.39 | 2160-2120 | Strong N=N=N stretching |
| | 1751.54 | 1770 - 1710 | Strong C=O stretching |
| | 1679.98 | 1685-1666 | Strong C=O stretching |
| **AZT-PLGA 85:15 physical mixture** | 3460.60 | 3500 - 3300 | Medium N-H stretching bands |
| | 3023.04 | 3000 - 2500 | Chelated O-H stretching bridge |
| | 2082.15 | 2160-2120 | Strong N=N=N stretching |
| | 1750.91 | 1770 - 1710 | Strong C=O stretching |
| | 1677.09 | 1685-1666 | Strong C=O stretching |

*Table C1.10: Thermal properties of AZT-PLGA loaded nanoparticles*

| Drug polymer combination | Mass loss events | $T_{onset}$ (°C) | $T_{deg.max.}$ (°C) | $T_{endset}$ (°C) | Total mass loss (%) |
|---|---|---|---|---|---|
| **AZT-PLGA 50:50 loaded** | $1^{st}$ | 225 | 414 | 415 | 100 |
| **AZT-PLGA 85:15 loaded** | $1^{st}$ | 234 | 334 | 335 | 93 |
| | $2^{nd}$ | 335 | 402 | 403 | |